January 2015

Two-Phase Flow Pressure Drop In Circular Small Channels With Abrupt Contraction And Expansion

Che-Hao Yang

TWO-PHASE FLOW PRESSURE DROP IN CIRCULAR SMALL CHANNELS WITH ABRUPT CONTRACTION AND EXPANSION

By

Che-Hao, Yang

Bachelor of Science, University of North Dakota, 2014

A Thesis

Submitted to the Graduate Faculty

of the

University of North Dakota

in partial fulfilment of the requirements

for the degree of

Master of Science

Grand Forks, North Dakota

August

2015

This thesis, submitted by Che-Hao.Yang in partial fulfillment of the requirements for the Degree of Master of Science from the University of North Dakota, has been read by the Faculty Advisory Committee under whom the work has been done and is hereby approved.

_____
Dr. Clement Tang, Chairperson

_____
Dr. Nanak Grewal,

_____
Dr. Yeo Howe Lim,

This thesis is being submitted by the appointed advisory committee as having met all of the requirements of the School of Graduate Studies at the University of North Dakota and is hereby approved.

_____
Dr. Wayne Swisher,
Dean of the School of Graduate Studies

_____
Date

PERMISSION

Title Two-phase flow pressure drop in circular small channels with abrupt contraction and expansion

Department Mechanical Engineering

Degree Master of Science

In presenting this thesis in partial fulfillment of the requirements for a graduate degree from the University of North Dakota, I agree that the library of this University shall make it freely available for inspection. I further agree that permission for extensive copying for scholarly purposes may be granted by the professor who supervised my thesis work or, in their absence, by the chairperson of the department or the dean of the School of Graduate Studies. It is understood that any copying or publication or other use of this dissertation or part thereof for financial gain shall not be allowed without my written permission. It is also understood that due recognition shall be given to me and to the University of North Dakota in any scholarly use which may be made of any material in my thesis.

Name: Che-Hao.Yang

Date: August 01, 2015

TABLE OF CONTENTS

Figure **LIST OF FIGURES** Page

Table **LIST OF TABLE** Page

ACKNOWLEDGMENTS

I will never be able to finish my thesis without help and guide from my committee members, friends, my family. Especially, I would like to express my deepest gratitude to my advisor, Dr. Clement Tang, for his great support, good patience, consistent encouragement and excellent guidance for my thesis and Master's program. I would like to express my sincere appreciation to Dr. Nanak Grewal and Dr. Howe Lim for their useful advices and experiences sharing. I also want to thank Jay Evenstad and Gary Dubuque for their expert manufacturing sharing and helping. I would like to thank my friends Sarbottam Pant, and Ashish Kotwal for their generous and valuable advises and help. Finally I want to thank my family for supporting and financing me.

ABSTRACT

Gas-liquid phase flow pressure drops occurred in circular channels with sudden contraction or expansion have been studied and investigated experimentally. Especially, water and nitrogen gas phases as experimental fluids were applied in this study. In this study, single phase, deionized water, and two phase, deionized water and nitrogen gas mixture, were under investigation and observation. The diameters of the test channels were 0.5, 0.375, 0.315, 0.19 and 0.14 inches. The setup of the contraction channels, 0.5 to 0.375 inches, 0.5 to 0.315 inches, 0.5 to 0.19 inches, and 0.5 to 0.14 inches were applied. For studying the expansion channels, the reverse of the contraction channels setup were used.

In single phase flow experiment, the ranges of the water mass flows were operated from approximately 5 to 30 g/s. The range of the Reynolds numbers in the smallest contraction channel, area ratio of 0.0784, was from 2016 to 10740. The pressure differences were obtained between 0.59 to 8.46 kPa. The loss coefficients were found to be approximately 0.85 when Reynolds number is above 8000. For the largest contraction channel, area ratio of 0.5652, the range of the Reynolds number became narrower, from 675 to 4014. The range of the pressure drop was to between 0.26 and 0.31 kPa. The loss coefficient remained constant value, which was 0.4, all measured flow rates. The range of Reynolds number in the smallest expansion channel, area ratio of 0.0784, was from 1958 to 10714. The pressure drops data was between 0.64 and 6.69 kPa. The value of the loss coefficient was a constant value of 0.849. In the largest expansion channels, area

ratio of 0.5652, the Reynolds number ranges between 780 and 3997. The pressure drops were between 0.18 to 0.295 kPa.

In two phase flow, the water flow rates were controlled between approximately 5 to 30 g/s. The nitrogen gas was added into the experimental test section. The flow rates of the nitrogen were from 0.00049 to 0.029 g/s. The experimental liquid Reynold numbers were recorded from 1310 to 7913 in the smallest contraction channel at the lowest gas mass flow rate. The pressure drops were measured between 0.64 and 3.78 kPa. The liquid Reynolds number range in the largest contraction channel, at the largest gas mass flow rate, was between 1326 and 4031. The range of the pressure drop was 0.19 to 0.46 kPa. For the smallest expansion channel, the range of liquid Reynolds number was from 1290 to 7899 at the smallest gas flow rate. The pressure drop results were between 0.51 and 1.2 kPa. In the largest expansion channel at the largest gas mass flow rate, the pressure drop was between 0.027 and 0.42. The liquid Reynolds number range was between 1323 and 4005. When comparing the experimental data with theoretical and semi-empirical equations, the conditions of incompressible flow, flat velocity profile, vena contracta, slip ratio, homogeneous two-phase flow, and void fraction effect were considered. In our experimental result, the two-phase flow pressure drop data agrees well with the correlations available in the literature. In addition, the two-phase flow pressure drops are observed to be very sensitive to the void fraction. In order to accurately predict the pressure drops with correlations, the void fractions have to be properly determined.

NOMENCLATURE

A	flow area [m^2]
C_C	vena-contracta coefficient
g	Gravitational acceleration [m/s^2]
k	Minor loss coefficient
$k_{d,}$	Momentum correction factor
$\dot{m}$	Mass flow rate [g/s]
P	Pressure [pa]
ΔP_e	Pressure drop due to sudden expansion [pa]
ΔP_c	Pressure drop due sudden contraction [pa]
Re	Reynolds number
v	Flow velocity [m/s]
T	Temperature [ºC]
L	Test section length [m]
h_f	Head loss due to friction [m]
f_D	Darcy friction factor
D	Pipe diameter [m]
$h_{turbine}$	Head loss due to turbine [m]
h_{pump}	Head loss due to pump [m]
σ_x	Standard deviation

N Number of the measured values

x_i The i-th measured value of x

$\bar{x}$ Meaning of the measured values

Greek Symbols

σ Area ratio

ρ Density [Kg/m^3]

μ Viscosity [pa s]

β Kinetic correction factor

Subscripts

1 Smaller channel

3 Bigger channel

c Contraction

e Expansion

G Gas

w Water

CHAPTER I

INTRODUCTION

1.1 Conception

Pressure drop, also called pressure loss, is a phenomenon of mechanical energy loss that occurs due to viscous effects when the fluid flows through a passage. There are many reasons that can cause pressure loss, for instance, surface roughness of the passage, a 90 degree elbow for changing the fluid direction, sudden contraction and sudden expansion in the fluid system, etc. In order to maintain the same efficiency of the work from input to output of the system, the conditions of the flow passage, the flow characteristics, and properties of the working fluids must be considered and understood in the system design.

1.2 Purpose

This proposal is to this study and analyzed how gas and liquid phases flow in contraction and expansion of small circular channels with diameters of 0.5 inches (0.127 mm) to 0.19 inches (0.0483 mm). Pressure loss, loss coefficient and mass flow rate were be observed in these channels. The channels have five different diameters, which allowed four area ratio variations for abrupt contraction and expansion conditions. The gas and liquid mass flow rates were be controlled separately in the beginning of the experiment. The experiment data were be collected by a data acquisition system. The data collected was analyzed and compare with previous work results and a new conclusion may be made.

1.3 Expectation

The anticipated results of this experiment will indicate the performance of the pressure drops in the pair channels with controllable mass flow rates. The results will provide useful data and benefits to engineering applications involving multiphase flow systems with complex flow geometries.

1.4 Scope of this experiment

In this thesis, the area ratios of the test sections were 0.0784, 0.1444, 0.3844 and 0.5625 inches. Liquid mass flow rates, approximately 5 to 30 g/s, were applied in the single and two phase flow in circular channels with contraction and expansion. In the two phase flow experiment, the nitrogen gas was added in to the test section and the flow rates of the nitrogen gas were from 0.00049 to 0.029 g/s. The pressure drop and loss coefficient were observed and estimated in this studying.

CHAPTER II

LITERATURE REVIEW

Phase flow is a system of fluid mechanics that contains one or more than one phase of gas, liquid or solid. The applications of phase flow are broadly used in various field in the modern society. The one of most recently popular application is nuclear reactors as large-scale power systems. Two-phase flow and heat transfer significantly important for the reactor's design and safe operation. Designs of large boilers are greatly required detail knowledge of two-phase flow, heat transfer and pressure drop performance. Climate control systems are also needed deep understanding of two-phase flow. The two-phase flow in large-scale systems is ubiquitous and significantly related in the modern society.

2.1 Pressure drop

Pressure drop or pressure loss is a pressure difference between two points when a fluid flows through these two points. There are many reasons lead to the pressure drop, for instance, resistance to flow, flow area, density, elevation, etc. Therefore, the accurate total pressure drop observation and estimate in a fluid flow could be helped to understand the behaviors and characteristic of the given fluid. The total pressure drop can be divided into two portions: the one irreversible pressure drop that is due to the conversion of the mechanical energy irreversible. The friction loss and local loss are the typical type of this kind pressure drop. The other called reversible pressure drop, for example elevation pressure drop and acceleration pressure drop. In our experiment elevation pressure drop can be neglected due to the horizontal test section applying.

2.2 Single phase and two phase flow performance in contraction and expansion

Yoda et al. [1], the annular flow in the channels was referred by Hewitt et al. [2] and the consideration of pressure drop at 600 to 1400 psia in two phase flow was referred by Jansen and Kervinen [3], conducted two phase flow, air and water, experiments on abrupt flow area contraction and expansion in small channels. Two diameter of channels were used in this test, the large channel was 1.6 mm and the small one was 0.84. The range of Reynolds number in the small diameter channel was from 870 to 12960. Furthermore, flow quality was found between 1.9×10^{-3} and 1.6×10^{-2} in the two phase flow experiment. The authors also demonstrated loss coefficients were different for gas and liquid in the contraction and expansion test section. However, the expansion loss coefficients were approximately constant in the single phase (water) flow.

2.2.1 Friction loss

Friction loss occurred due to several reasons

1. Viscosity of fluid in motion
2. Fluid molecules against each other
3. Fluid layers moving in different velocities
4. Inter-phase friction between gas-liquid phases
5. Channel inside surface roughness

However, the friction loss can be expressed as Darcy–Weisbach equation

$$h_f = f_D * \frac{L}{D} * \frac{v^2}{2g} \tag{2.1}$$

where:

h_f = Head loss due to friction, given in units of length

f_D = Darcy friction factor

L = Pipe length

D = Pipe diameter

v = Flow velocity

g = Gravitational acceleration

The friction loss also can be described by pressure loss formation

$$\Delta P = f_D * \frac{L}{D} * \frac{\rho v^2}{2} \quad (2.2)$$

Where ΔP presents pressure drop in the flow system and ρ is the density of fluid.

2.2.2 Local loss, acceleration, and total pressure drop

Local loss caused by formation of vortices and strong turbulence in the flow, local disturbances of the flow, etc.

Acceleration pressure drop can be found in the flow area changing or density changing in two-phase flow system.

However, single phase flow total pressure drop and two-phase flow total pressure drop have defined into different equations in the research paper [1]. The total pressure drop of the single phase flow in the expansion channels demonstrated, as the previous discussion, into two parts: reversible pressure loss and irreversible pressure loss. Another majority factor in contraction and

expansion system is minor loss. The minor loss was happened at when a fluid flows through joints, valves, filters, contraction system, expansion condition, etc. The loss can cause a significant effect in the pressure drop in a small system, such as our setup. For the relationship of the total pressure loss, minor loss, reversible pressure loss and irreversible pressure loss, the equations described as below:

2.2.3 Single phase in expansion channels

The pressure drop in the expansion channels equations will be:

$$\Delta P_e = P_{2,1} - P_{2,3} = \Delta P_{e,r} - \Delta P_{e,i} \tag{2.3}$$

Flat velocity profiles were assumed, where:

ΔP_e = Pressure drop in the expansion channel

$P_{2,1}$ = Pressure measured from the flow area change to the small channel (See Figure 6)

$P_{2,3}$ = Pressure measured from the flow area change to the large channel (See Figure 6)

$\Delta P_{e,r}$ = Reversible pressure drop in the expansion channels (Elevation loss and acceleration loss)

$\Delta P_{e,i}$ = Irreversible pressure drop in the expansion channels (Friction loss and local loss)

$$\Delta P_{e,r} = -\frac{{v_1}^2}{2} * \rho_L * (1 - \sigma^2) \tag{2.4}$$

where $\sigma = \frac{A_1}{A_3}$:

v_1 = Velocity in the small channel

ρ = Density

A_1 = Area of the small channel

A_3 = Area of the large channel

$$\Delta P_{e,i} = K_e * \rho_L * \frac{v_1{}^2}{2} \quad (2.5)$$

$$k_e = (1-\sigma)^2 \quad (2.6)$$

where:

k_e = loss coefficient in the expansion channels

The pressure difference of the expansion channels in single phase could would also be claimed by I.Y.Chen et al. [4], similar to Schmidt [5] and Attou [6] studyings. The pressure drop can be related to the kinetic energy of the flow and be described into three parameters: density, velocity and area ratio of the channels. The equation expression as below:

$$\Delta P_e = \rho_L * v_1{}^2 * \sigma * (1-\sigma) \quad (2.7)$$

2.2.4 Single phase in contraction channel

The point vena contracta takes place when a fluid flows through the minimum cross section of a channel where fluid velocity reach its maximum. The sudden contraction is the case of this condition. Vena contracta occurs at a place slightly downstream of the changing area of the channel. Figure 1 illustrates how and where the vena contracta happens. Vena contracta point condition was also considered into the pressure loss at contraction channels. Normally, the coefficient of the vena contracta describes as area at vena contracta divides by area of orifice.

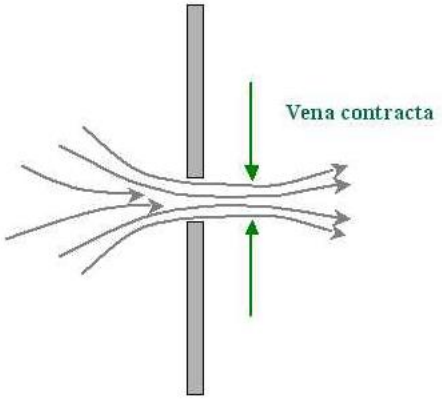

Figure 1: Schematic diagram of vena contracta [7]

The pressure drop in the contraction channel equations in Yoda et al. was formulated as velocity of the small channel, kinetic energy correction factor (β), area ratio, vena contracta coefficient (C_C) and momentum correction factor (k_d). For laminar flow in the channels, the kinetic energy correction is going to be 2 and the momentum factor equals to 1.33, are defined. However in the fully turbulent flow situation, both two factors will be approximate to one. The general equation can be expressed:

$$\Delta P_c = P_{2,1} - P_{2,3} = \Delta P_{c,r} + \Delta P_{c,i} \tag{2.7}$$

$$\Delta P_c = \frac{\rho_L * {v_1}^2}{2} * \frac{1 - \beta_3 * \sigma^2 * {C_C}^2 - 2 * C_C + 2 * {C_C}^2 * k_{d1}}{{C_C}^2} \tag{2.8}$$

The contration coefficient (C_C) in single phase flow referred to Geiger's thesis in 1964 [8]. The expression formula shown as below:

$$C_C = \frac{1 - \sigma}{2.08 * (1 - \sigma) + 0.5371} \tag{2.9}$$

For the laminar flow, the equation can be shown as (β = 2, k_d = 1.33):

$$\Delta P_c = \frac{\rho_L * {v_1}^2}{2} * [\frac{1}{{C_C}^2} - \frac{2}{C_C} + 2 * (1.33 - \sigma^2)] \tag{2.10}$$

In this case, flat velocity profiles or fully turbulent flow were postulated. The pressure drop in the contraction channel equations will be:

$$\Delta P_c = \frac{\rho_L * {v_1}^2}{2} * [(1 - \frac{1}{C_C})^2 + 1 - \sigma^2] \tag{2.11}$$

Single phase flow pressure drop in contraction channels was also defined in the Geiger's thesis, the equation used as following equation:

$$\Delta P_c = \frac{\rho_L * {v_1}^2}{2} * (\frac{1}{C_C} - 1)^2 \tag{2.12}$$

Chisholm [9] found total pressure drop could be associated with the static pressure drop to the vena contracta (ΔP_{SC})and pressure recovery downstream of the vena contracta (ΔP_{RC}) for single phase flow in contraction channels. The application of the contraction coefficient in Chisholm's report was slight different with Geiger's [8]. The formulas can be described as below:

$$\Delta P_c = \frac{\rho_L * {v_1}^2}{2} * [\left(\frac{1}{(\sigma * C_C)^2}\right) - 1 - \frac{2 * ({C_C}^{-1} - 1)}{\sigma^2}] \tag{2.13}$$

$$C_C = \frac{1}{0.639 * (1 - \sigma)^{0.5} + 1} \tag{2.14}$$

2.2.5 Two-phase in expansion channel

The two-phase flow in the expansion channels were assumed as both liquid and gas phases were incompressible and void fraction kept same in this case. The pressure drop in the expansion channel was going to be:

$$\Delta P_e = \Phi_{L0,e} * \Delta P_{L0,e} \tag{2.15}$$

where:

$\Phi_{L0,e}$ = Two-phase flow multiplier at all liquid condition in expansion channel

$\Delta P_{L0,e}$ = Pressure drop at all liquid condition in expansion channel

$$\Delta P_{L0,e} = \frac{\dot{m}_1{}^2}{\rho_L * A_1 * A_3} * (\sigma - 1) \tag{2.16}$$

where:

$\dot{m}_1$ = Mass flow rate at small channel

$$\Phi_{L0,e} = \frac{\rho_L}{\rho'} \tag{2.17}$$

$$\rho' = [\frac{1 - x^2}{\rho_L * (1 - \alpha)} + \frac{x^2}{\rho_G * \alpha}]^{-1} \tag{2.18}$$

$$\frac{x}{(1 - x)} = S * \frac{\rho_G * \alpha}{\rho_L * (1 - \alpha)} \tag{2.19}$$

$$S = \frac{v_G}{v_L} \tag{2.20}$$

$$x = \frac{\dot{m}_G}{\dot{m}_G + \dot{m}_L} \tag{2.21}$$

where:

ρ_L = Density of liquid

ρ' = fictitious mixture densities

ρ_G = Density of gas

x = Flow quality

α = Volumetric void fraction

S = Slip ratio

$\dot{m}$ = Mass flow rate

The homogeneous flow assumption was also applied in Yoda's [1] experimental report. Due to the assumption the velocity of liquid and gas were same, therefore slip ratio equaled to one. The relationship of the void fraction and quality were shown as following formula:

$$\alpha = \frac{\frac{x}{(1-x)} * \frac{\rho_L}{\rho_G}}{1 + \frac{x}{(1-x)} * \frac{\rho_L}{\rho_G}} \tag{2.22}$$

Substitution was applied:

$$\xi = \frac{x}{(1-x)} * \frac{\rho_L}{\rho_G} \tag{2.23}$$

The void fraction relative equation could be simplify into:

$$\alpha = \frac{\xi}{1+\xi} \tag{2.24}$$

For ideal annular flow situation, Zivi [10] proposed the minimum entropy generation assumption, the outcome of the slip ratio was different. The slip ratio expression was:

$$S = 0.7 * (\frac{\rho_L}{\rho_G})^{1/3} \tag{2.25}$$

To repeat the process of the substitution Eq. 2.19 and Eq. 2.22.

$$\varpi = \frac{x}{(1-x)} * \frac{\rho_L}{\rho_G} * (\frac{\rho_G}{\rho_L})^{1/3} \tag{2.26}$$

The void fraction relative equation could be simplify into:

$$\alpha = \frac{\varpi}{1+\varpi} \tag{2.27}$$

An equation of two phase flow pressure drop, which illustrated the pressure recovery in sudden diffuser, was generated by Wadle [11]. Wadle proposed constant minor loss coefficients in different fluid applications. For steam and water, the coefficient was 0.667. The coefficient was 0.83 in the application of air and water. The final pressure drop equation derivation was shown as:

$$\Delta P_e = (1-\sigma^2) * \frac{k * G^2}{2} * (\frac{(1-x)^2}{\rho_L} + \frac{x^2}{\rho_G}) \tag{2.28}$$

Where:

G = mass flux = $\rho * v = \frac{\dot{m}}{A}$

Collier and Thome [12] derived and rearranged the non-friction loss mechanical energy equation of two phase flow of the pressure drop in expansion channels. The pressure drop performances were proportional to its void fraction behaviors. The derivation could be expression as below:

$$\Delta P_e = \frac{-(1-\sigma^2)*G^2}{2*(\frac{x}{\rho_G}+\frac{1-x}{\rho_L})} * [\left(\frac{(1-x)^3}{(1-\alpha)^2*{\rho_L}^2}+\frac{x^3}{\alpha^2*\rho_G}\right)] \tag{2.29}$$

where void fraction was proposed by Kawahara et al. [13], the heat transfer concept was referred by Hewitt et al. [14]:

$$\alpha = \frac{0.03*\beta^{0.5}}{(1-0.97*\beta^{0.5})} \tag{2.30}$$

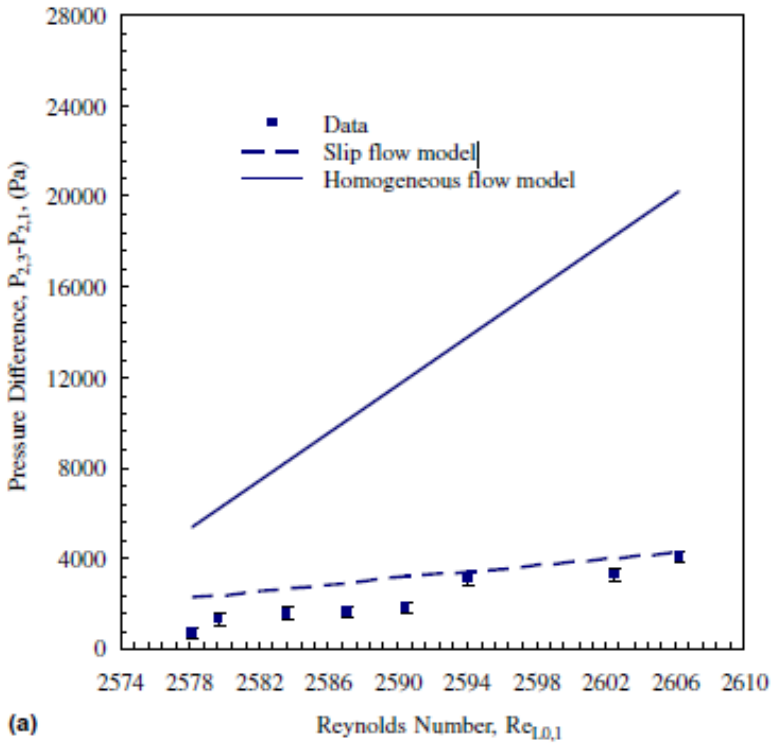

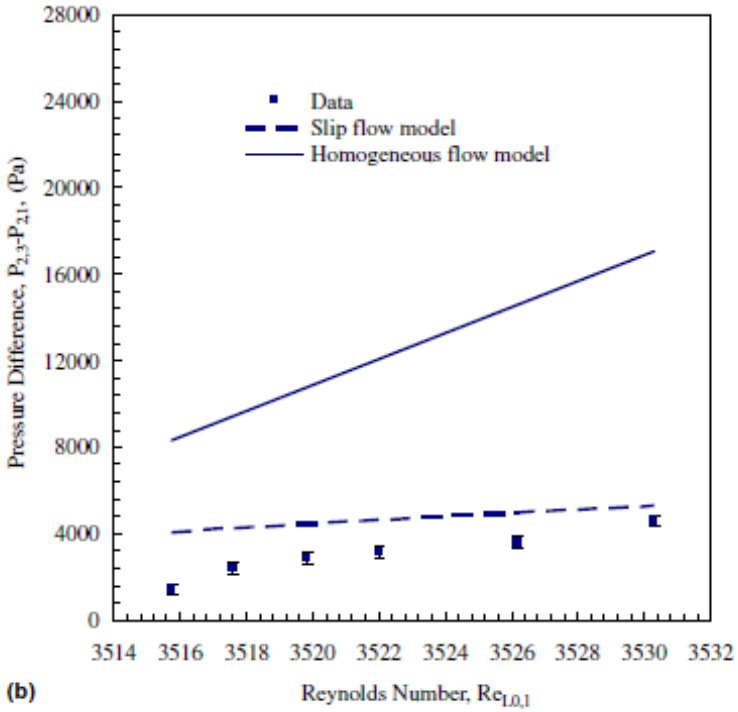

Figure 2: The two phase flow pressure difference vs Re in sudden expansion from Yoda data result [1]

The experimental data was predicted in two methods, slip flow model and homogeneous flow model in Figure 2. From the result of the two methods comparison, slip flow model which the value was obtained by using Eq. 2.25, demonstrated the great agreement of the prediction than the model of homogeneous flow for either Reynolds number big or small than 3000. The similar data pattern and slop with slip flow model were found in the plots.

2.2.6 Two-phase in contraction channel

Yoda et al [1]. considered the effect of the vena contracta unleashed downstream of the channels when two phase flow across abrupt contraction channels. The postulate incompressible gas and liquid and void frication and qualities were same and unchangeable. Geiger's [8] Vena contracta coefficient (C_C) was applied in the case. Total pressure difference could be described as:

$$\Delta P_c = {G_1}^2 * [\frac{\rho_h}{2 * \rho''^2} * \left(\frac{1}{{C_C}^2} - \sigma^2\right) + \frac{1}{\rho'} * (1 - C_C)] \quad (2.31)$$

where:

$$\rho'' = [\frac{(1-x)^3}{{\rho_L}^2 * (1-\alpha)^2} + \frac{x^3}{{\rho_G}^2 * \alpha^2}]^{-1/2} \quad (2.32)$$

To receive a better result, the assumption of homogeneous were made which the slip ratio equaled to one.

$$\Delta P_c = \Phi_{L0,c} * \Delta P_{L0,c} \quad (2.33)$$

where:

$\Phi_{L0,c}$ = Two-phase flow multiplier at all liquid condition in contraction channel

$\Delta P_{L0,c}$ = Pressure drop at all liquid condition in contraction channel

$$\Delta P_{L0,c} = \frac{{\dot{m}_1}^2}{2 * \rho_L * {A_1}^2} * [\left(\frac{1}{C_c} - 1\right)^2 + (1 - \sigma^2)] \quad (2.34)$$

$$\Phi_{L0,c} = 1 + \frac{x * (\rho_L - \rho_G)}{\rho_L} \quad (2.35)$$

$$C_c = 1 - \frac{1 - \sigma}{2.08 * (1 - \sigma) + 0.5371} \quad (2.36)$$

The Eq. 2.24 was applied in the Eq. 2.32. Furthermore, Yoda et al [1]. continued to make other postulate circumstance that fluids flow through the abrupt contraction channels without vena contracta. The value of the vena contracta coefficient was going to be one under this assumption. The liquid and gas density ratio to the power 1/3 which proposed by Zivi [10] was joint the estimate comparison. Collier and Thome recommended the estimation of the two phase flow pressure drop

in sudden contraction by using homogeneous flow. The Geiger's [8] vena contracta coefficient was applied. The formula shown:

$$\Delta P_c = \frac{G^2}{2 * \rho_L} * \left[\left(\frac{1}{C_C} - 1\right)^2 + (1 - \sigma^2)\right] * [1 + x * \left(\frac{\rho_L}{\rho_G} - 1\right)] \tag{2.37}$$

The plots of the Yoda's [1] experimental two phase flow pressure difference against Reynolds number in fully liquid flow condition were drawn and exhibited.

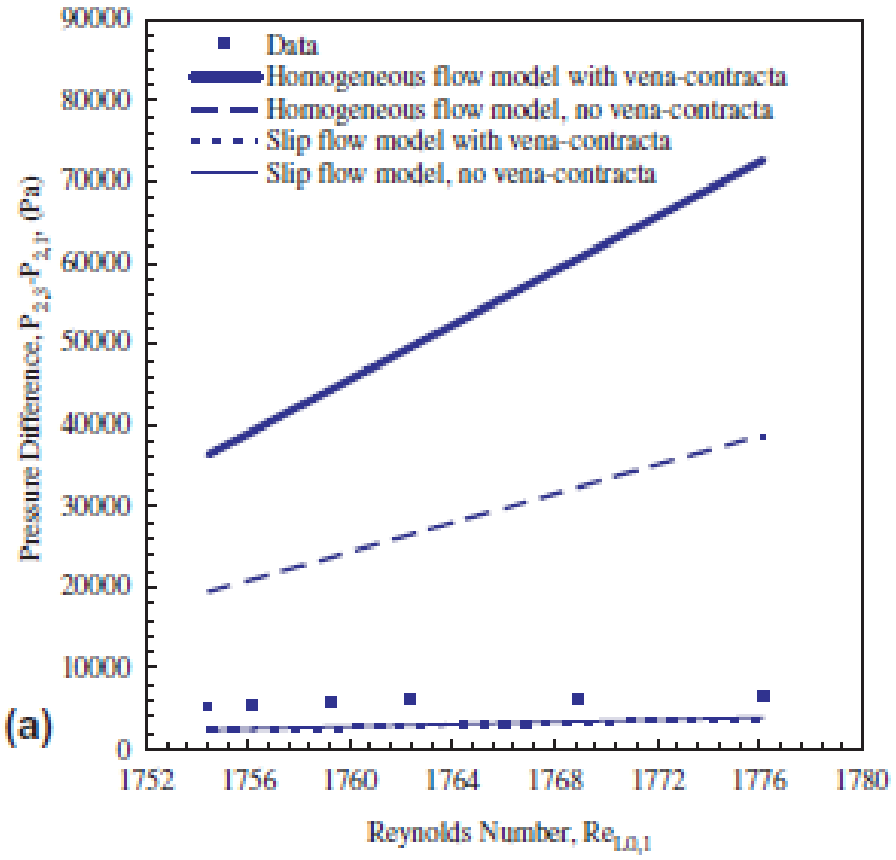

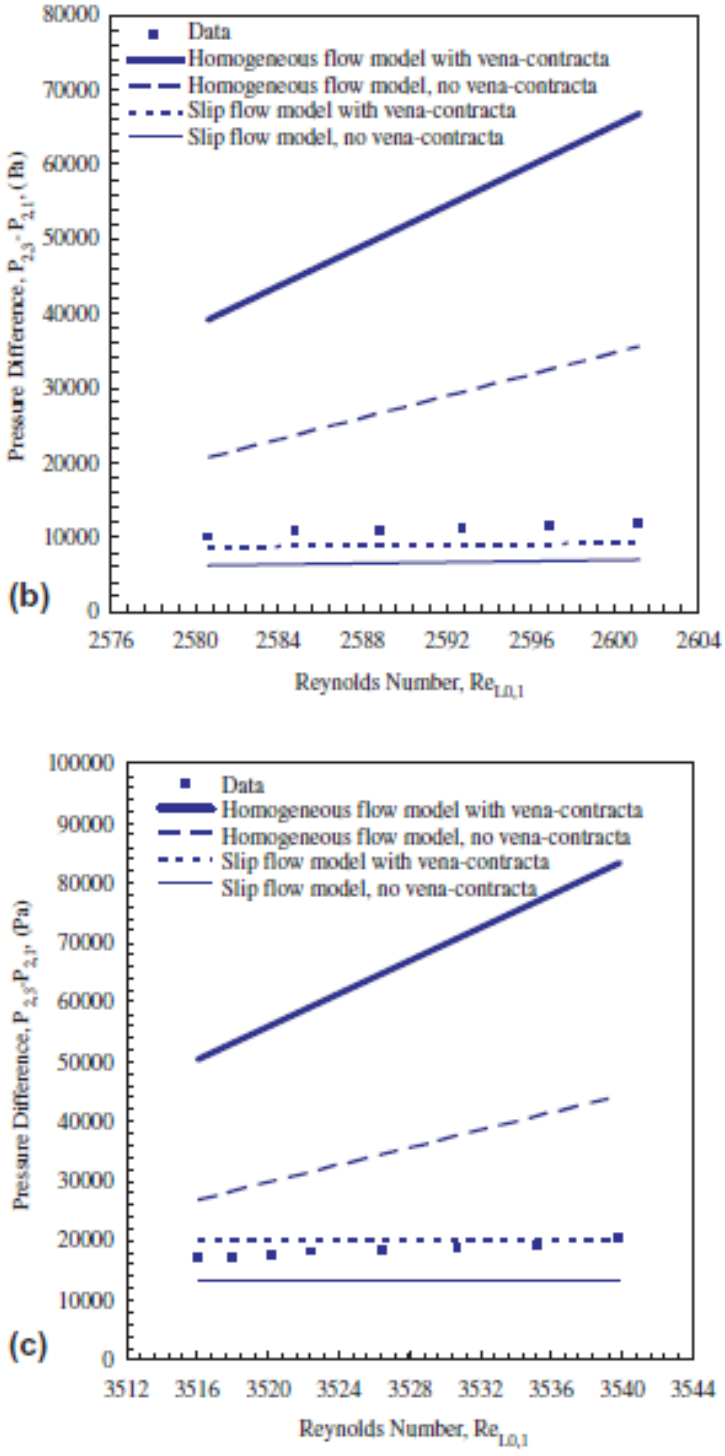

Figure 3: The two phase flow pressure difference vs Re in sudden contraction from Yoda data result [1]

Four difference of the prediction model were used for the pressure drop in Figure 3. The homogeneous flow model with vena contracta which Eq. 2.33 - Eq. 2.36 were applied. The prediction from the homogeneous model was far from the experimental data. The homogeneous model without vena contracta result predicated by applying Eq. 2.33 - Eq. 2.35 with C_C= 1. The prediction were even not close to the experimental pressure drop data whatever lower or higher Reynolds number. The slip ratio with or without vena contracta consideration could receive the rough agreement with Reynolds number lower than 1800. Therefore, the good pressure drop prediction of Reynolds number from 2580 to 3540 occurred only the vena contracta was accounted in slip flow model. The pressure drop pattern was agreed perfectly when the range of Reynolds number from 2580 to 2600.

2.3 Minor loss coefficient

In this experiment, each test section length was considered as the short pipe length, so major loss was neglected in the experiment. Due to change velocities and flow fluid accelerations in the geometrical construction of channels when fluid flow through them, the minor loss occurred and considered into the loss calculation was needed.

2.3.1 Single phase in expansion channels

To estimate the minor loss coefficient (k), the application and derivation of the general energy equation is necessary. The energy equation can be written as:

$$\frac{P_1}{\rho_1 * g} + \frac{{v_1}^2}{2 * g} + z_1 + h_{pump} = \frac{P_3}{\rho_3 * g} + \frac{{v_3}^2}{2 * g} + z_3 + h_{turbine} + h_{loss} \quad (2.38)$$

Assuming there are no additional work done by and into pumps and turbines in the system. The flow fluid is under incompressible which density is going to remain constant everywhere.

The test sections are under level condition, no elevation head generates at this time. The equation becomes:

$$\frac{P_1}{\rho * g} + \frac{{v_1}^2}{2 * g} = \frac{P_3}{\rho * g} + \frac{{v_3}^2}{2 * g} + h_{loss} \tag{2.39}$$

The pressure difference can be found as:

$$\Delta P_{1,3} = \frac{\rho * ({v_3}^2 - {v_1}^2)}{2} + \rho * g * h_{loss} \tag{2.40}$$

Minor head loss can be expressed as:

$$h_{loss} = k * \frac{{v_1}^2}{2 * g} \tag{2.41}$$

The single phase minor loss coefficient in expansion channels is united by pressure drop, fluid density, fluid velocity and area ratio which described in Yoda's [1] report. For determining the loss coefficient, the equation is going to be:

$$k_e = -\frac{2 * \Delta P}{\rho_L * v_L} - (\sigma^2 - 1) \tag{2.42}$$

However, the loss coefficient in the expansion channels also can be estimated in different methods. The parameters in this method are different. This loss coefficient is highly determined by the area ratio and momentum factor. The equation can be:

$$k_e = 1 - 2 * k_{d1} * \sigma + \sigma^2 * (2 * k_{d3} - 1) \tag{2.43}$$

Where k_d is momentum correction factor. Let k_{d1} and k_{d3} equals to one, the flat velocity profiles are generated the formula can be simplified into:

$$k_e = (1 - \sigma)^2 \tag{2.44}$$

2.3.2 Single phase in contraction channels

For determining the single phase minor loss coefficient in contraction channels, the formula of the loss coefficient in expansion should be changed the signs in the right side of the equation. The equation can be shown as:

$$k_c = \frac{2 * \Delta P}{\rho_L * v_L} + (\sigma^2 - 1) \tag{2.45}$$

Geiger [8] indicated the correlation between momentum factor (k_d) and kinetic energy factor (β), and loss coefficient. There are three known cases, for a laminar velocity profiles $k_{d2} = k_{d3}=1.33$, $\beta_1 = \beta_2 = 2$, for a turbulent flow but not completely uniform $k_{d2} = k_{d3}=1.1$, $\beta_1 = \beta_2 = 1.1$, the last one is uniform velocity profile $k_{d2} = k_{d3}=1$, $\beta_1 = \beta_2 = 1$. The equation will be:

$$k_c = (\sigma^2 - 1) + 2 * \left(k_{d3} - \frac{k_{d2}}{C_C}\right) + \left(\frac{\beta_2}{{C_C}^2} - \beta_1 * \sigma^2\right) \tag{2.46}$$

The loss coefficient in Kays [15] proposed that the fluid flow in the abrupt contraction channels always faces the vena contracta situation. In this case the uniform velocity assumption is made. Therefore, the loss coefficient formula becomes as:

$$k_c = (1 - \frac{1}{C_C})^2 \tag{2.47}$$

where C_C is used from the correlation of Geiger's [8] thesis. (Eq. 2.9)

Toufik et al [16] mentioned that under low values of Reynolds numbers, the loss coefficient can be estimated natural log of the Reynolds numbers themselves. The equation shown as:

$$k_c = 0.0588 * \ln(Re) + 0.0218 \tag{2.48}$$

2.4 Nitrogen and water phase flow in different circular channels

In order to verify the effect of channel diameter on adiabatic two-phase flow characteristics in microchannels, Chung and Kawaji [17] and Chisholm [18], conducted experiments with a mixture of nitrogen gas and water in circular channels of 530, 250, 100, and 50 μm in diameter. Chung and Kawaji [17] clarified the flow characteristics of 530 and 250 μm channels were similar to the microchannel ≈ 1 mm diameter as described by Triplett et al [19]. Yet in the 100, and 50 μm channels, turbulence flow did not be generated due to the effect of surface tension and liquid viscosity in the channels. However, Chung and Kawaji [17] built a predicable model based on Darcy–Weisbach equation, Blasius formula, the Armand [20] correlation, etc. Figure 4 and 5 represented the model of the 50 μm channel appeared a good prediction than the 100 μm because of the absence of the multiple flow pattern in 50 μm channel.

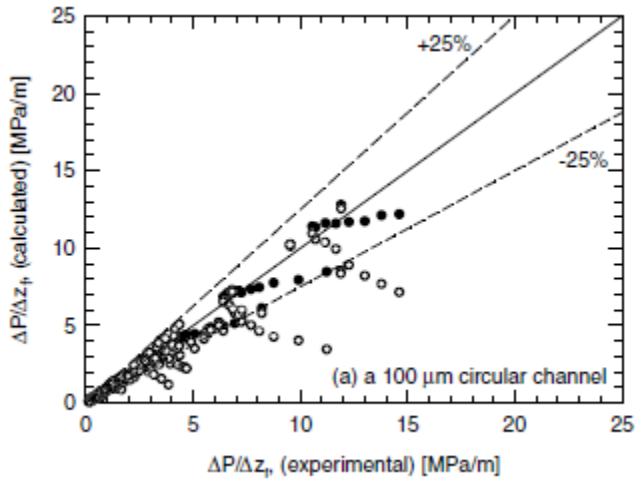

Figure 4: Comparison of model predictions with experimental results for the two-phase pressure drop in microchannels in 100 μm channel. ●: using experimental void fraction ○: using void fraction from the Armand [20] correlation [17].

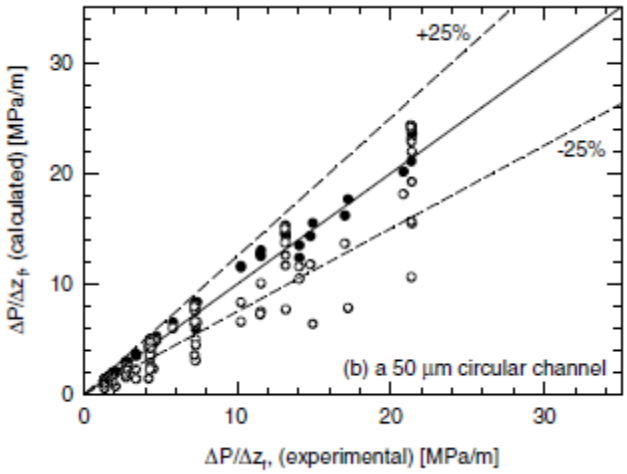

Figure 5: Comparison of model predictions with experimental results for the two-phase pressure drop in microchannels in 50 μm channel [17].

2.5 Oil and water phase flow performance in contraction and expansion

Without phase change in microchannel as discussed above, nothing more than focusing on phase frictional pressure drops and thermal resistance effects and superficial surface roughness behavior and heat transfer coefficients, and geometrical channel shape were quite different from the conventional correlations. However, these acquaintances had been obtained on multi-phase flow in microchannel. Ching-Yi J. Hwang and Rajinder Pal [21], two phase oil and water application also discussed in Pal studying [22] and the pressure drop obtained from resistance loss method was referred by Sookprasong [23], experimentally measured the pressure drop along the circular stainless steel pipes which the two-phases flow went through sudden expansions and contractions. The inner diameters of the pipe were 0.802 and 1.624 inches, and the oil and water mixture were tested on the examination. The obtained pressure profiles was used for evaluating the pressure loss data furthermore, the loss coefficients were collected from the pressure loss and velocity data. Figure 6 illustrated the frictional loss in the upstream and downstream pipes

accompany with the performance of the pressure drop. While the flow compassed the transitional region, the pressure was abrupt by increased.

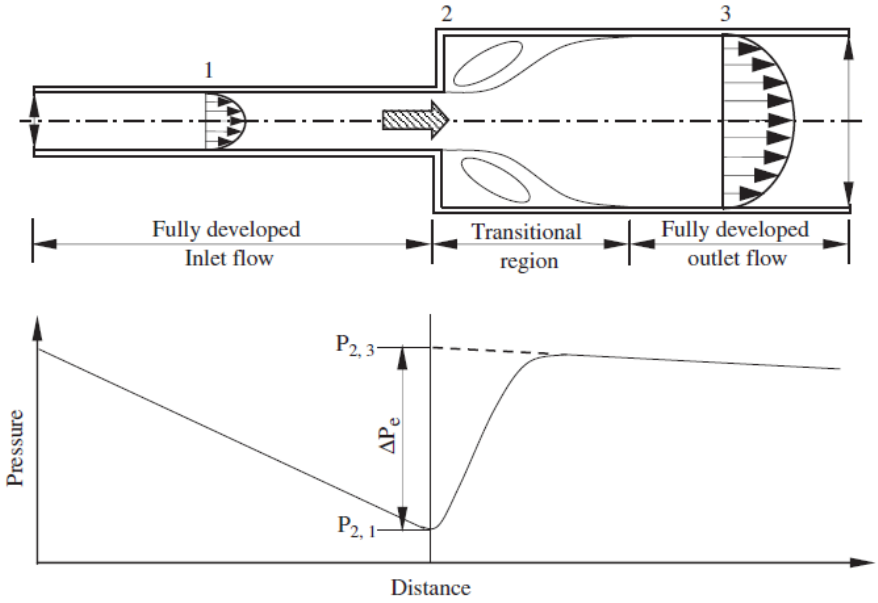

Figure 6: Pressure profile for a sudden expansion [21].

The concentration of oil was an observation point that the authors focused on it. It depended on the proportion of the oil concentration, either oil in water or water in oil emulsion, was flowing through the pipe. The volume fraction of oil in the emulsion control the behavior of pressure drop Figure 7 showed the pressure profile was different before and after the expansion and also various by changing volume fraction. However, the behave comparison of oil in water and water in oil emulsion was quite similar in the experiment, Figure 8 represented the pressure profiles for water in oil emulsion [21].

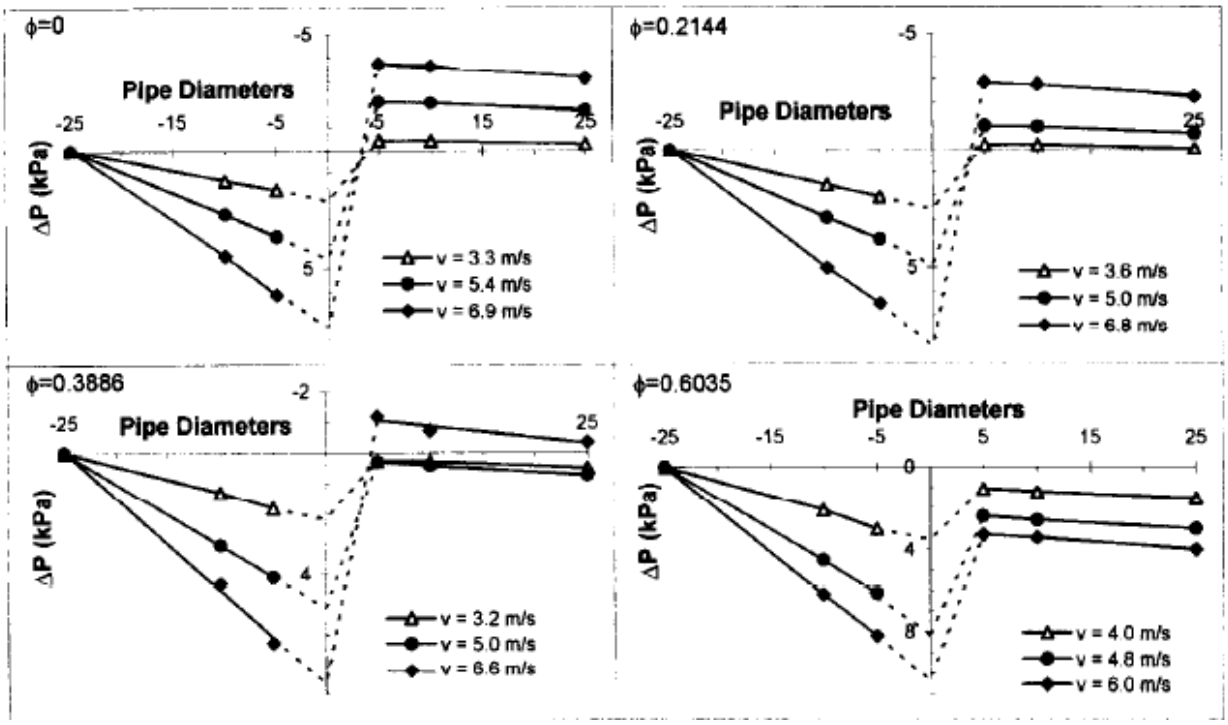

Figure 7: Pressure profiles for oil-in-water emulsions in a sudden expansion [21].

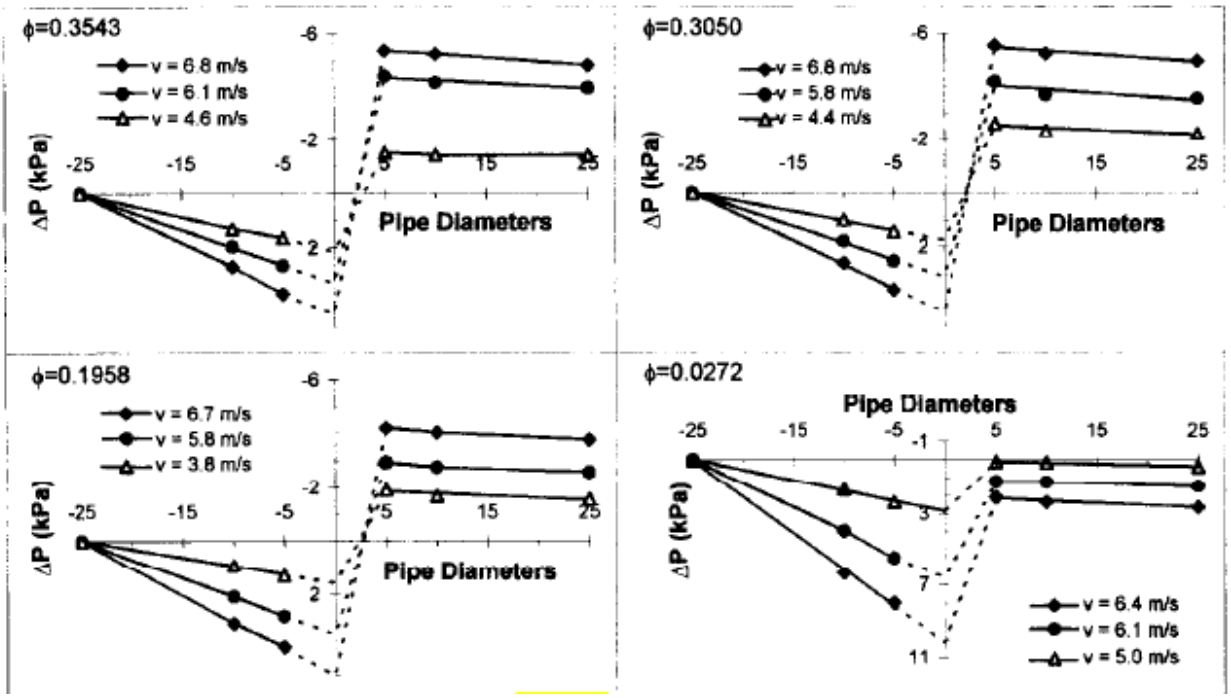

Figure 8: Pressure profiles for water-in-oil emulsions in a sudden expansion [21].

The loss coefficient were insignificant on both the emulsions flowing through expansions or contractions. The range of loss coefficient, K_e were around 0.4 to 0.6 in the emulsions flowing through expansions. Figure 9 demonstrated, no matter what, the emulsions flowing through contractions had found different values of pressure drop and loss coefficient, but the behavior of these two factors were similar.

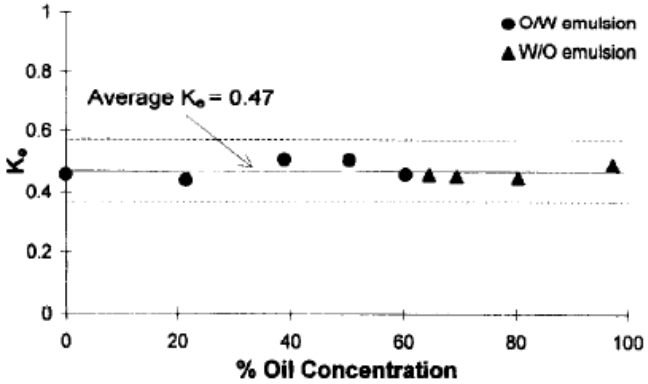

Figure 9: Expansion loss coefficient as a function of oil concentration [21].

2.6 Two phase flow in circular and semi-triangular channels

In the same year, K.A. Triplett et al. [24], about upward liquid flow observation was referred by Oya [25] and air-water phase flow in narrow channel concept was considerred from Fouran and Bories [26] conducted experiments on air-water two-phase flow in microchannels. The flow patterns, transition boundaries, void fraction and pressure drop were reported in the investigation. Two types of the microchannels had been used, the one was circular microchannels with 0.0433 and 0.0570 inches inner diameters. The other was semi-triangular microchannels with 0.0429 and 0.0586 inches. No surprise, bubble flow, slug flow, churn flow, and annular flow were the flow patterns in the test sections. Yet, these flow regimes for these two types of microchannels were very similar from slug to slug-annular flow patterns.

K.A. Triplett et al. [19], frictional pressure drop calculation method notation was referred by Beattie and Whalley [27] and performance of the two phase flow concept was referred by Chen and Spedding [28] also reported that in the bubble and slug flow regimes, and high Reynolds number, the predictions of experimental data were quite precise, therefore, in the slug-annular and annular flow patterns, and low Reynolds number of slug low would come out significant deviations result. Figure 10 expressed the result of pressure drops normalization.

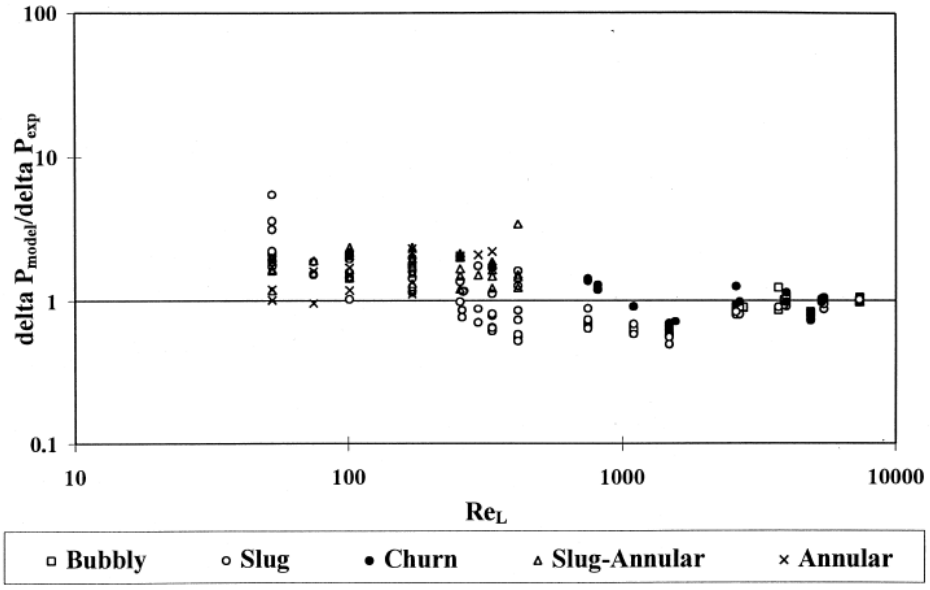

Figure 10: Model-predicted pressure drops normalized with experimentally-measured pressure drops [19].

2.7 Flow regimes and bubbles

Two years late, in order to understand these knowledge thoroughly in two-phase minichannels, flow regime pattern identification, transition criteria, void fraction and interfacial concentration are priority for consideration. Xu et al. [29], modeling flow pattern in for two phase flow in the tubes was referred by Taitel [30] and Flow regime transition concept was from Mishima [31] in Xu et al. [29] report, conducted adiabatic experiments in a vertical rectangular channels with narrow gaps of 0.3, 0.6 and 1.0 mm. The experiment illustrated flow regimes cap-bubbly flow, slug-droplet flow, churn flow and annular-droplet flow are normally occurred in the narrow small gap 0.3 or less due to the small bubbles squeezing and merging with each other. Yet, the flow regimes were converted and dominated by bubbly flow, slug flow, churn-turbulent flow in the channels with medium size gaps as the gaps of 0.6 and 1.0 mm. Figure 11 represented the flow regimes in 0.3 mm channel. Figure 12 presented the flow regimes in the channels with medium size gaps as the narrow gaps of 0.6 and 1.0.

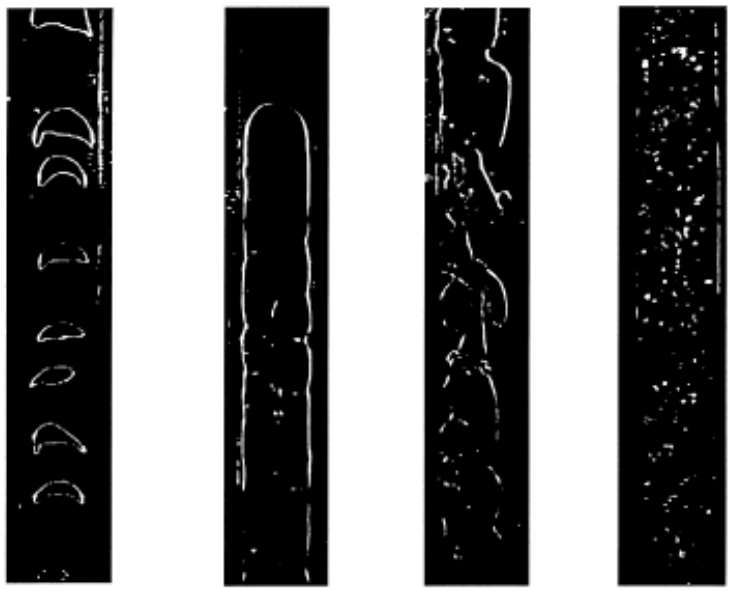

(a) cap–bubbly flow; (b) slug–droplet flow; (c) churn flow; and (d) annular–droplet flow.

Figure 11: Flow regimes in 0.3 mm channel *[29]*.

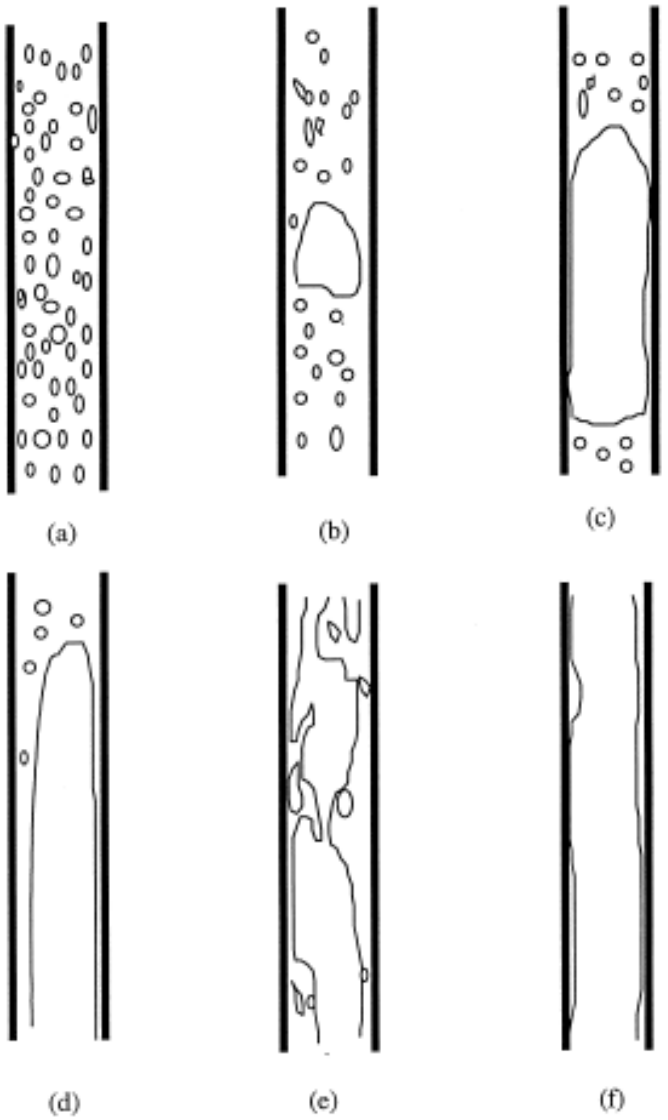

(a) bubbly flow; (b) cap–bubbly flow; (c) slug flow; (d) slug–churn flow; (e) churn–turbulent flow; (f) annular flow.

Figure 12: Flow regimes in channels with medium size gaps [29].

This experiment also found that the flow regimes would be small in gas velocity- liquid velocity diagram since the gap channel decreased and friction shear stress increased. The authors also reported that bubbly flow appeared only in the gap channel which was greater than 0.3 mm the different flow would develop when the gap channel smaller than 0.3 mm [29].

2.8 Fins or channels effect

Knight et al. [32] entirely optimized the microchannel experimental application from three published researches, this studying in single phase heat transfer portion was referred by Kakac and Aung [33]. In the first case, the comparison of Knight et al [32]. research to Tuckerman and Pease [34] was practiced. The Table 1 indicated that all dimensions were remained same except the values of the ratio of fin thickness to channel width, laminar friction factor, and Nusselt number depends on the ratio of the hydraulic diameter to the fluid thermal conductivity and the state of the flow development. No matter what, the optimal channel and fin dimensions were found by the conditions mentioned above and the thermal resistance is reduced by 35% from that of Tuckerman and Pease.

Table 1 : Comparison of Knight et al. result to the work of Tuckerman and Pease [32].

	Tuckerman and Pease	*Present Study*
CONSTRAINTS		
Size, Length (L) by Width (W)	1 cm × 1 cm	same
pressure drop, Δp	206.8 kPa	same
% infinite fin performance, β	76%	unrestricted
Fin length, μm	unrestricted	365
Coolant	water	same
Prandtl number, Pr	3.77	same
Fin Material	Silicon	same
$k_{\text{fluid}}/k_{\text{fin}}$	0.00464	same
Fin to channel thickness ratio, Γ	1	unrestricted
Nusselt Number	6	unrestricted
Type of flow	laminar	laminar or turbulen
γ_1, laminar friction factor	96	not applicable
DIMENSIONLESS GROUPS		
L/W	1	same
Maximum $N_{\Delta p}$	2.82×10^{10}	same
Maximum N_{work}	3.62×10^{13}	unrestricted
CALCULATED RESULTS	Laminar	Turbulent
n, number of channels	88	22
Depth, D, μm	365	365
Fin to channel width ratio, Γ	1	0.215
Fin thickness, μm	57	81
Channel thickness, μm	57	377
Reynolds Number	730	8459
Volumetric Flow Rate, cm^3/s	11	59.2
Aspect Ratio, α	6.4	0.97
Nusselt Number	6	85.6
Laminar friction factor γ_1	96	not applicable
$N_{\Delta p}$	2.82×10^{10}	2.82×10^{10}
N_{work}	3.62×10^{13}	1.95×10^{14}
Capacity Thermal Res, °C/W	0.022	0.006
Convective Thermal Res, °C/W	0.064	0.050
Total Thermal Resistance, °C/W	0.086	0.056
Change in Thermal Resistance, $\Delta\Theta$		35%

The relationship among number of channels and thermal resistance with various ratio of fin thickness to channel width shown in Figure 13. The dashed line in the laminar regime with ratio of fin thickness to channel width, equals to one, has the best value of number of channels around 88 [32]. The optimal ratio of fin thickness to channel width in the laminar regime was 0.32 expressed as the solid line. However, the plot demonstrated the lowest thermal resistance occurred in turbulent regime when the ratio of fin thickness to channel equals to 0.215 as the solid line shown. The optimal number of channels under this situation was around 22.

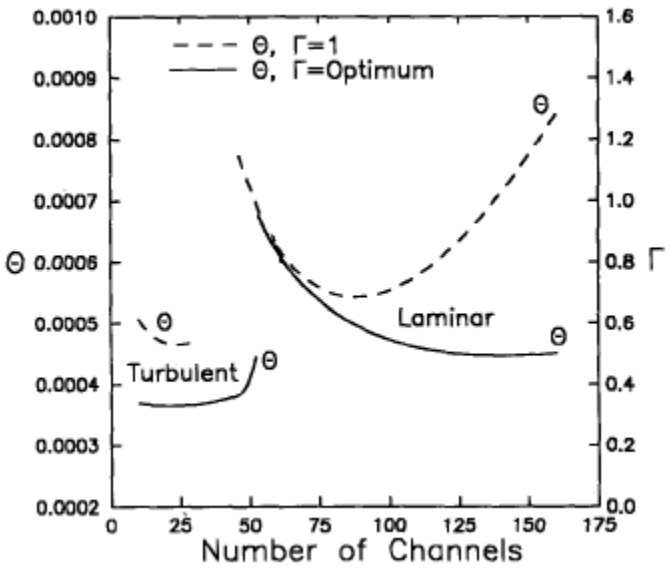

Figure 13: Thermal resistance as a function of the number of channels for the heat sink described in Table 1 [32].

In the secondary case, they remained the dimension of heat sink same but ratio of fin thickness to channel width, aspect ratio, flow regime and volumetric flow rate were flexible compared to the studying of Goldberg [35]. The optimal comparison result between Goldberg and Knight et al. shown on the Table 2 below. The optimal result happened only on two situations in which the pressure drop is same or the power consumed is equally.

Table 2: Comparison of Knight et al. result to the work of Goldberg [32]. n: Number of cooling channels, Γ: Ratio of fin thickness to channel width, ΔΘ: Improvement in thermal resistance.

	Researcher	n	Γ	Δp kPa (in H_2O)	$\dot{w}$, Watt	$\dot{V}$, liter/min	$\Delta\Theta$
Case I (Goldberg's $\ell = 0.127$ mm)	Goldberg	25	1	1.17 (4.68)	0.583	30	—
	Present Study same Δp	24	0.435	1.17 (4.68)	1.747	89.9	32.4%
	Present Study same $\dot{w}$	20	0.390	0.73 (2.92)	0.583	48.2	15.4%
Case II (Goldberg's $\ell = 0.254$ mm)	Goldberg	12.5	1	0.29 (1.17)	0.146	30	—
	Present Study same Δp	18	0.315	0.29 (1.17)	0.239	49.2	18.4%
	Present Study same $\dot{w}$	20	0.390	0.26 (1.06)	0.146	32.8	11.4%
Case III (Goldberg's $\ell = 0.635$ mm)	Goldberg	5	1	0.047 (0.19)	0.024	30	—
	Present Study same Δp	12	0.250	0.047 (0.19)	0.018	22.4	38.6%
	Present Study same $\dot{w}$	15	0.320	0.075 (0.30)	0.024	19.1	46.2%

Table 3 represented the comparison of Knight et al [32]. result to the work of Phillip [36]. In this case, Knight et al. [32], however, increased almost the twice number of channels and reduced the ratio of fin thickness to channel width to 0.66 given the improvement result decreasing the thermal resistance to 21 percent. The above cases illustrated that without the needless and useless limitation, for example to constrain the state of flow in laminar regime, brought the remarkable thermal resistance performance in heat sink applications.

Table 3: Comparison of Knight et al. result to the work of Phillip [32].

	Phillips	*Present Study*
CONSTRAINTS		
Size, Length (L) by Width (W)	1 cm × 1 cm	same
pressure drop, Δp	68.9 kPa	same
Aspect Ratio	4.0	unspecified
Fin Length, microns	unspecified	1889
Coolant	water	same
Fin Material	Silicon	same
Fin to channel thickness ratio, Γ	1	unrestricted
Nusselt Number Correlation	(37)	same
Type of flow	laminar or turbulent	same
DIMENSIONLESS GROUPS		
L/W	1	same
Maximum $N_{\Delta p}$	8.86×10^9	same
Maximum N_{work}	1.45×10^{14}	same
CALCULATED RESULTS		
n, number of channels	11	19
Depth, D, μm	1889	1889
Fin to channel width ratio, Γ	1	0.66
Fin thickness, μm	472.1	215
Channel thickness, μm	472.1	323
Volumetric Flow Rate, cm^3/s	145	145
$N_{\Delta p}$	8.86×10^9	8.86×10^9
N_{work}	1.45×10^{14}	1.45×10^{14}
Capacity Thermal Res, °C/W	0.0016	0.0016
Convective Thermal Res, °C/W	0.064	0.049
Total Thermal Resistance, °C/W	0.066	0.052
Change in Thermal Resistance, $\Delta\Theta$		21%

The small rectangular channels having hydraulic diameters of 0.133 – 0.367 mm and unique geometric configurations were investigated in the single-phase convective heat transfer and flow friction studying of Peng and Peterson [37], about behavior of the fluid flow through the small channels was referred by Pfahler et al. [38]. Peng and Peterson further demonstrated the

geometric configuration is a significant factor in their studying. The working fluid was water, moreover, the stainless steel was used in the microchannel structure rather than fused silica which used in Tuckerman and Pease studying. There were twelve different geometric configuration setup shown as Table 4 below.

Table 4: Geometric parameters of the test sections [37]. W: Width of microchannel,
W_c: Center-to-center distance of microchannel,
W_t: Width of rnicrochannel structure,
D_h: Hydraulic diameter,
Z: Dimensionless variable ($\frac{\text{Min(H,W)}}{\text{Max(H,W)}}$),
$C_{f,l}$: Coefficient for laminar flow friction,
$C_{f,t}$: Coefficient for turbulent flow friction

Plate	W [mm]	W_c [mm]	W_t [mm]	L [mm]	H [mm]	D_h [mm]	D_h/W_c	H/W	Z	$C_{f,l}$	$C_{f,t}$
1	0.4	4.5	18	45	0.2	0.267	0.0593	0.5	0.5	28 600	40 400
2	0.4	2.8	18	45	0.3	0.343	0.1225	0.75	0.75	44 800	34 200
3	0.4	2.0	18	45	0.3	0.343	0.1715	0.75	0.75	44 800	34 200
4	0.3	4.6	18	45	0.2	0.24	0.0533	0.667	0.667	42 600	18 200
5	0.3	2.8	18	45	0.3	0.30	0.107	1.00	1.00	109 000	38 600
6	0.3	2.0	18	45	0.3	0.30	0.15	1.00	1.00	109 000	38 600
7	0.2	4.5	18	45	0.2	0.20	0.0444	1.00	1.00	32 400	20 100
8	0.2	2.8	18	45	0.3	0.24	0.0857	1.50	0.667	42 600	18 200
9	0.2	2.0	18	45	0.3	0.24	0.12	1.50	0.667	42 600	18 200
10	0.1	4.5	18	45	0.2	0.133	0.0296	2.0	0.50	5200	1820
11	0.1	2.8	18	45	0.3	0.15	0.0536	3.0	0.333	24 200	6920
12	0.1	2.0	18	45	0.3	0.15	0.075	3.0	0.333	24 200	6920

The aspect ratio and the ratio of the hydraulic diameter represented a significant heat transfer effect in the laminar regime. Therefore, the heat transfer in turbulent regime was indicated to and the ratio of the hydraulic diameter and a new dimensionless variable, Z. The friction factor or flow resistance reached a minimum value as Z = 0.5. Comparing Figure 14 and 15, it is obvious to recognize that the geometric configuration is definitely a significant element in the minimizing friction factor no matter in the laminar or turbulent flow. There results indicated that laminar and turbulent flow resistance was usually smaller than that predicted by classical relationships, and the Reynolds number for flow transition to fully developed turbulent flow became much smaller than

the ordinary channel flow. Empirical correlations were suggested for calculating both the heat transfer and pressure drop.

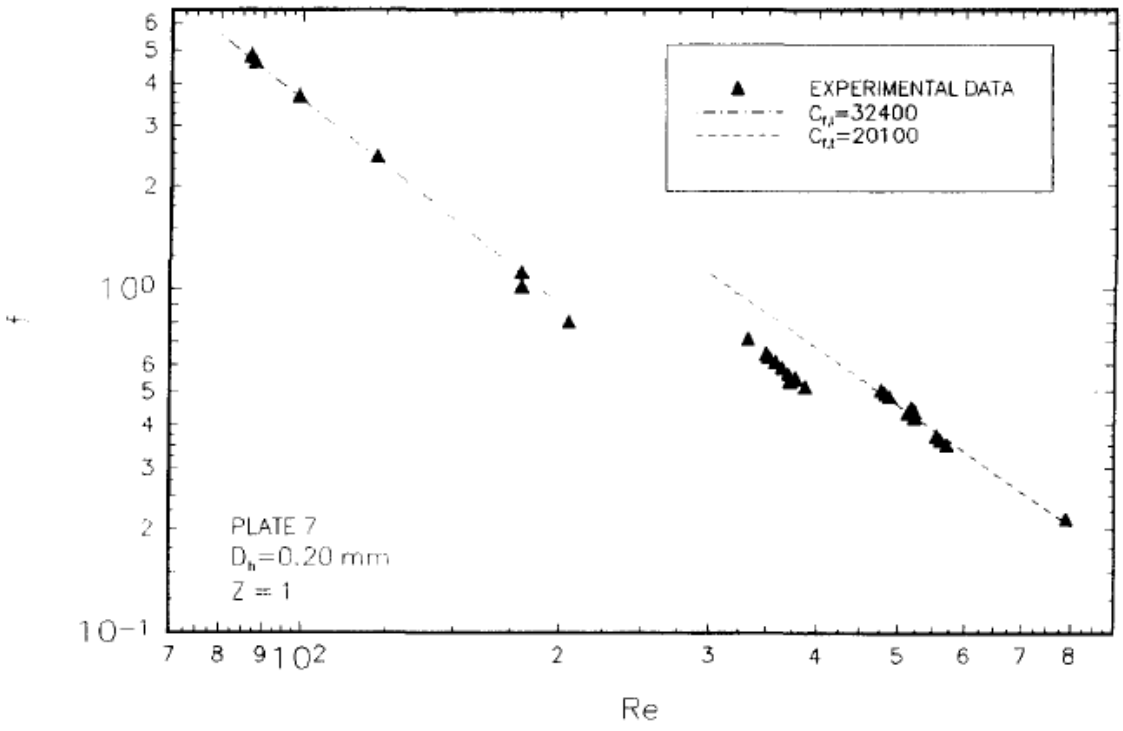

Figure 14: Friction factor of plate 7 [37] refers to Table 4.

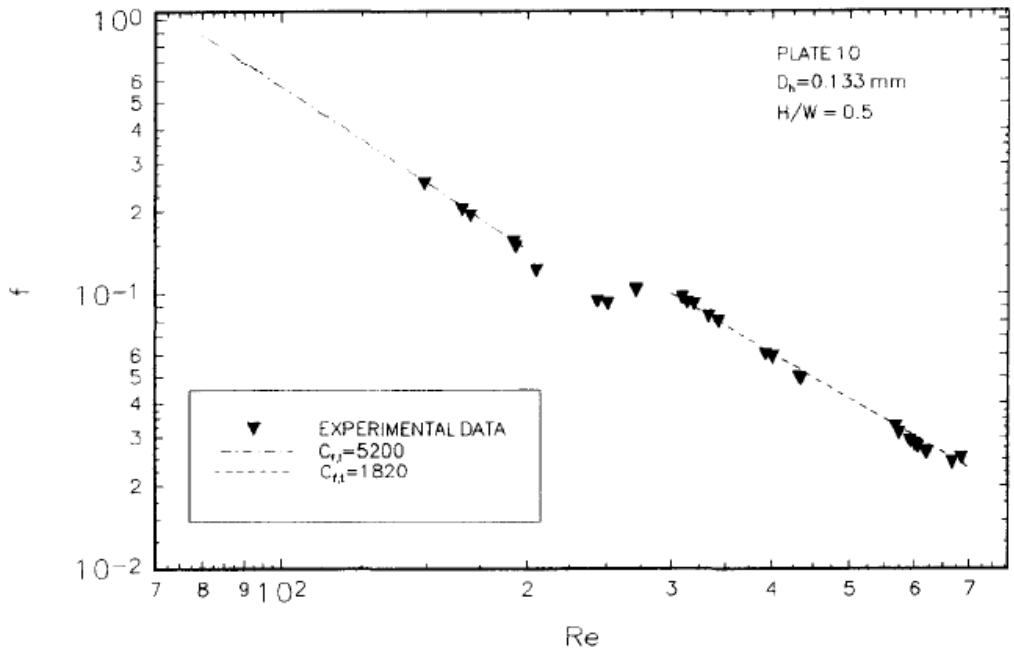

Figure 15: Friction factor of plate 10 [37] refers to Table 4.

2.9 Reynolds number and pressure difference

Mala and Li [39], the concept of liquid and gas transport in small channels referred by Pfahler et al. [40],experimentally tested two types of circular microchannels or microchannels that made in stainless steel and fused silica, furthermore the range of the diameters used in the studying from 50 to 254 µm. It is well known the critical Reynolds number is for transition from laminar to turbulent flow. The critical Reynolds number is about 2300 under the some certain condition. However the studying indicated the critical Reynolds number is affected by external disturbances. In other words, as long as the flow remain undisturbed, the critical Reynolds number could be very large values unless the flow keeps laminar regime. Yet turbulent flow could be occurred for the Reynolds number in small values Figure 16 clearly illustrated the pressure gradients of the fused silica channels are larger than the stainless steel channels. Moreover, the higher pressure gradient occurred at smaller diameter channels, rather than larger diameter channels. However, the plot also demonstrated the classical theory is less significant when the channel diameter is getting larger.

This experiment looks like that the tests were under the laminar regime due to the Reynolds number less than 2100 but the pressure drops between the experimental results and theory are so different could be an early transition from laminar to turbulent flow or the surface roughness effects on the channel flow. Figure 16 shows the comparison of the different Reynolds number regions with conventional laminar flow theory equation. Figure 16(a) roughly indicated the agreement between the experimental result and the theory, moreover Figure 16(b) represented the transition from laminar flow. Finally, Figure 17(c) demonstrated a fully developed turbulent flow was occurred in this region.

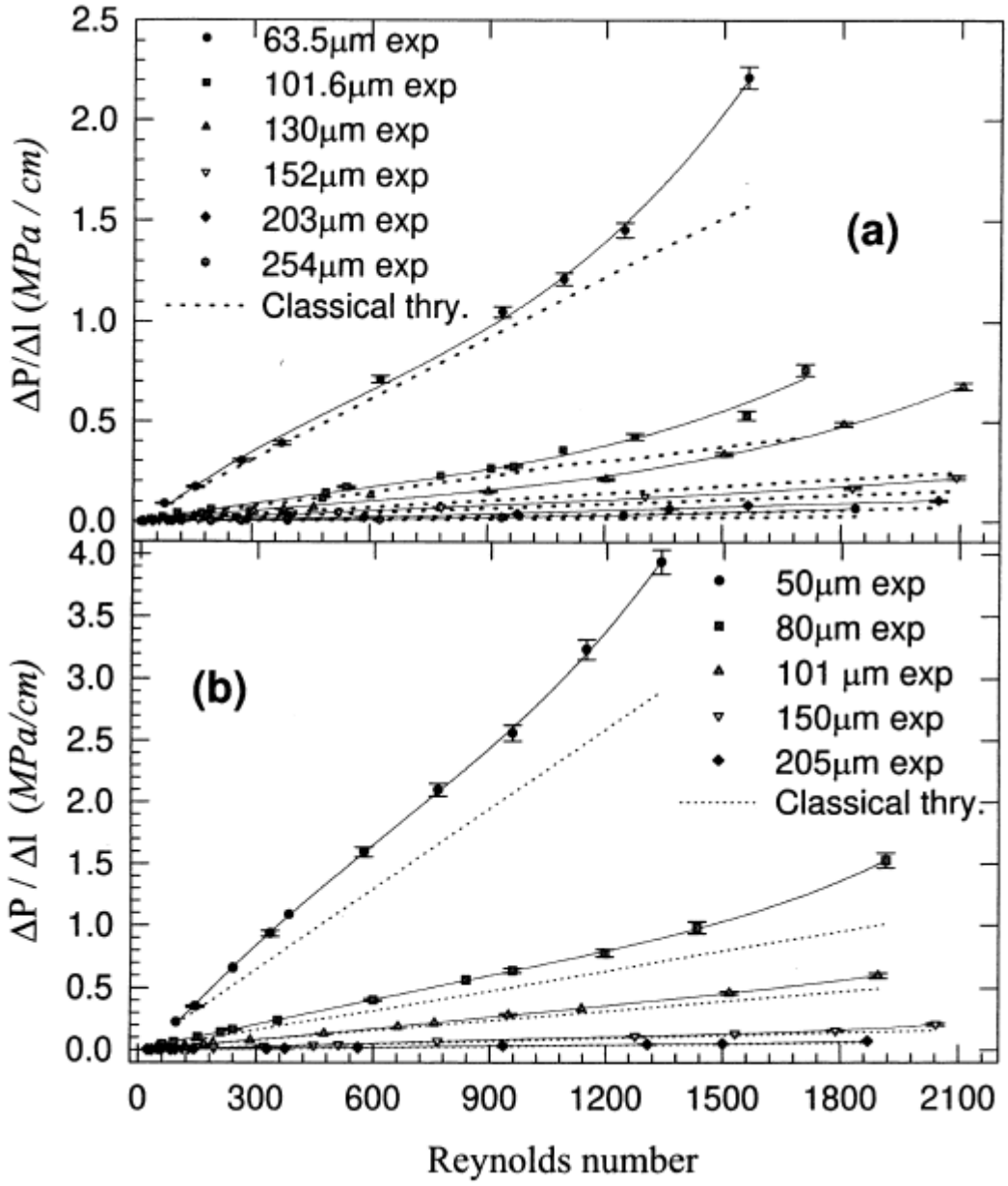

Figure 16: ΔP/Δl vs. Re for (a) Stainless steel (b) Fused silica channels and comparison with classical theory Poiseuille flow equation [39].

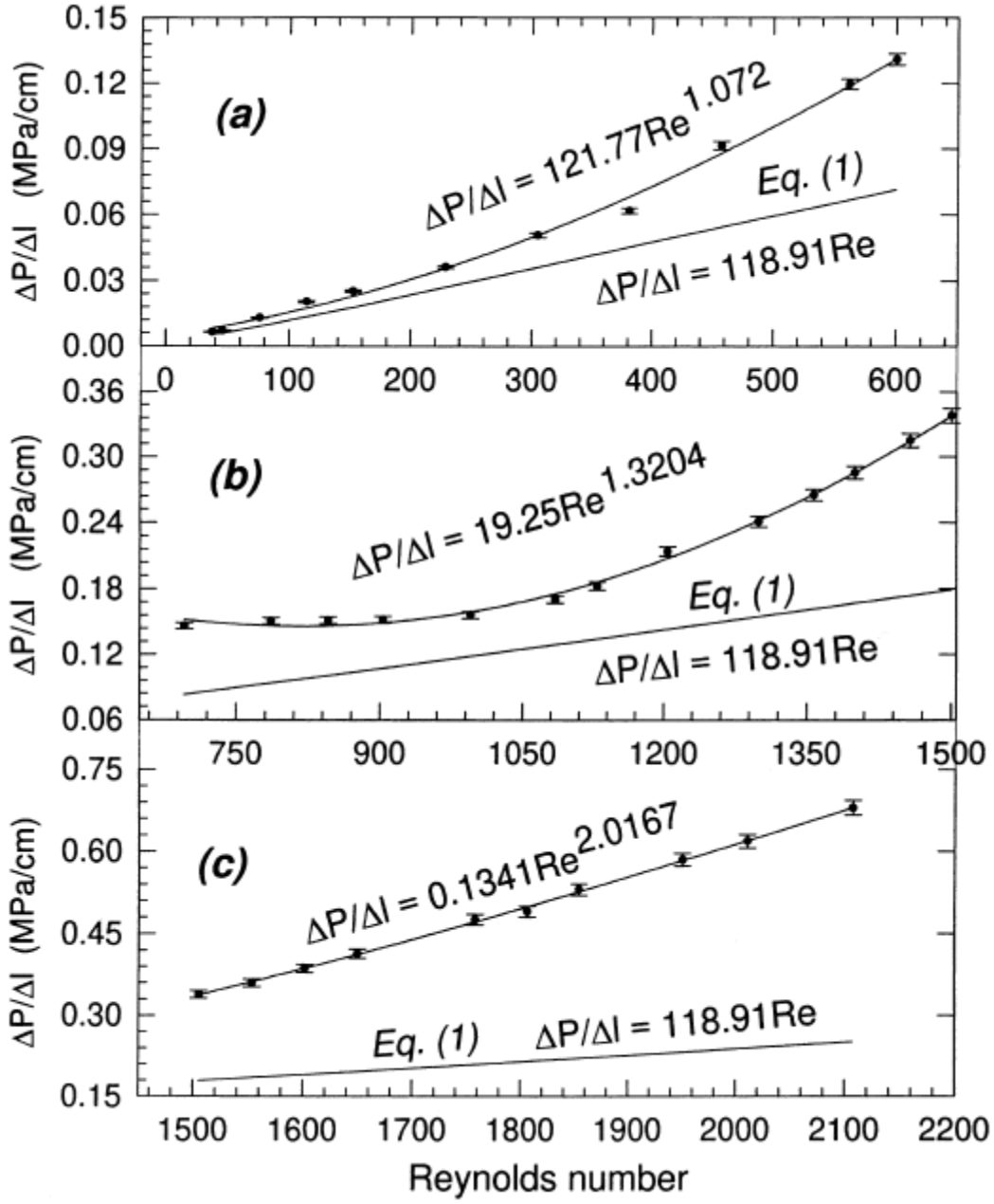

Figure 17: ΔP/Δl vs. Re for Stainless steel in three regions for 130 μm [39].

2.10 Friction factor and Reynolds number

From Figure 18, the experiment results were considered reasonable for the conventional theory in the region Ⅰ where might be laminar flow regime. Yet the region II, the range of Reynolds number from 500 to 1500 were regarded as a transition flow regime. The most difference between the experiment values and the theory curve in region III was discussed as fully developed turbulent flow. The friction factor was getting to a constant value gradually from the beginning of region III. However, Blasius equation curve matched the experiment data very well in the region III. The authors indicated the Blasius Equation gives the friction factor for turbulent flow in smooth pipes for Reynolds number $\leq 10^5$. Thus, Blasius Equation can be used to determine the friction factor in microchannels for Reynolds number $\geq$ 1500 with reasonable accuracy [39]. Figure 19 simply interpreted the ratio of roughness –viscosity is larger when it closes to the wall and approaches to zero when it closes to center of the microchannels. The fused silica microchannels with small size hold the higher roughness –viscosity ratio than the stainless steel channels. Apparently, the roughness-viscosity is proportional to Reynolds number the authors concluded it.

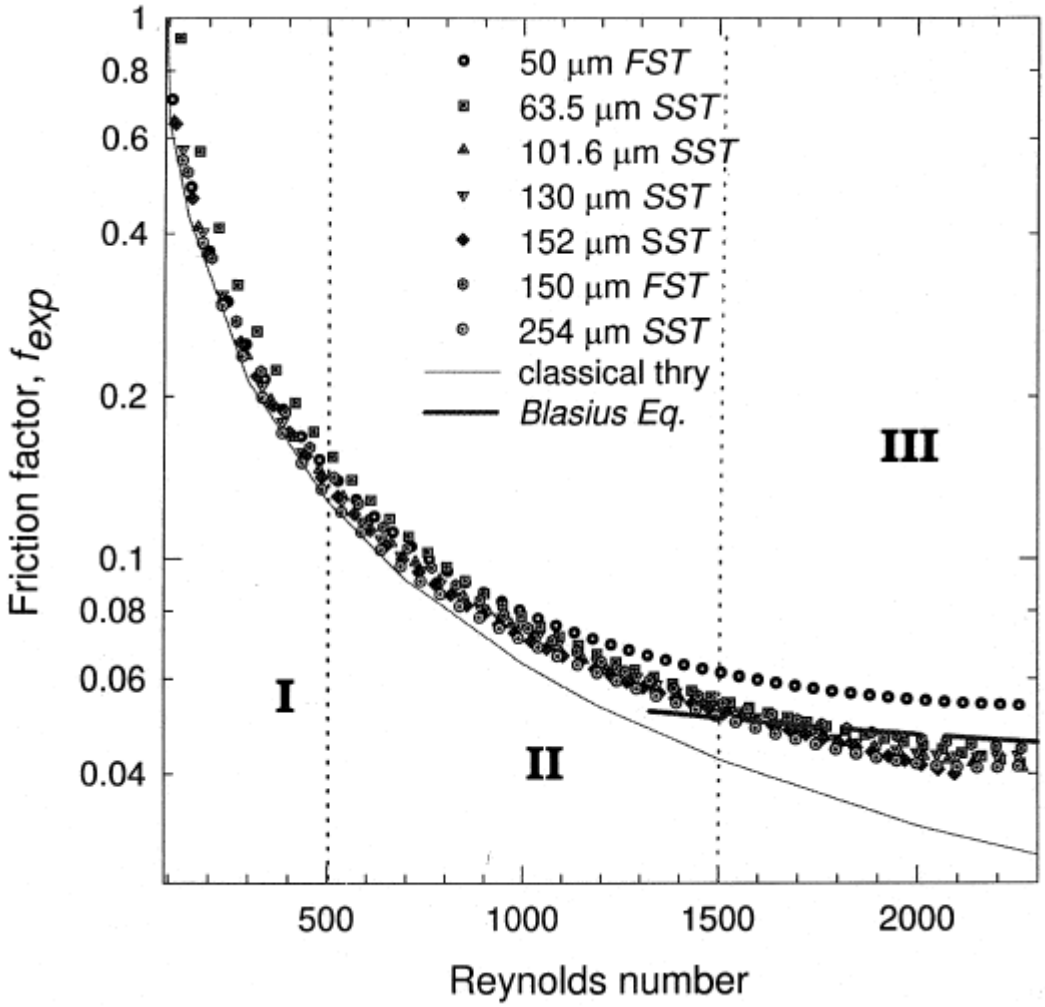

Figure 18: Friction factor vs. Reynolds number for stainless steel and fused silica microchannels and comparison with the classical theory and Blasius Eq. [39].

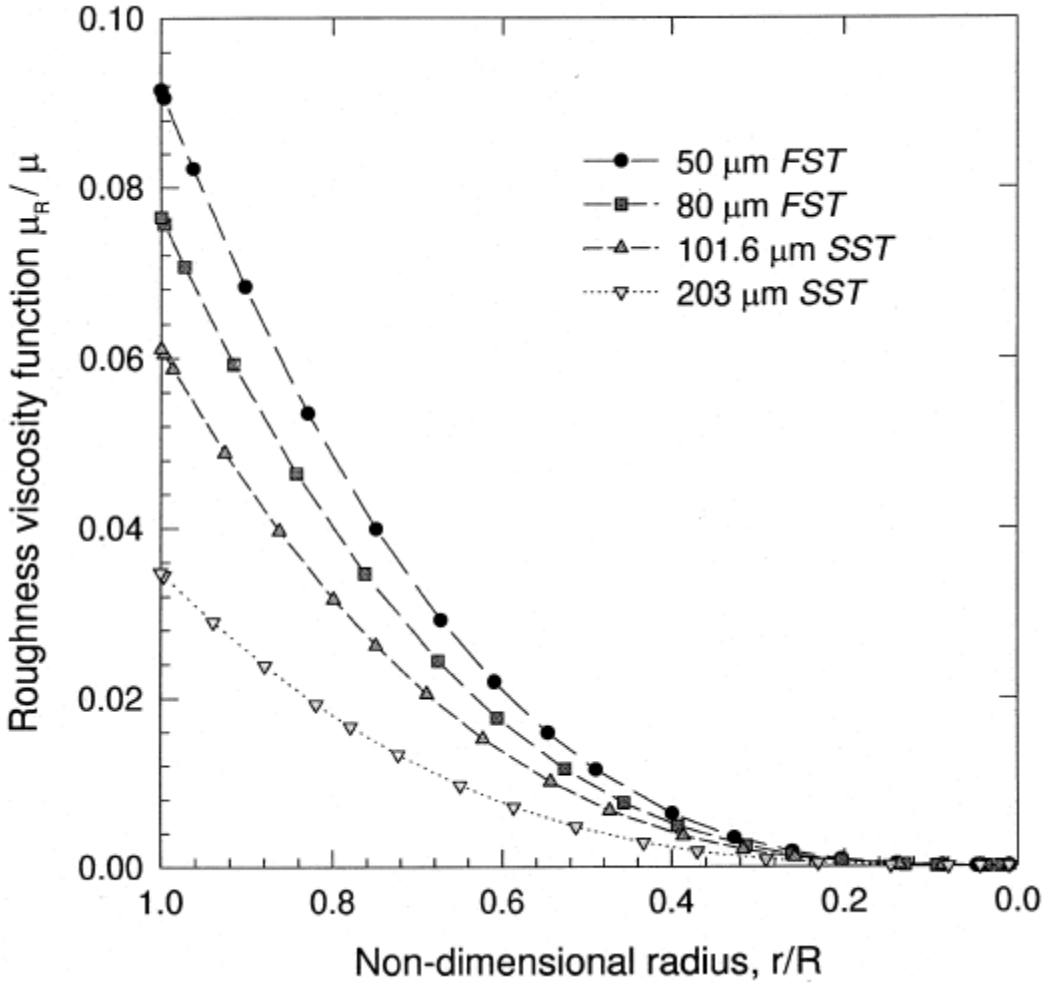

Figure 19: Variation of roughness-viscosity ratio with non-dimensional radius for some stainless steel and fused silica microchannels at Reynolds number 950.
r: Radial coordinate,
R: Radius of the microchannel,
μ_R: Roughness viscosity of water,
μ: Dynamic viscosity of water [39].

2.11 The performance of trapezoidal channels

Weilin et al. [41] conducted adiabatic experiments in trapezoidal silicon microchannels with a hydraulic diameter ranging from 51 to 169 mm, the general concept of the pipe flow was referred by Benedict [42] and laminar flow behavior in ducts was considered from Shah's studying [43]. In the experiment, six different geometric microchannels were tested and the volume flow

rate and the pressure drop across the microchannel were measured. The six various dimensions of the trapezoid showed on Table 5. The author concluded there were several factors could deviate the experiment result far from the theory. The one of the factors that the author indicated is the curve of experiment result of pressure gradient were always higher than the prediction at a given flow rate, especially the Reynolds number over 450 the experiment curve start to increase greatly. The comparison result showed on the Figure 20. Moreover, the flow friction was considered as the one of effects in the experiment. No surprising, again, the flow friction was higher than the theoretical prediction in the studying. A roughness viscosity model, which could have better agreements between the experimental result and theoretical outcome, is used to explain the effect of the surface roughness on laminar flow in microchannels. The Figure 21 demonstrated the improvement of deviation between theoretical result and experiment data by using roughness viscosity model.

Table 5: Types of the trapezoidal silicon microchannels [41].
a and b: Base of the trapezoid, h: Height of the trapezoid,
dh: Hydraulic diameter, k: surface roughness

Channel. No.	a (μm)	b (μm)	h (μm)	d_h (μm)	k (μm)
1	405.27	359.72	28.06	51.3	0.8
2	148.33	94.83	44.44	62.3	0.8
3	162.11	105.43	45.47	64.9	0.8
4	237.01	66.11	109.77	114.5	2.0
5	318.81	150.24	113.84	142.0	2.0
6	523.20	356.32	111.14	168.9	2.0

[a] Length of the microchemicals = 2.8 cm and number of microchannels per plate = 5.

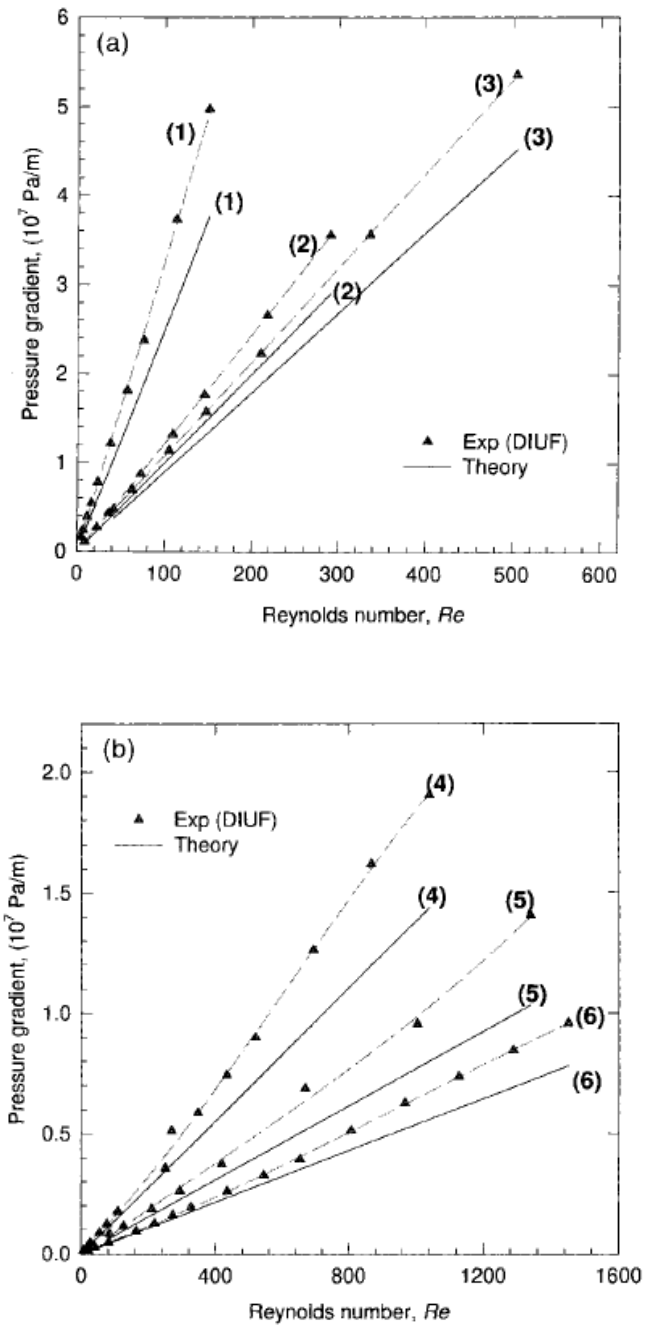

A comparison of the measured data of pressure gradient vs. Reynolds number with the predictions of conventional laminar flow theory. (a) (1) d_h = 51.3 μm; (2) d_h = 62.3 μm; (3) d_h = 64.9 μm; (b) (4) d_h = 114.5 μm; (5) d_h = 142.0 μm; (6) d_h = 168.9 μm.

Figure 20: The comparison of experiment result with predictions result in the chart of pressure gradient vs. Reynolds number [41].

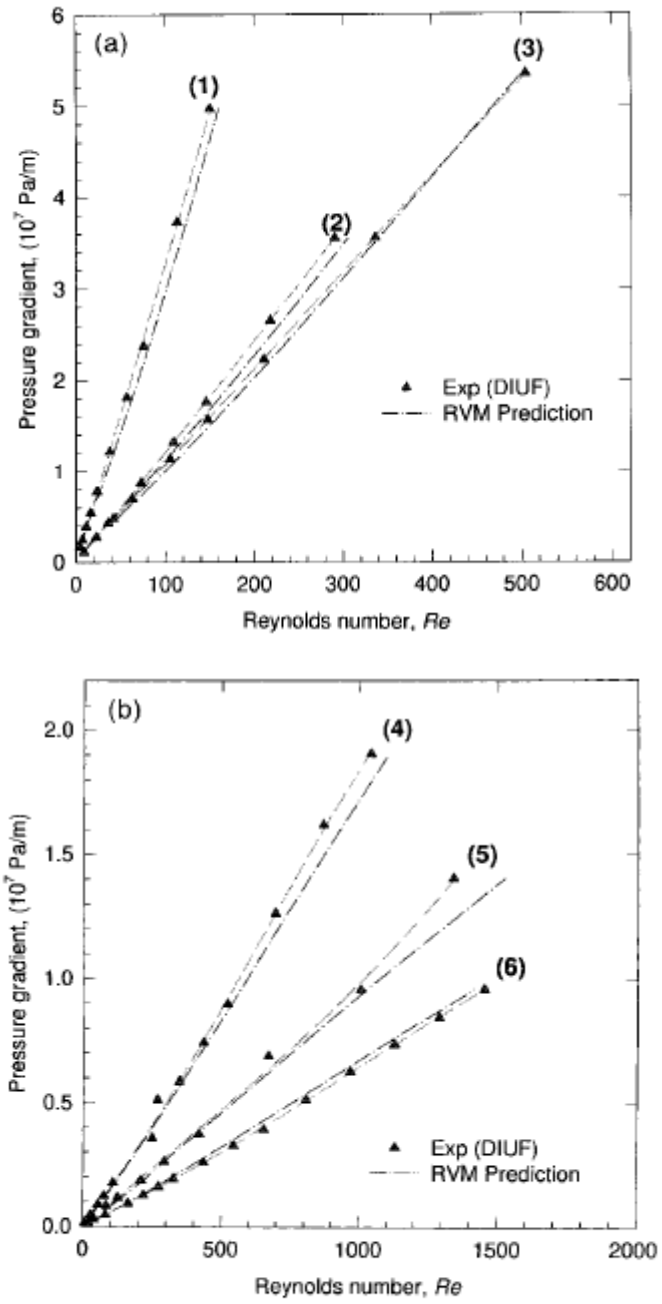

A comparison of experimental data of pressure gradient vs. Reynolds number with the predictions of the roughness-viscosity model: (a) (1) $d_h = 51.3$ μm; (2) $d_h = 62.3$ μm; (3) $d_h = 64.9$ μm; (b) (4) $d_h = 114.5$ μm; (5) $d_h = 142.0$ μm; (6) $d_h = 168.9$ μm.

Figure 21: The comparison of experiment result with predictions result in the chart of pressure gradient vs. Reynolds number with the roughness viscosity model [41].

2.12 Power density and channel width

The notion of the phase flow is not only studied and used in large-scale systems but also in small dimensional scale. Tuckerman and Pease [34] were the first who used heat transfer application in the mini-channel applied by single-phase flow the similar studying and test had done by Kay [44] [45]. The research successfully demonstrated single-phase forced convective cooling in microchannel, circuit power densities more than 1000 W/cm^2, is feasible to remove a power density of 790 W/cm^2 from a substrate temperature 71 °C above the input water. This exciting research result, as a landmark paper, widely expressed in this field, more single-phase flow researchers involved in this studying area. The relative research further developed and concentrated on optimization and analysis of single-phase flow in minichannel and microchannel. Goldberg [35] investigated three different channel widths, 5, 10, and 25 mils in his research. The air flow rate of 30 L/min was applied in these three heat sinks, the heat transfer performance was referred by Ozisik [46]. The limitation of this research were kept the flow in laminar regime and ratio of fin thickness to channel width equals to one. Unsurprised, the experiment result, match to the expectation, shown smallest channel width and largest pressure drop generated the smallest thermal resistance.

The report by Sasaki and Kishimoto [47] indicated that the channel width, finned heat sink constructed on a silicon chip, could be reduced while the cooling capability with a constant rate of coolant flow is increasing. Furthermore, the report shown channel cross-section is inversely proportional to the pressure drop from coolant inlet to outlet. Figure 22 shows the relationship between allowable power density and channel width. The report demonstrated the optimal channel widths could be 400 and 250 μm for a pressure drop of 200 and 2000 kg/m^2. The correlation between optimal channel width and cooling fin length shown in Figure 23. The plot illustrated

that the optimal channel width would be magnified once the pressure drop decreases in order to remain the fin length same.

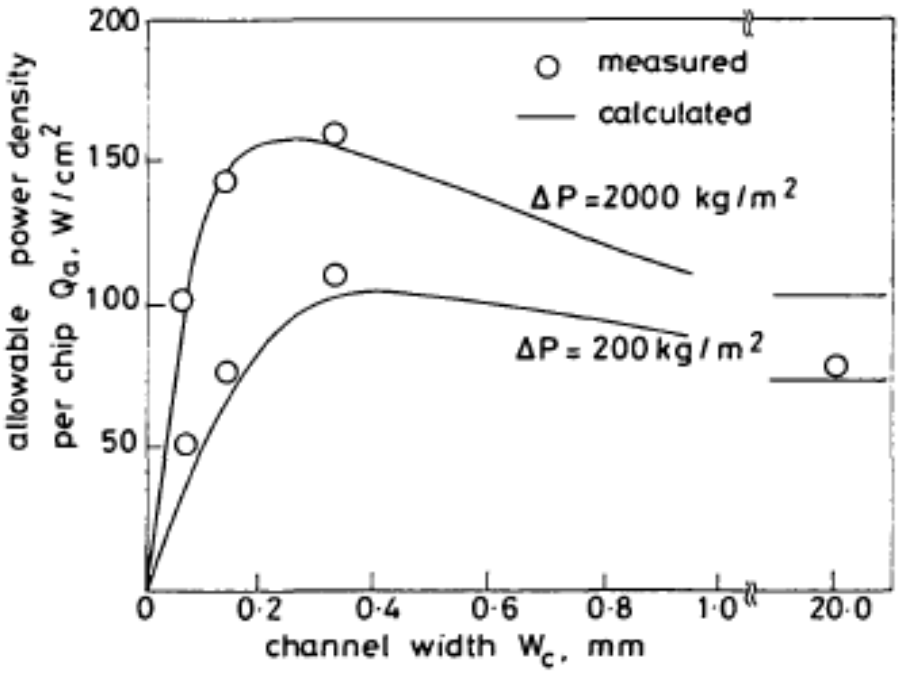

Figure 22: Allowable power density per chip as a function of channel width Wc, with pressure drop ΔP as a parameter [47].

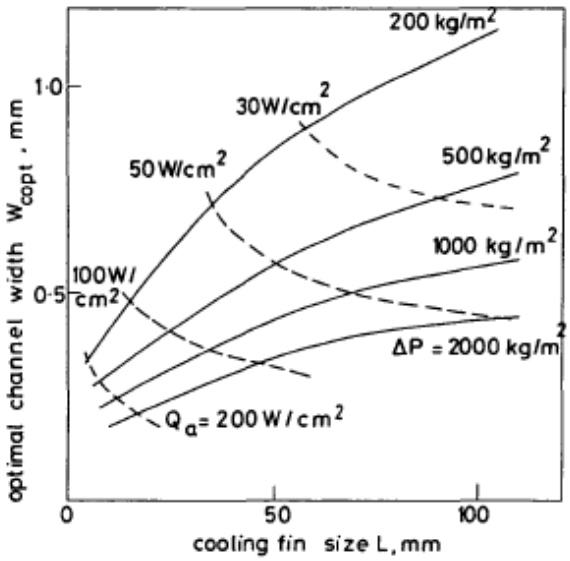

Figure 23: Optimal channel width as a function of cooling fin length, with pressure drop ΔP as a parameter [47].

Samalam [48] was also one of researchers who tended to optimize the Tuckerman and Pease's work. The purpose of his studying was to make the solutions simple enough and can be used to design advantageous cooling structure and also be applied first-order solutions to appraise order corrections.

2.13 Thermal resistance

The innovation of design measure of water cooled microchannel heat sinks was recorded in the research of Phillips [36]. The laminar and turbulent flow regimes were regarded for developing flow and fully developed flow where limitation were set on aspect ratio of channel width to fin width. The thermal resistances presented as a function of channel width are the major discussions in his design that allowed turbulent flow yielded the smallest thermal resistance. Figure 24 indicated that the curve of R''_{bulk} (Coolant bulk temperature rise thermal resistance) decreasing accompanies by increasing channel width. R''_{conv} (Convective thermal resistance) curve shows it is going to increase for laminar flow; it is smaller for turbulent flow. The plot also

demonstrated that small channel widths are dominated by R''_{bulk}, yet R''_{conv} is the main factor for larger channel widths shown in the graph for the presenting of R''_{tot} (Total thermal resistance).

The consequence of the various channel length in the heat-sink performance shown by the blue and red curves in Figure 25. The blue line, shown on the up-plot, resulted the shorter channel length accompanies by the lower total thermal resistance, however the down-plot, the one presented pump power versus channel width, unfortunately indicated to acquire this lower resistance, the high pump power is required. Although, the resistance performance of red line, the one represented the longer channel length, is not as good as shorter length channel, but the pump power cost is quite low in the experience. Freon has commonly used as refrigerants and as aerosol propellant. Freon (CCI_2F_2) as the liquid coolant rather than water is applied in the studying of Phillips [36]. The total thermal resistance of Freon is higher than the total thermal resistance of water as showing in the up-plot, however, it is not hard to see the pump power of Freon and the power of water is quite similar as showing in the down-plot.

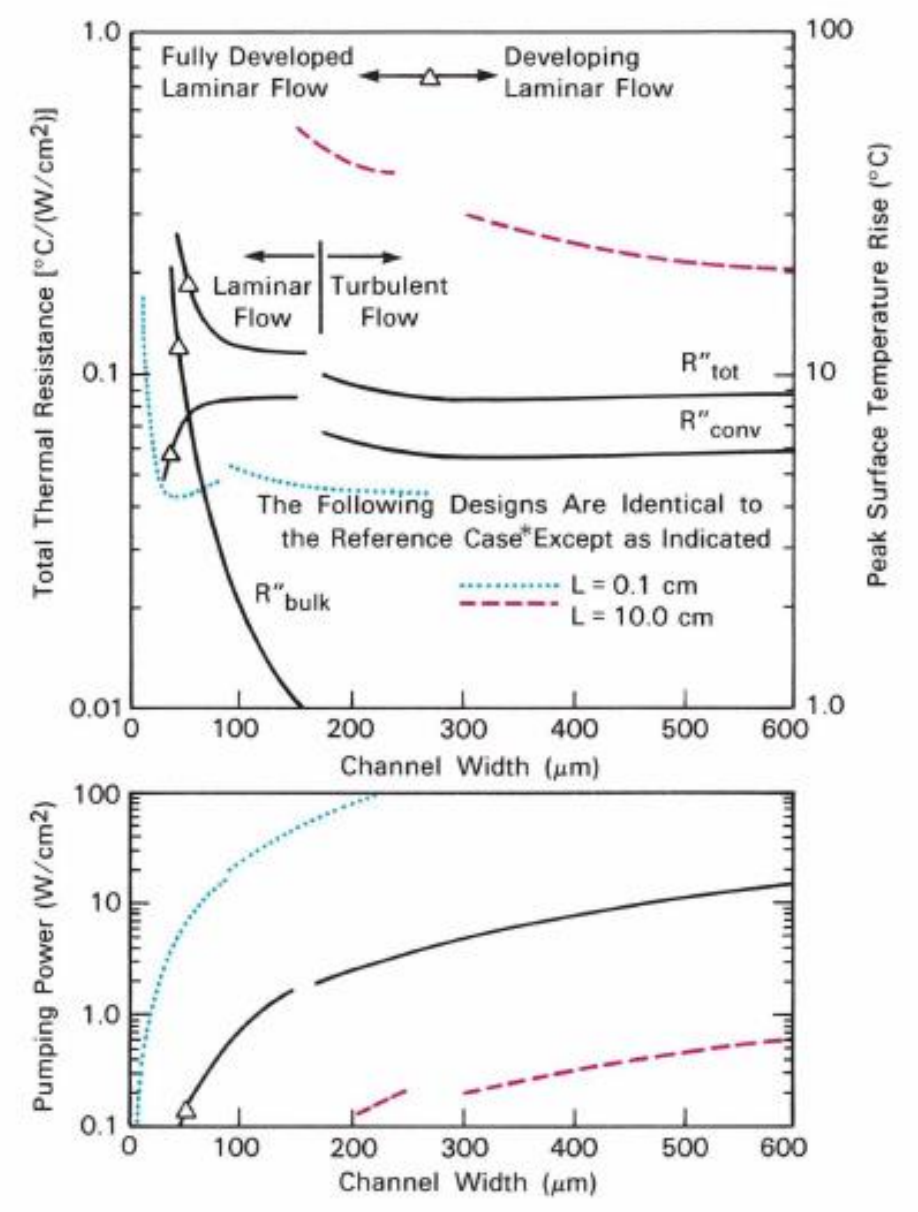

Figure 24: Total thermal resistance and pumping power requirements are shown as functions of channel width. The pressure drop is held constant for these curves [36].

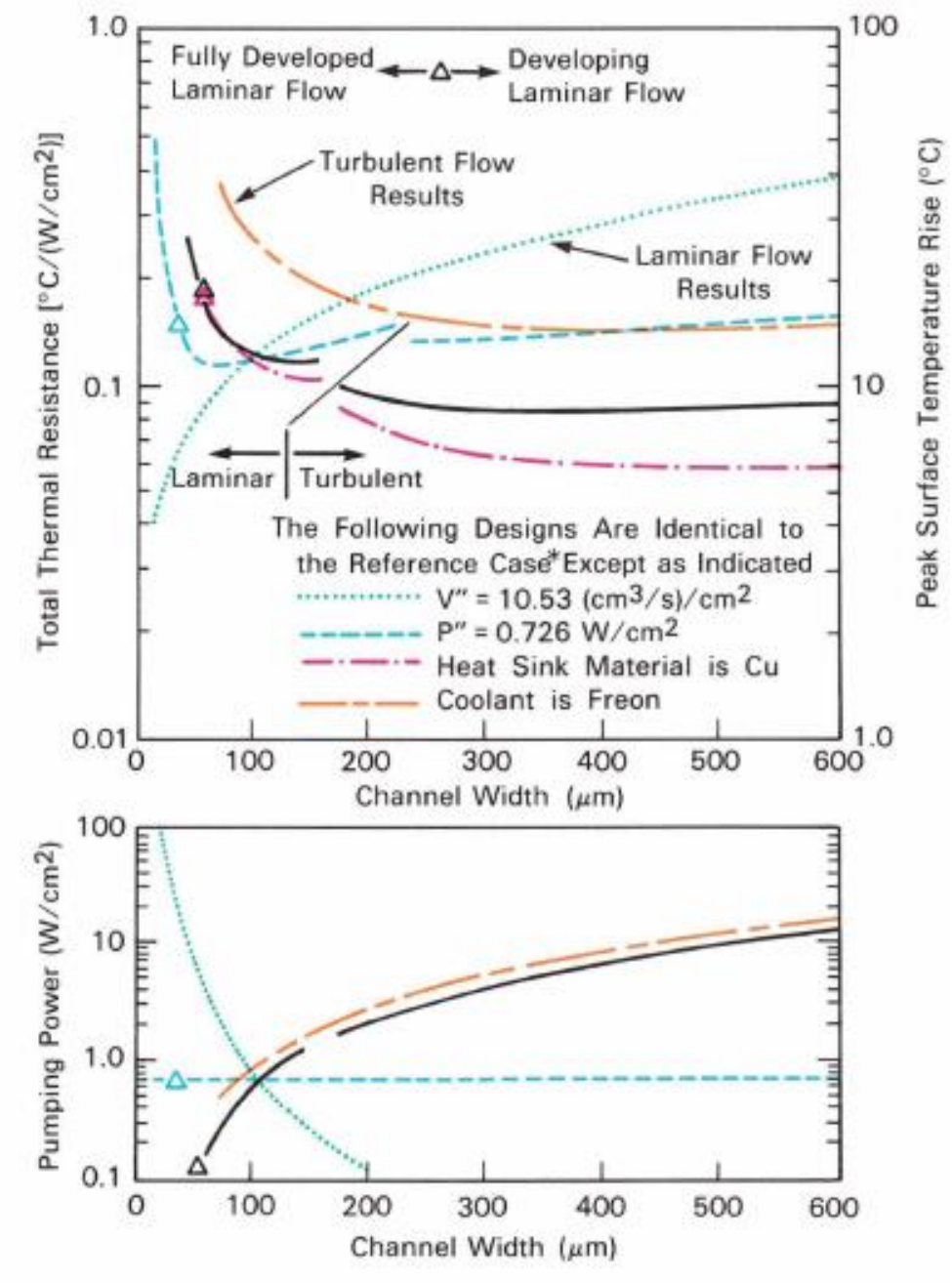

Figure 25: Total thermal resistance and pumping power requirements are shown for various coolants, heat-sink materials, and coolant flow-rate constraints [36].

2.14 Heat power

In single-channel measurements, Lian Zhang et al [49]. found that the pressure change in single-channel against heat power result was similar to the outcome of the multi-channel, except the onset of boiling point where was at 1.32 W less than the 2.14 W where the onset of boiling point of multi-channel was at. Figure 26 showed the pressure against heat power curve.

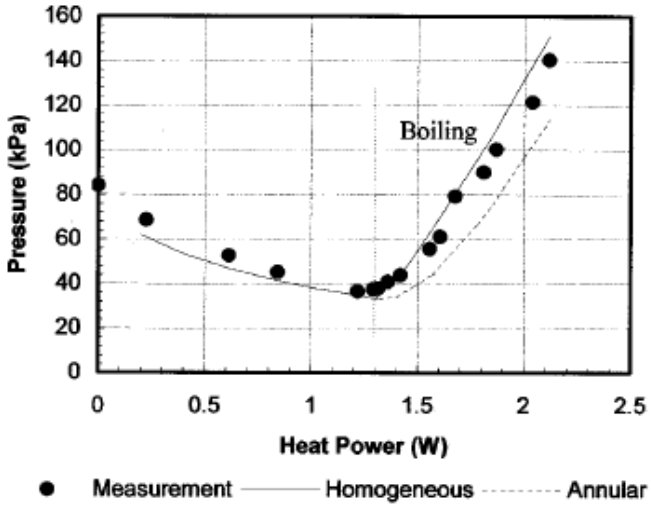

Figure 26: A single-channel device, as a function of heat power at the flow rate of 0.1 ml/min [49].

2.15 Boiling flow

Lian Zhang et al. [49], two phase flow concept was referred by Stanley et al. [50] and concept of the boiling in low flow rate was considered from Bowers [51] conducted experiments on boiling flow in single microchannel which the hydraulic diameter was 58 μm and multi-microchannel that the hydraulic diameter was 31 μm, both experiments were tested at 0.1 ml / min flow rate. The measurements in the multi-channels reported that pressure of the channels decreased with increasing heat power in single phase flow, but the pressure increased suddenly at the water boiling point where indicated the beginning point of two phase flow. Figure 27 illustrated the result of the experiment, the boiling point occurred at the heat power of 2.14 W. In

the experiments, the authors also claimed that the electrical signals of data acquisition system could be a significant indicator for seeking the water boiling point. The test result pointed in Figure 28, it is obviously to found every point begins fluctuating after the onset of boiling water.

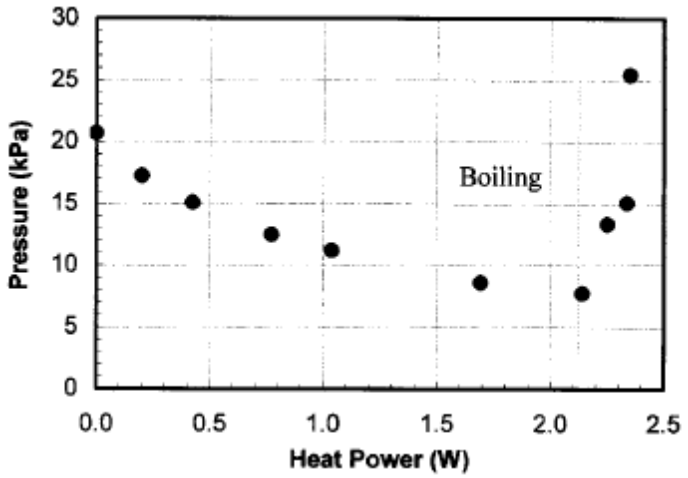

Figure 27: Pressure change in the multi-channel measured as a function of heat power at the flow rate of 0.1 ml/min [49].

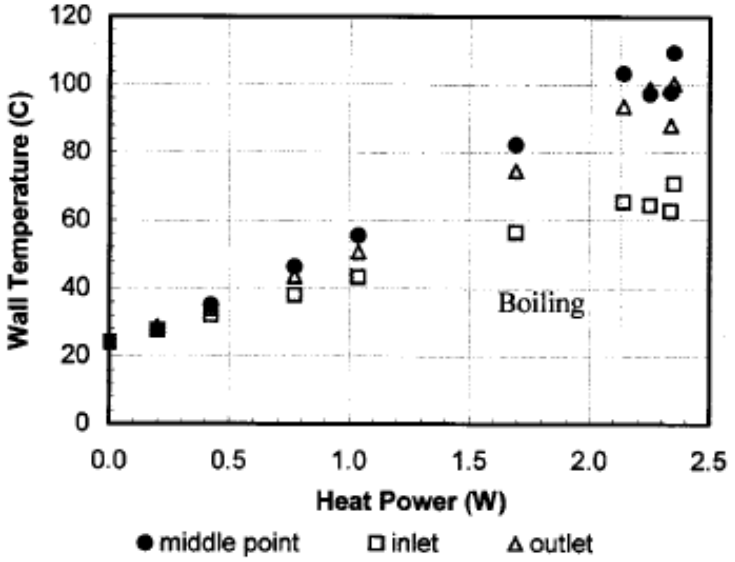

Figure 28: The temperature of multi-channel measured as a function of heat power [49].

CHAPTER III

EXPERIMENTAL FACILITY AND PROCEDURE

3.1 Experimental Facility

An experimental facility for our test requires some specific instruments to complete this study. In this experiment, pressure drop, mass flow rate, temperature difference, Reynolds number, etc. are the major parameters for analyzing and understanding the behaviors of the phases flow in the contraction and expansion channels. Figure 29 shows that the closed-flow loop system was used to gather the data in the experiment. The deionized water storage tank, standard duty gear pump, mass flow meter, thermocouples, contraction and expansion channels, pressure transmitters, static pressure transducers, data acquisition system, heat exchanger and pipes system.

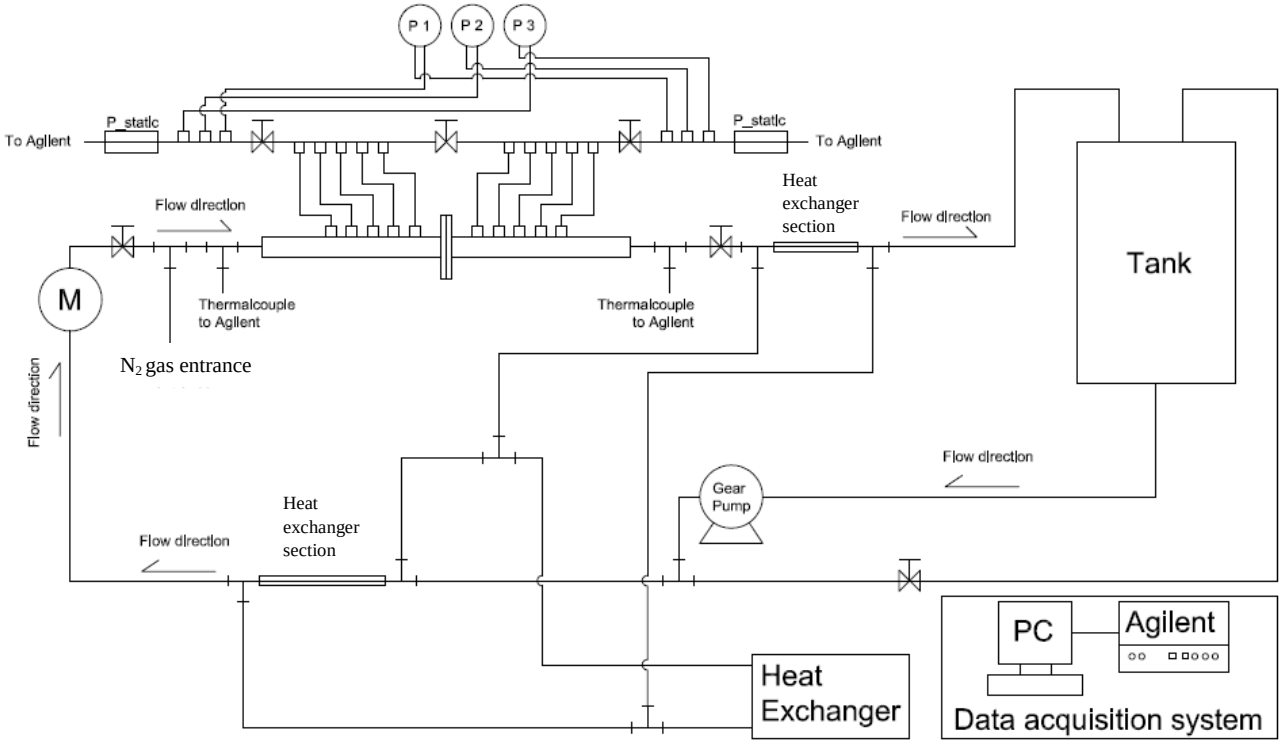

Figure 29: Schematic diagram of the experimental system

3.1.1 Storage Tank

The cylindrical tank was made by using PVC material with the diameter 0.25 m, height 0.3048 m. The capacity of the tank volume is 15 liters. The PVC cover is placed and sealed entirely on the top of the tank, the reason is to avoid any potential effect from outside the tank. Furthermore, due to reasons of saving amount of energy consume in the pump and keeping the same required power output, the potential energy theory is applied, the tank is installed at 1 m above the pump. In order to maintain the purity of deionized water, the deionized water in the tank is checked every time at the beginning of the experiment. Figure 30 shows completely the configuration of the storage tank.

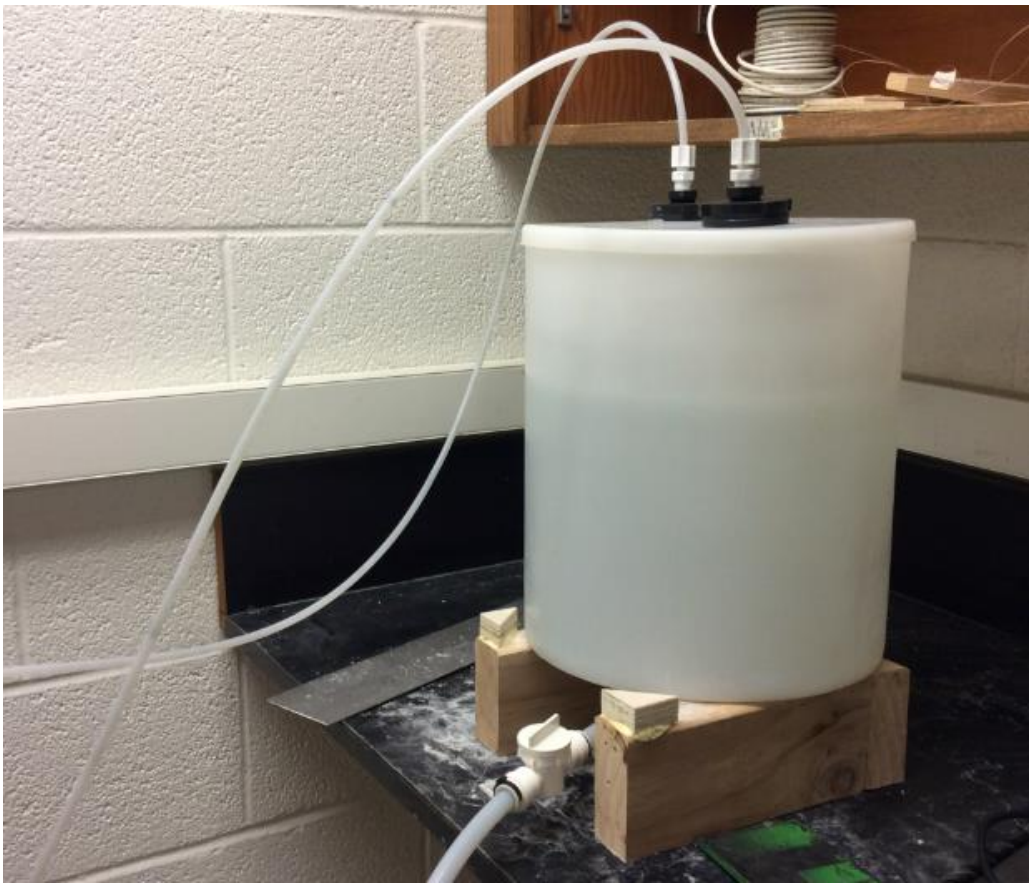

Figure 30: The DI water storage tank

3.1.2 Standard duty gear pump

Figure 31 presents the Liquiflo 35F gear pump set up. The pump is designed to operate within ambient temperature range of -20 ºC and 40 ºC. Its maximum flow can be operated to 13.0 LPM and maximum speed can be applied to 1750 RPM. The maximum pressure drop, shows in the pump specifications, is 6.9 bar. Deionized water is feeding by the PVC hose from right side of the pump and flowing into the pipes system from left side of the pump. Figure 32 shows the performance of the gear pump when it operates with either water or oil.

Figure 31: Liquiflo gear pump

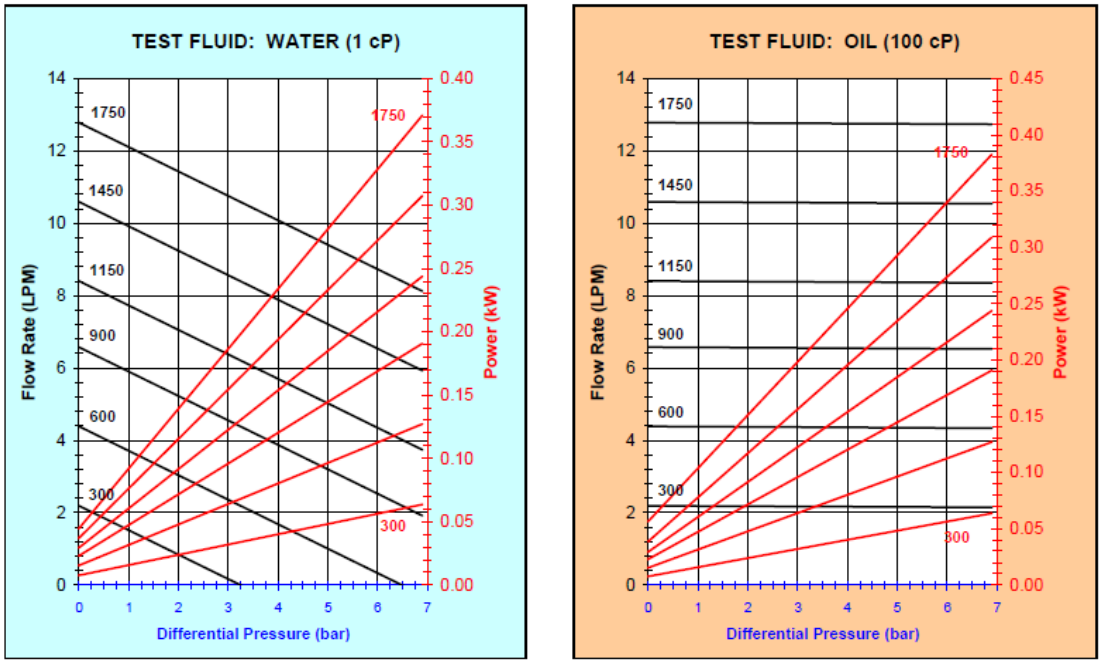

Figure 32: The performance curves of the 35F gear pump with the test fluid water and oil. (http://www.liquiflo.com/v2/gears/3/35f.htm)

3.1.3 Mass flow meter

Figure 33 shows the CMFS010M model micro mass flow sensor. It can be operated, the mass flow rate, approximate 30 g/s. The mass flow accuracy of this sensor is ± 0.05 % on liquids and ± 0.25 % on gases. For the temperature accuracy is ± 1 ºC ± 0.5 % of reading on both liquids and gases fluid. The mass flow rate is measured by vibrations of two parallel measuring channels in the sensor. When flow is introduced, the channels are going to twist and cause the inlet vibration frequency and outlet vibration frequency difference shows as Figure 34. This sort of difference is proportional to the mass flow rate.

Figure 33: Mass flow meter

Figure 34: Mass flow rate measurement

3.1.4 Test section

Figure 35 shows the aluminum test section are 0.5, 0.375 and 0.14 inches on the top, and 0.19 and 0.3 inches on the bottom. In the experiment, the 0.5 inches diameter test section is irreplaceable no matter the contraction or expansion tests. Figure 36 illustrates the configuration of the test section. The given fluid are flowing through the test section from left side and leaving on the right side. Ten pressure taps were installed in the bottom of the test section, the distance of a tap to another is approximately 1 inch, will provide us the local pressure data and help us to find static pressure. However 1/8 inches flexible PVC channels are connected with taps. In order to collect the accurate and efficient data, bubbles are not allowed in the internal flexible PVC channels before the fluid are introduced into the test section.

In the experiment, the constant mass flow rate and temperature are required. The inconstant mass flow rate will cause various velocities in the test section during a time period. The uncertainty velocities are going to affect the static pressure data we are expected. The constant temperature or the isothermal condition is also an important factor during the experiment, because the temperature difference can make unnecessary thermal properties change especially when the phase change occurs.

Figure 35: Various diameters test sections

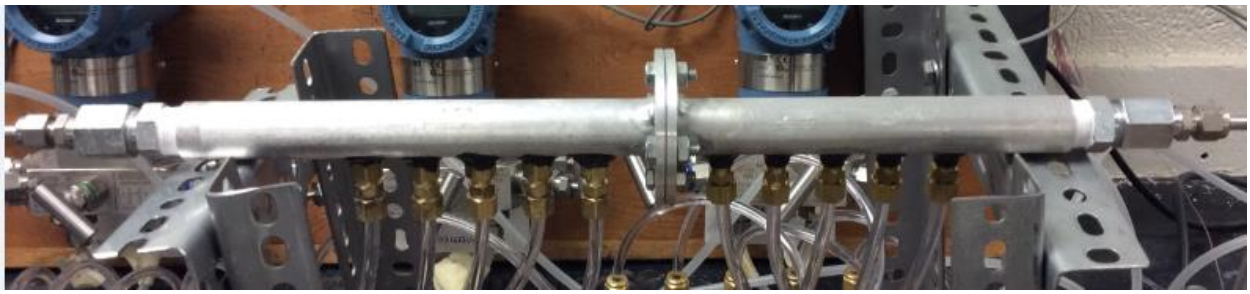

Figure 36: The schematic of the test sections with upstream 0.5 in. - diameter (Left side) and downstream 0.14 in. – diameter (Right side).

3.1.5 Thermocouples

Six inches long TMQSS-020U-6 quick disconnect thermocouples with miniature connectors are used to measure the bulk temperature of the fluid at inlet and outlet. Figure 37 is the thermocouple set up downstream of the test section. The tip of thermal probe is inserted in the center of the channel perpendicularly in order to get the accurate temperature data. The purpose in this studying, the inlet temperature is expected to be approximately same as the outlet temperature. The other side of the connector is connected to the acquisition system. All of the temperature reading data are collected by the acquisition unit.

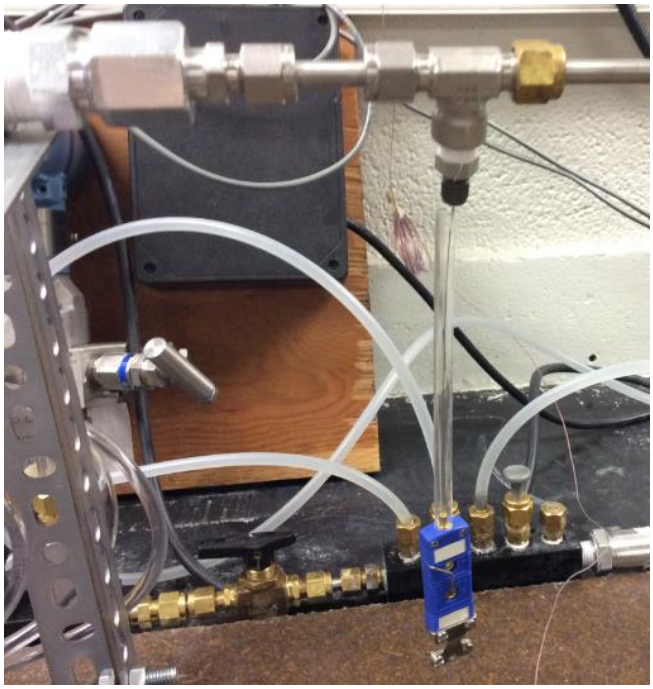

Figure 37: TMQSS-020U-6 Thermocouple at downstream

3.1.6 Pressure transducers

From left to right 300, 36 and 9 psi Rosemount differential pressure (DP) transmitters, with ± 0.65 % accuracy, are applied in the experiment as shown in Figure 38. There are the manifolds, which are installed between the test section and the pressure transmitters, on both upstream and downstream test sections. Therefore one 50 psi static pressure transducers is also installed individually on the upstream manifold and the downstream manifold. The differential pressure data can be read by the acquisition unit.

Normally, pressure drop is getting small when the diameters of the channel become small. However these three DP transmitters are going to be inaccurate for pressure drop measurement when the larger diameter channels were applied. Because the DP transmitters could not receive the accurate value when the larger diameter was used, the 50 psi static pressure transducers are the reliable and accurate measuring transducers.

Figure 38: Rosemount differential pressure transmitters

3.1.7 Heat exchanger

The heat exchanger is used to keep the temperature of fluid same during the entire experimental period. In our case, two heat exchangers are applied in our flow system. One is set up before the inlet test section in order to guarantee the isothermal process when the fluid flows through the test section. The other one is placed at outlet downstream section for removing the extra heat which are generated by the flowing fluid through the test section.

3.1.8 Gas flow mass controller

Since the flow rate of the liquid is controlled by gear pump regulator, Alicat flow mass controller is used for operating the gas flow. Figure 39 shows the outward appearance of the controller. The range of the volumetric flow rate can be applied the minimum flow rate from 0.025 to maximum flow rate 5 standard liter per minute (slpm). In our experiment, nitrogen was used as the gas portion in this two phase flow experiment. The volumetric flow range was operated 0.025 to 1 slpm for each test section. The reading data from the experiment can be collected by RS -232 terminal program on Microsoft Windows operating system in the acquisition system. Pressure, temperature, volumetric flow rate and mass flow can be read and collected in the system.

Figure 39: Alicat MC5 slpm full scale flow mass controller

3.1.9 Data acquisition system

This system consists of two major devices, one is an Agilent 34972 and the other one is a computer center. This system will read and collect the data from the CMFS010M model micro mass flow meter, TMQSS-020U-6 quick disconnect thermocouples and pressure transducers including three Rosemount meters and two static pressure transducers in an excel format. Yet we can organize, analyze and plot the data easily on the computer screen. Figure 40 is the Agilent acquisition.

Figure 40: Agilent/HP 34972A LXI data acquisition switch unit

3.2 Experimental procedure

Leakage free checking in the flow loop is a first step and a necessary procedure in the beginning of the experiment, in order to guarantee the entire experimental test data are effective and usable. DPG-107 Dwyer digital pressure gauge and A T-970 Ametek pneumatic hand air calibration pump are used for preventing and calibrating the possibility of the flow loop leakage. The pressure range of the digital pressure gauge can be applied up to 300 psi (20.69 bar) and the hand pump allows pressure range from 0 to 580 psi (0 to 40 bar). Figure 41 shows the gauge and the hand pump combination. In this step, the inlet valve, which was setup after the mass flow meter and before the test section, and outlet valve, which was located after the test section and before the heat exchanger, were closed. Therefore the hand pump was connected the gas inlet entrance and continually giving the pressure by press and unlash the handle until the pressure reach the maximum which the handle was hardly to apply the pressure anymore. In this moment the pressure vent valve was closed, the whole test section acted as a close system, and the gauge was

observed in few minutes. If the pressure reading doesn't change on the gauge display means the leakage test is successful, otherwise to check and replace leakage parts are necessary.

Figure 41: The combination of DPG-107 Dwyer digital pressure gauge and A T-970 Ametek pneumatic hand air calibration pump

3.2.1 Single phase flow experimental procedure

3.2.1.1 Equipment and requirement setup

The properties and behaviors of the single phase flow observation was a step before the application of the two phase flow. In this step the gas entrance valve was turned off, the mass flow 5, 10, 15, 17.5, 20, 22.5, 24.5, 26.5, 28.5 and 30 g/s were given sequentially for each contraction and expansion test sections. The five pressure taps were located at upstream pipe and other five were set at downstream, the five pressure drop data were observed and collected by the acquisition system from these taps. The static pressures were also considered to gather as the required data in

the experiment. The operating fluid temperature was required as a constant value by the heat exchanger. After a test section had been installed in the flow loop, the flexible plastic channels, which connect the pressure taps to valves that were installed on the pressure gauge manifold, had to be checked whether or not bubbles inside the channels before the beginning of the experiment. The bubble could cause an unwilling influence in the reading result. Before start collecting the effective data in the acquisition, turn on the gear pump and let the fluid flow through entire flow loop for five minutes in order to reach stable condition of the mass flow rate. After the five minutes, the data could be collected by different types of stop scanning. The contraction experiment had been done, and yet reverse the test section in order to acquire the expansion data, furthermore replaced the next test section and so on so forth.

3.2.1.2 Data reading setup

The pressure drop, temperature and mass flow data reading setup were needed for the acquisition system. There were five locations required for measuring the data. Each location was applied by different type of stop scanning. The first location stop scanning setup was after 100 scans. The second location stop scanning setup was 50 seconds elapsed time. Third location stop scanning was set elapsed time for 40 seconds. Fourth location stop scanning was after 150 scans. The final location stop scanning was 90 sec elapsed time. Each experimental required flow rate was run three times in order to collect accurately reading data in the experiment.

3.2.2 Two phase flow experimental procedure

The gas entrance valve was opened in order to pass the required nitrogen gas mass flow rate through the test section. Five gas mass flow rates, which units is Standard liter per minutes (SLPM), were applied in the experiment: 0.025 (≈ 0.00048 g/s), 0.1 (≈ 0.0019 g/s), 0.5 (≈ 0.0095 g/s), 1(≈ 0.019 g/s), 1.5 (≈ 0.028 g/s). Each giving gas flow rate remained constant and run with

single water flow 5, 10, 15, 17.5, 20, 22.5, 24.5, 26.5, 28.5 and 30 g/s individually. The data of the water behaviors were still collected and presented by Agilent software, the gas performances were received by HyperTerminal which menu on Microsoft windows. After the whole data readings were acquired, flip the test section to receive the opposite section data for either contraction or expansion. The test section changed one by one after the process was done, and so on so forth.

3.3 Data analysis

The thousand data were measured in the experiment, the value of data could not be claimed as true value. The experiment data are always contained and companied with errors of the outcome values. To receive precision and accuracy experimental data, the experimental uncertainty and percent error are going to apply in the correction of the result. The equations are shown as below and APPENDIX A is the estimation result:

Standard deviation (SD):

$$\sigma_x = \sqrt{\frac{1}{N-1}\sum_{i=1}^{N}(x_i - \bar{x})^2} \tag{3.1}$$

where:

N = Number of the measured values

x_i = The i-th measured value of x

$\bar{x}$ = Meaning of the measured values

Standard error of mean (SEM)

$$SEM = \frac{\sigma_x}{\sqrt{N}} \tag{3.2}$$

The percent of error:

$$\%\ Error = \frac{Value\ of\ the\ experiment - Value\ of\ the\ acceptance}{Value\ of\ the\ acceptance} \tag{3.3}$$

CHAPTER IV

RESULT AND DISCUSSION

4.1 Minor loss coefficient observation

The Eq. 2.46 is used to predict the loss coefficient with contraction channels. Assumption of turbulent flow not completely uniform velocity profiles and total uniform velocity profiles are made. The result indicates the loss coefficient with not completely uniform assumption is around 0.5 and the loss coefficient of the full uniform assumption is lower than 0.4. In the lower Reynolds number situation the Eq. 2.47 is suggested for prediction. However, the prediction equation suggest the loss coefficient should be 0.85 roughly, especially Reynolds number after 6000.

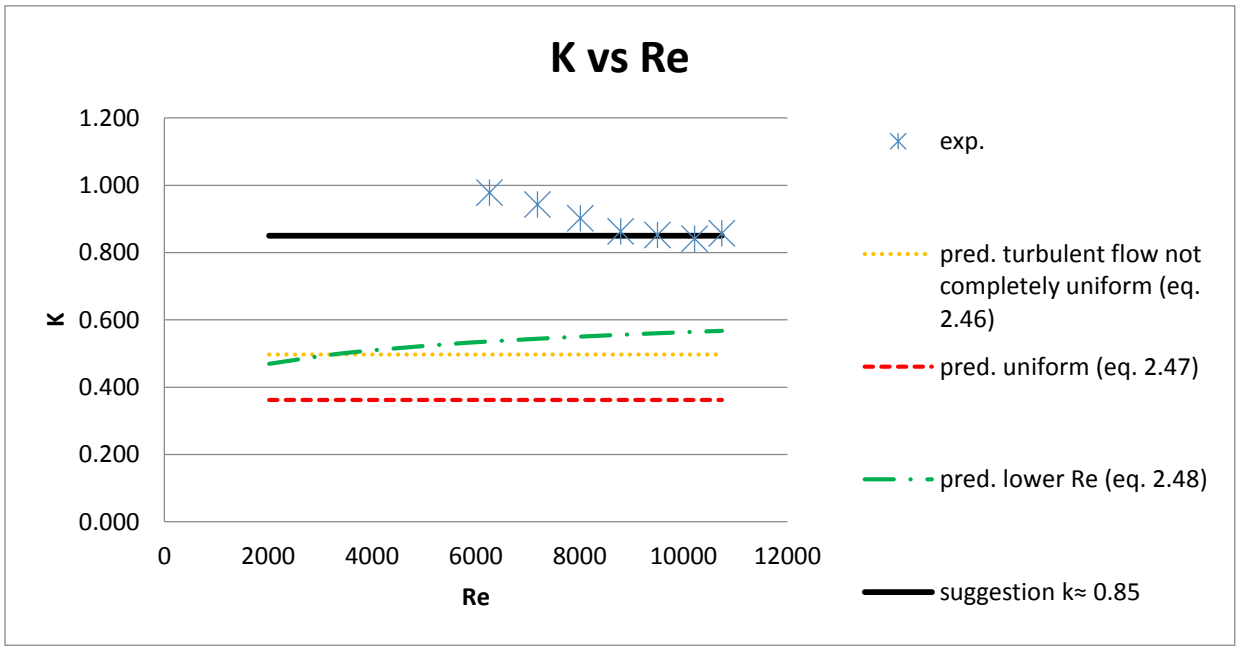

Figure 42: Multiple predictions for σ_c = 0.0784, $\dot{m}_L$ (g/s) =5.63-30

Figure 43 shows loss coefficient against velocity from experimental data and previous experimental result from Yoda's [1] report. The previous data expresses that the loss coefficinet seems decreasing when the velocity is increased. In our experiment, the loss coefficeint is also reducing when the velocity is getting faster. To neglect the singularities, the loss coefficient of the experimental data can be expected affirmatively that the loss coefficient is inversely proportional to the velocity.

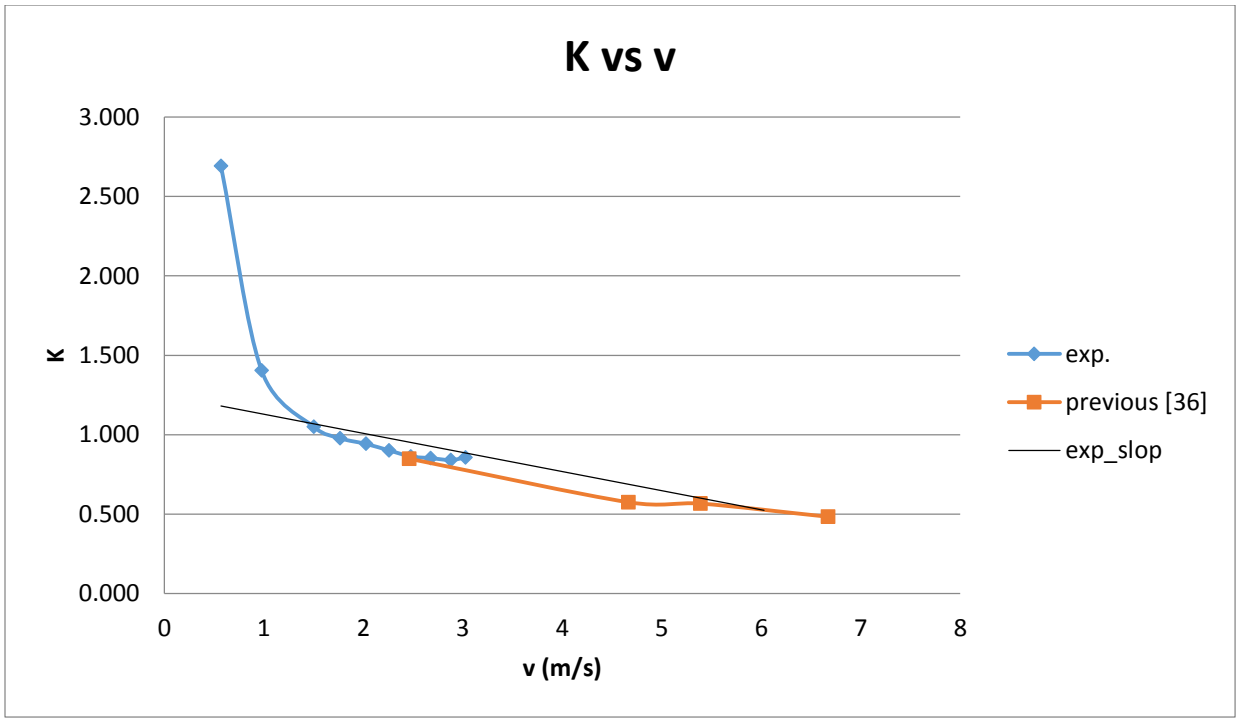

Figure 43: Velocity influence on loss coefficient for exp. v (m/s) = 0.56-3.03 and previous v (m/s) = 1.25-6.67

The minor loss coefficient is suggested around 0.67 in this case which shows in Figure 44. The turbulent flow not completely uniform prediction in this area ratio 0.1444 will be 0.47. The uniform prediction is 0.34 at this time. All result indicates that the loss coefficient is reduced when area ratio is increased. The experimental data of the loss coefficient becomes flat and predicable after Reynolds number equals 6000.

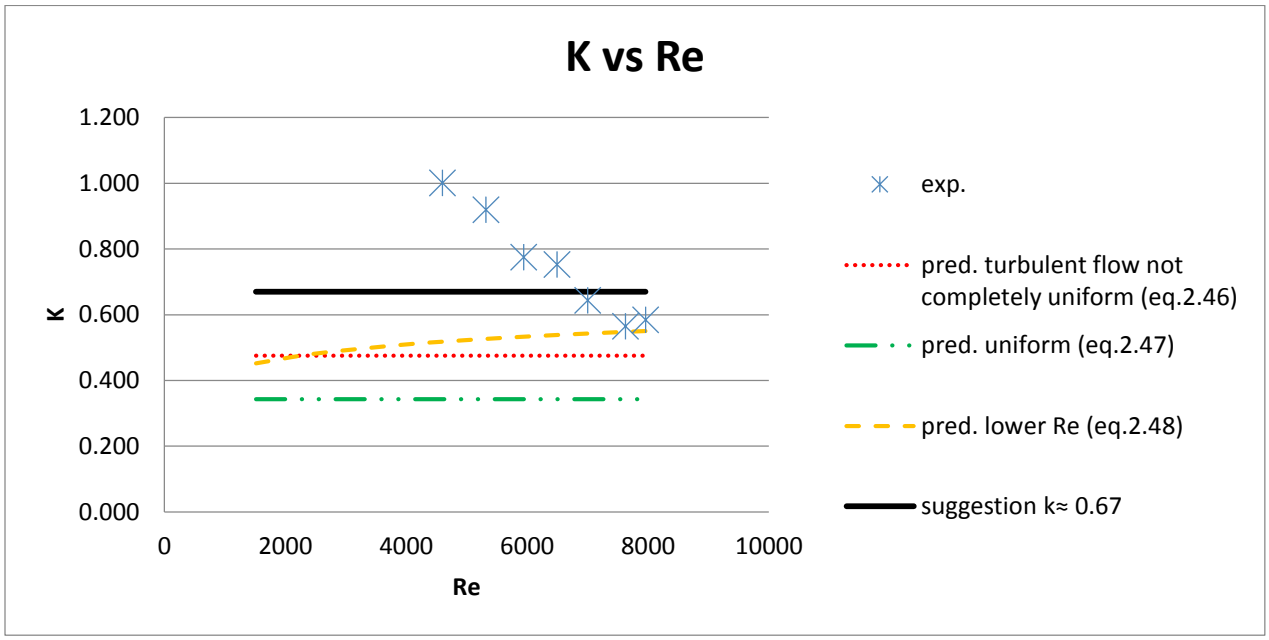

Figure 44: Multiple predictions for σ_c = 0.1444, $\dot{m}_L$ (g/s) =5.74-30.16

The loss coefficient performance in our experiment can be predicable at higher velocity which is great than 1.5 m/s. The experimental data begins decreasing slowly and the slop of the loss coefficients are getting flat and constant when Reynolds number after 6000.

4.2 Pressure drop observation

4.2.1 Single phase performance

The pressure drop can be estimated from the point of the upstream trend line where the distance equals to zero subtracts the point of the downstream trend line where the distance.

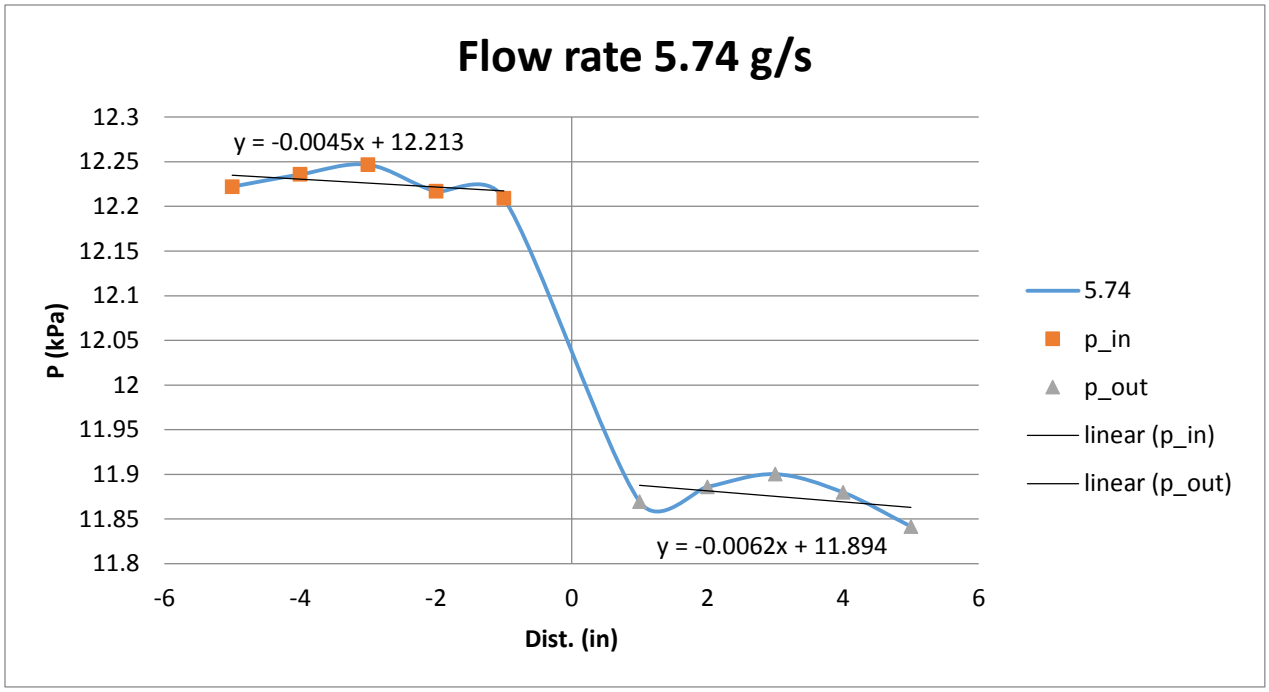

Figure 45: Pressure drop performance for σ_c = 0.1444, $\dot{m}_L$ (g/s) = 5.74

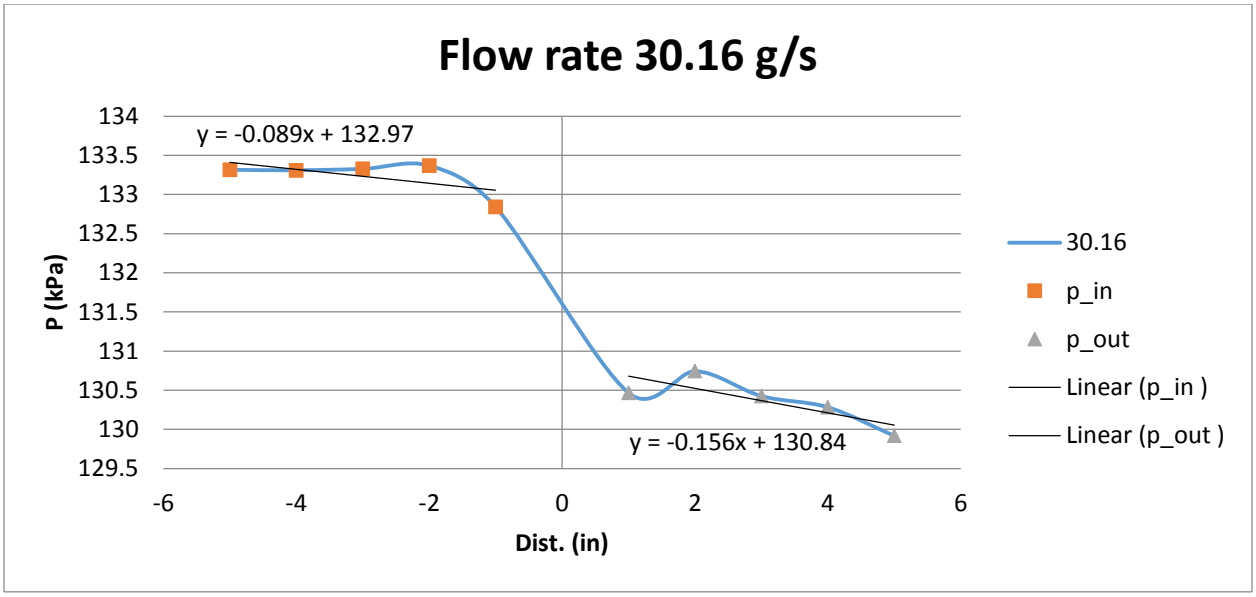

Figure 46: Pressure drop performance for σ_c = 0.1444, $\dot{m}_L$ (g/s) = 30.16

The comparison of these three flows illustrates the slop of the pressure drop is elevated gradually and the slop of the pressure differences can be expected to reach the maximum when the highest of the experimental mass flow rate is operated.

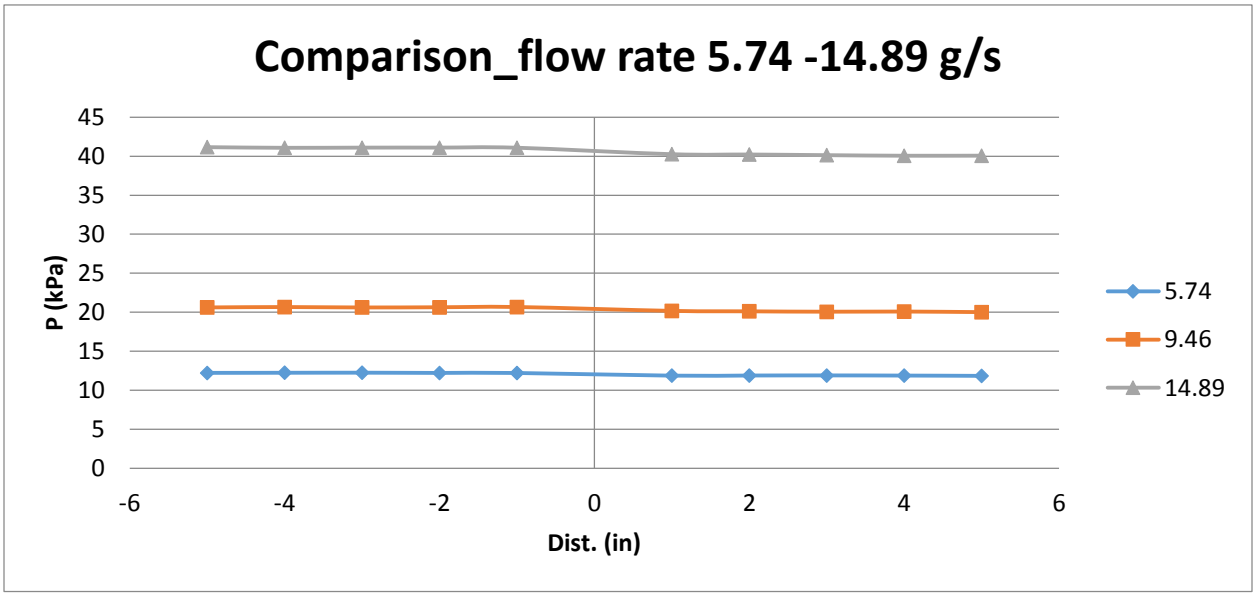

Figure 47: Pressure drop performance for σ_c = 0.1444, $\dot{m}_L$ (g/s) = 5.74, 9.46 and 14.89

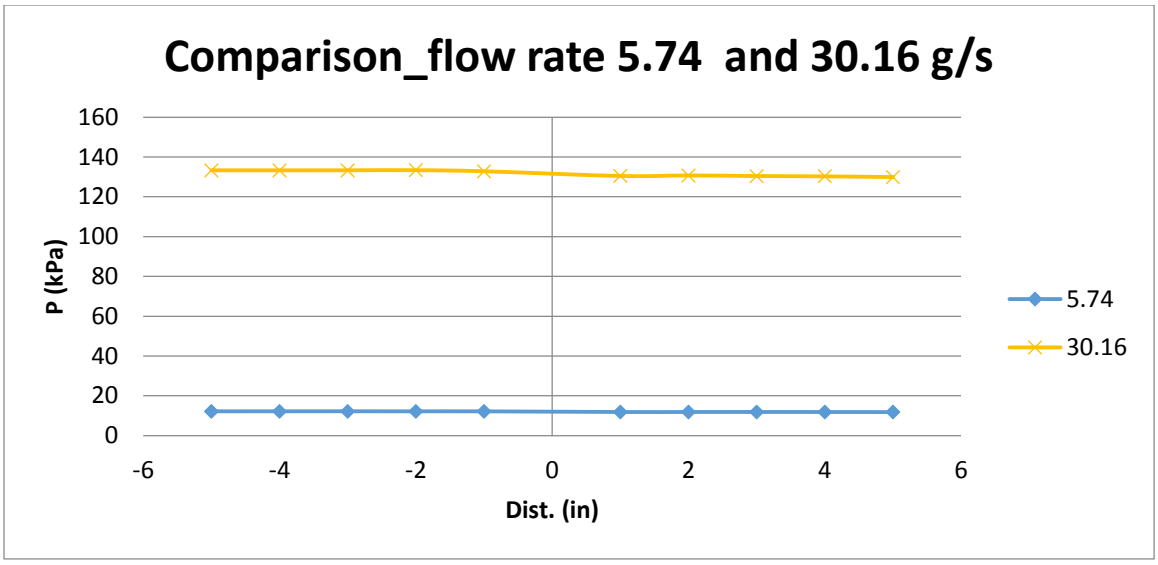

Figure 48: Pressure drop performance for σ_c = 0.1444, $\dot{m}_L$ (g/s) = 5.74 and 30.16

To ensure the formula of prediction can perfectly work on our data, the equation check is definitely needed from the previous data which obtained from Yoda's [1] report. The checking result seems fine when the range of Reynold number from 1000 to 6000 and pressure drop up to 45 kPa. Figure 49 shows the result of the formula checking.

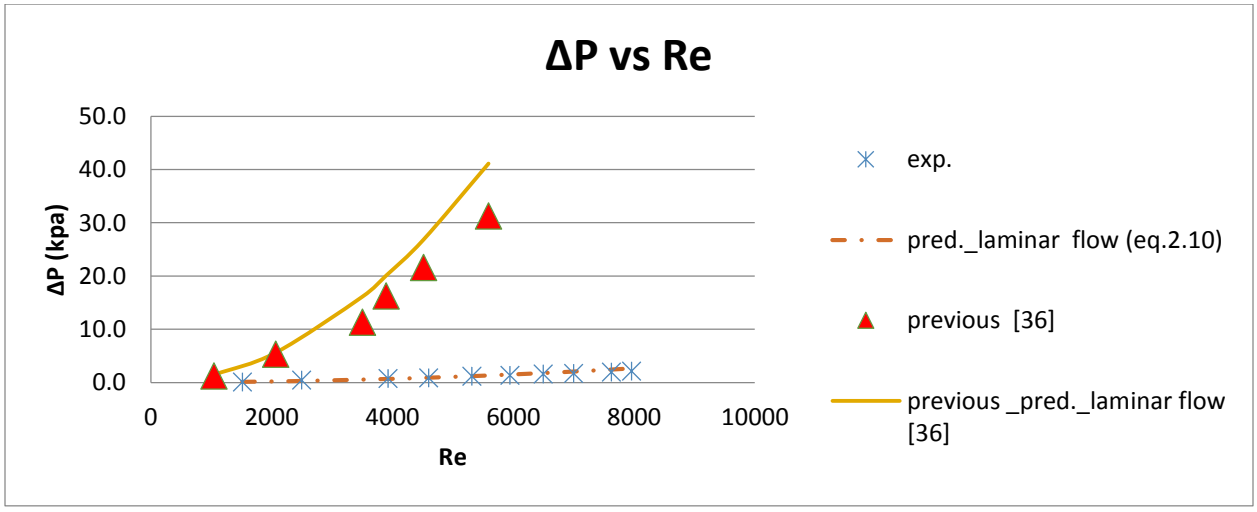

Figure 49: Pressure drop performance for σ_c = 0.1444, $\dot{m}_L$ (g/s) = 5.74 and 30.16 and previous data

Figure 50 illustrates the multiple pressure drop behavior predictions. According to Eq. 2.8, laminar flow prediction, shows better agreement than other predictions. Figure 51 demonstrates the data can be predicted within ± 20%.

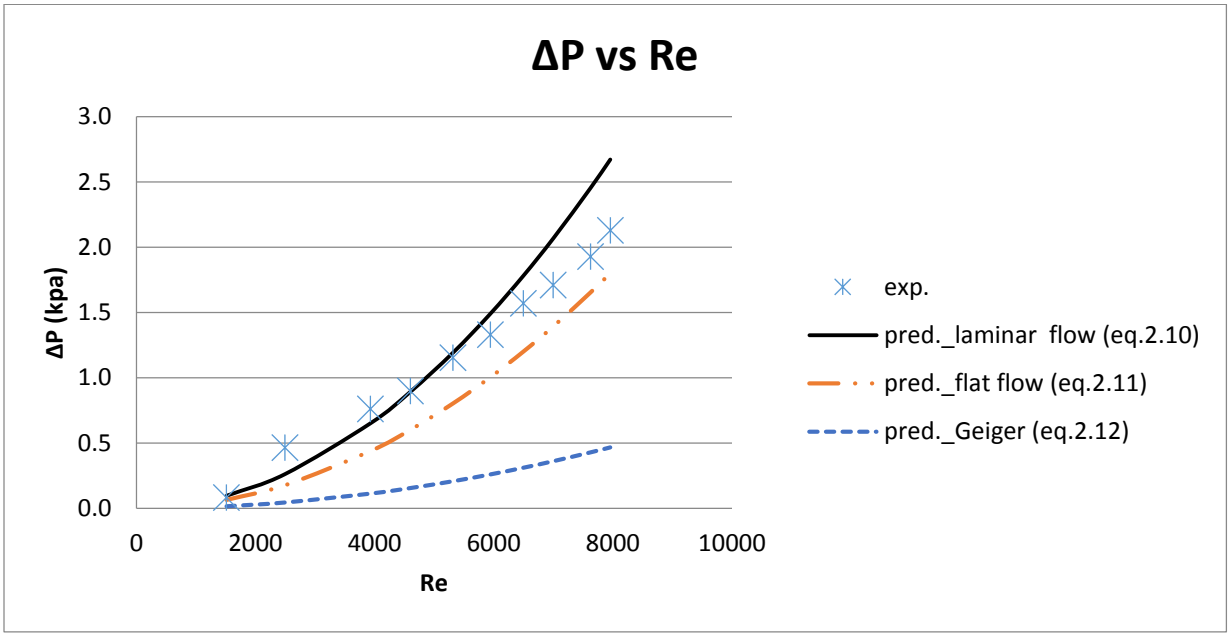

Figure 50: Pressure drop performance and predictions for σ_c = 0.1444, $\dot{m}_L$ (g/s) = 5.74-30.16

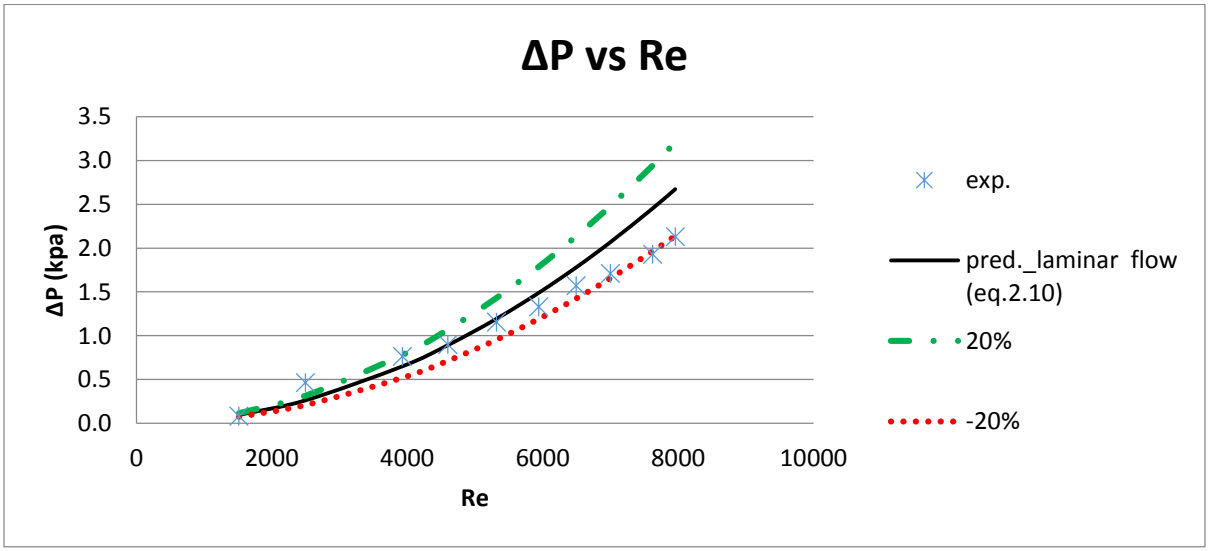

Figure 51: Pressure drop performance with ± 20% for σ_c = 0.1444, $\dot{m}_L$ (g/s) = 5.74-30.16

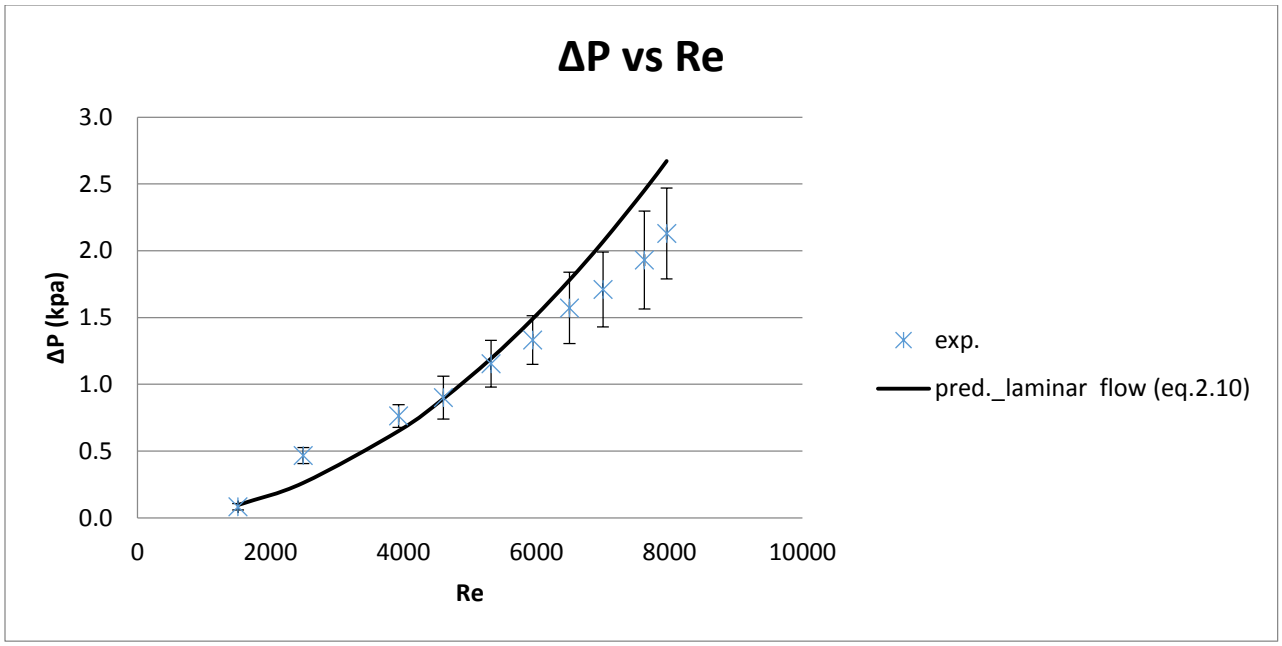

Figure 52: Pressure drop standard deviation for σ_c = 0.1444, $\dot{m}_L$ (g/s) = 5.74-30.16

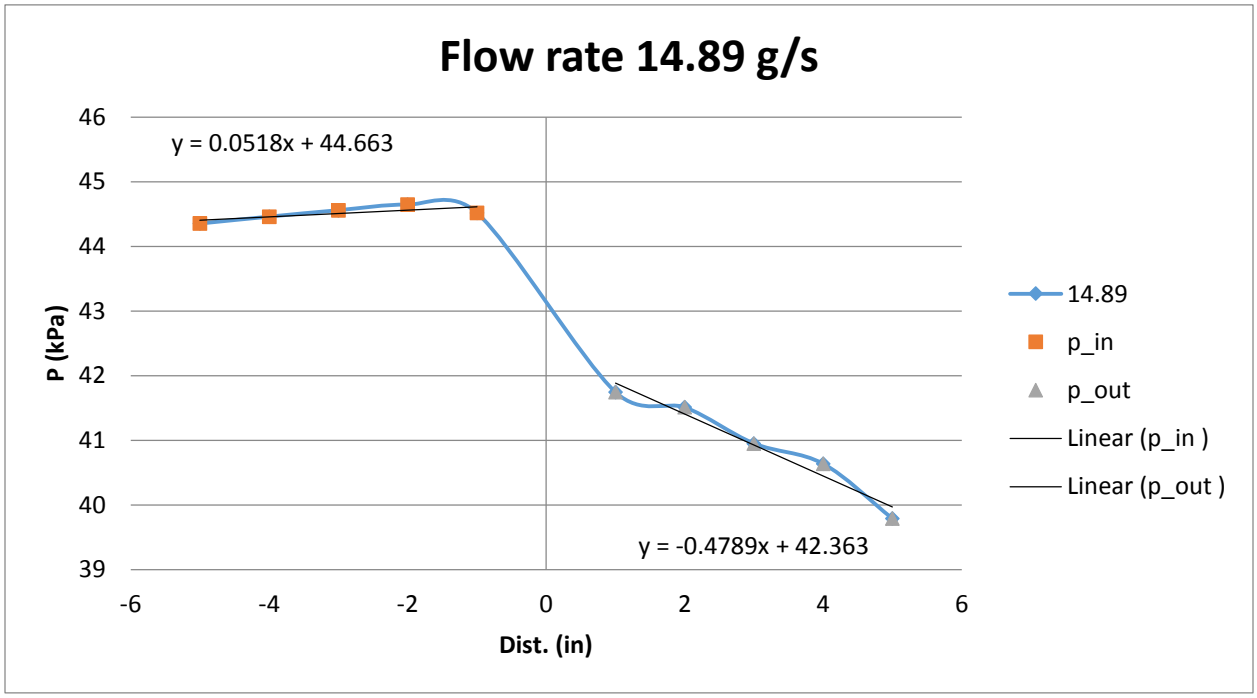

Figure 53: Pressure drop performance for σ_c = 0.0784, $\dot{m}_L$ (g/s) = 14.89

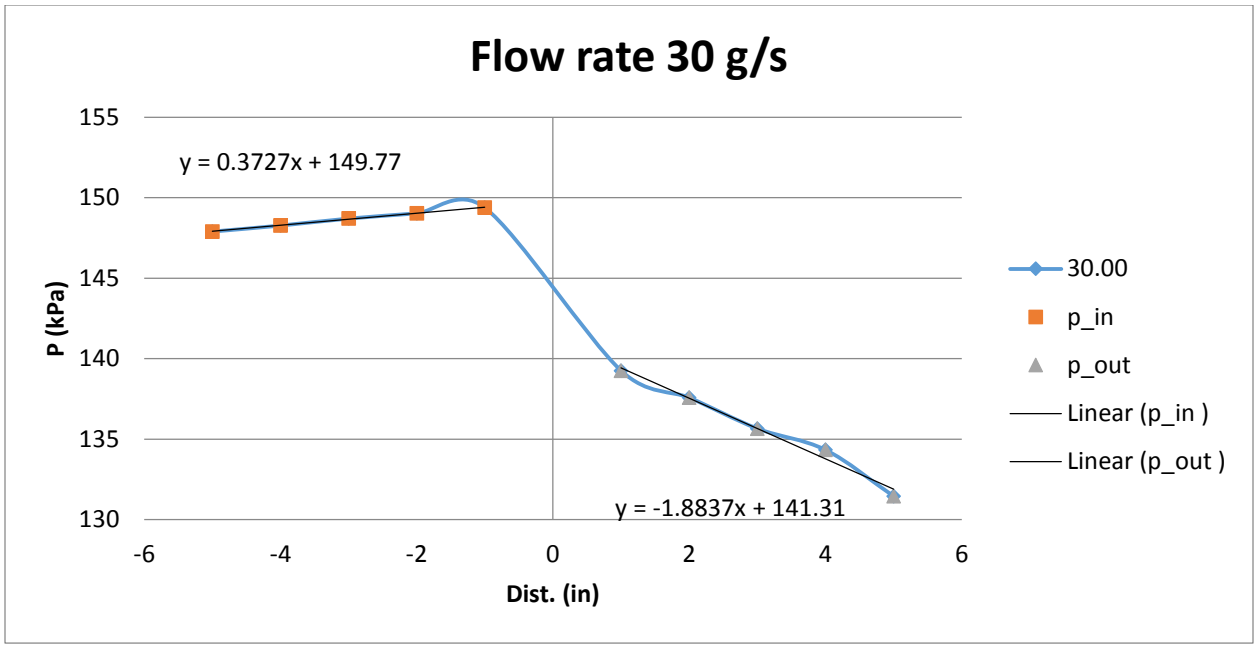

Figure 54: Pressure drop performance for σ_c = 0.0784, $\dot{m}_L$ (g/s) = 30

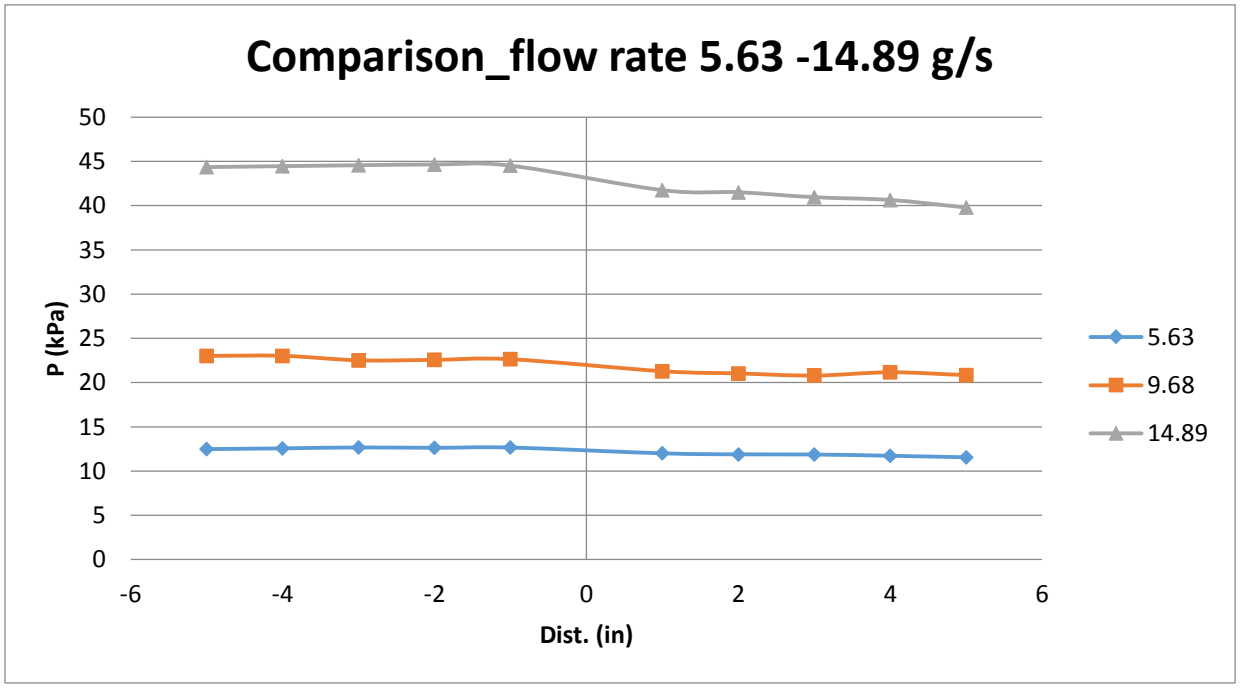

Figure 55: Pressure drop performance for σ_c = 0.0784, $\dot{m}_L$ (g/s) = 5.63, 9.68 and 14.89

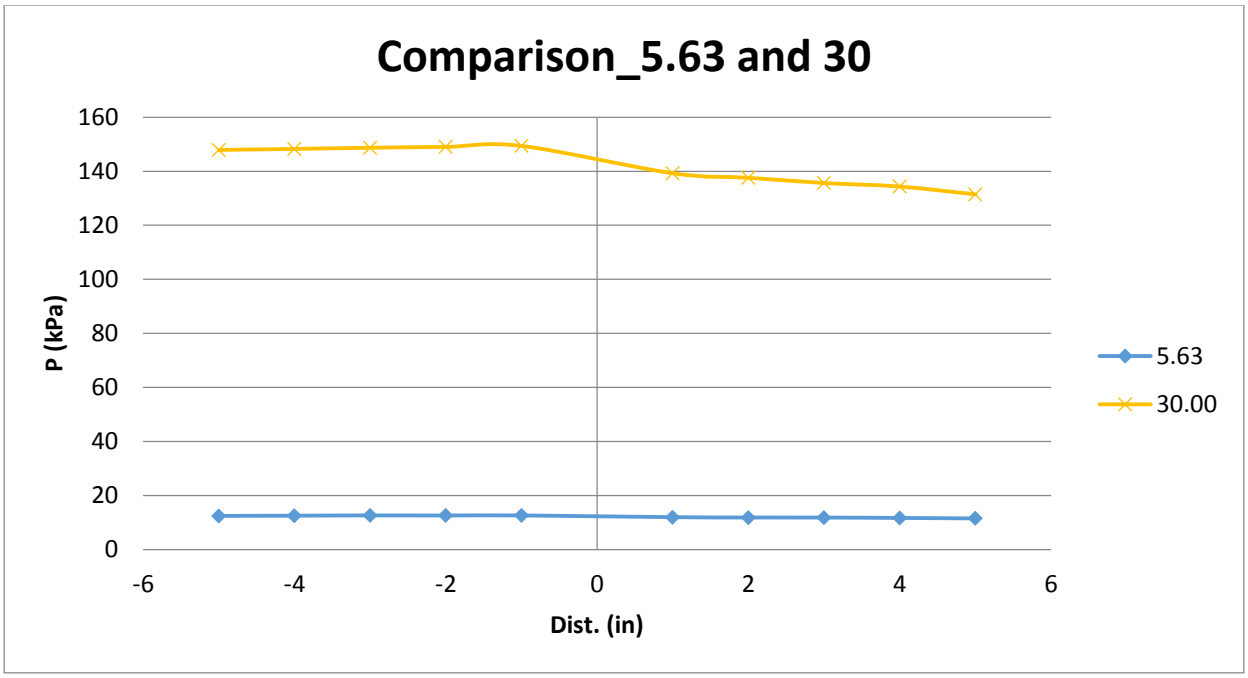

Figure 56: Pressure drop performance for σ_c = 0.0784, $\dot{m}_L$ (g/s) = 5.63 and 30

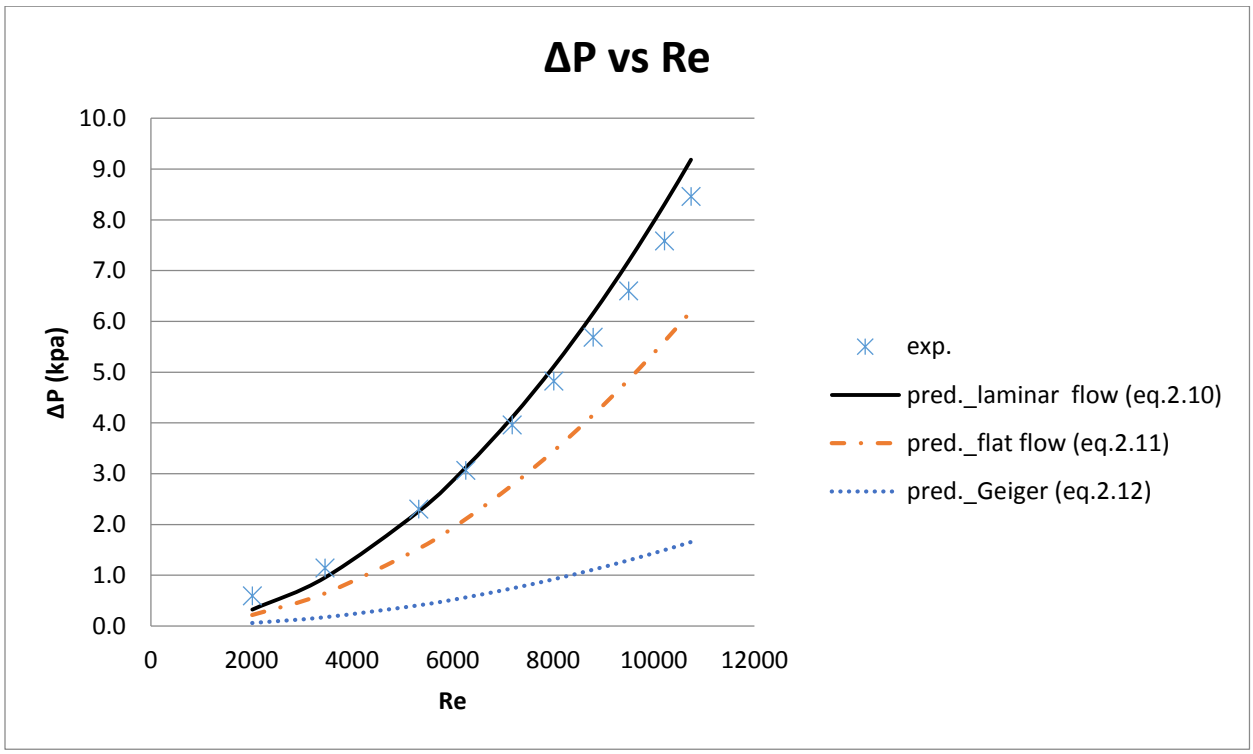

Figure 57: Pressure drop performance and predictions for σ_c = 0.0784, $\dot{m}_L$ (g/s) = 5.63-30

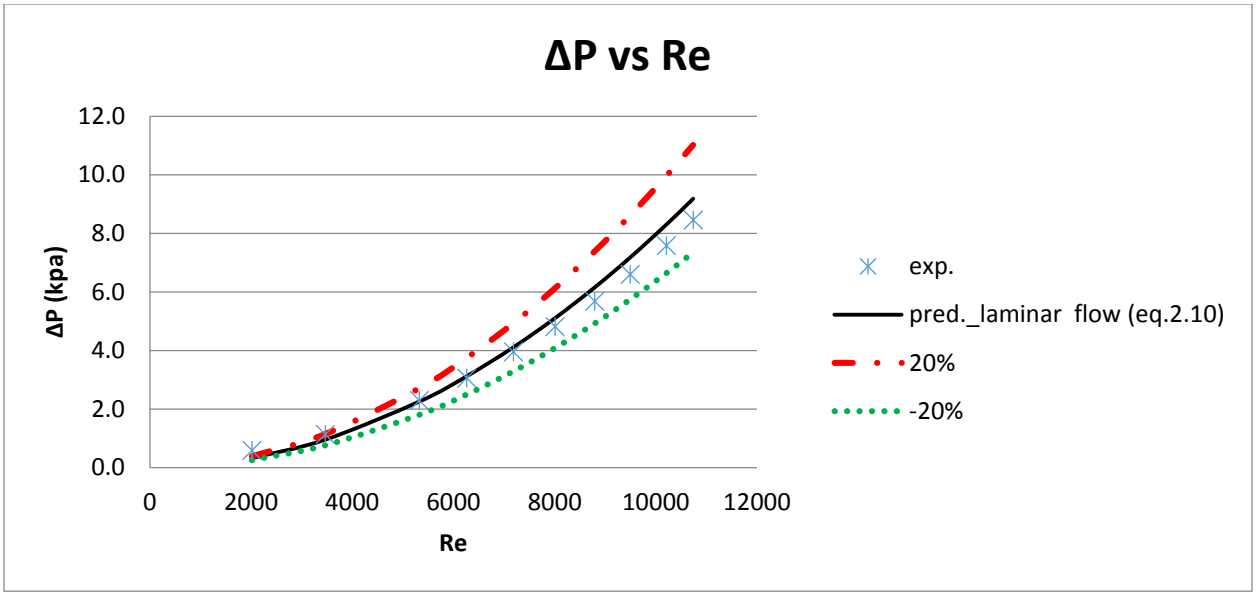

Figure 58: Pressure drop performance with ± 20% for σ_c = 0.0784, $\dot{m}_L$ (g/s) = 5.63-30

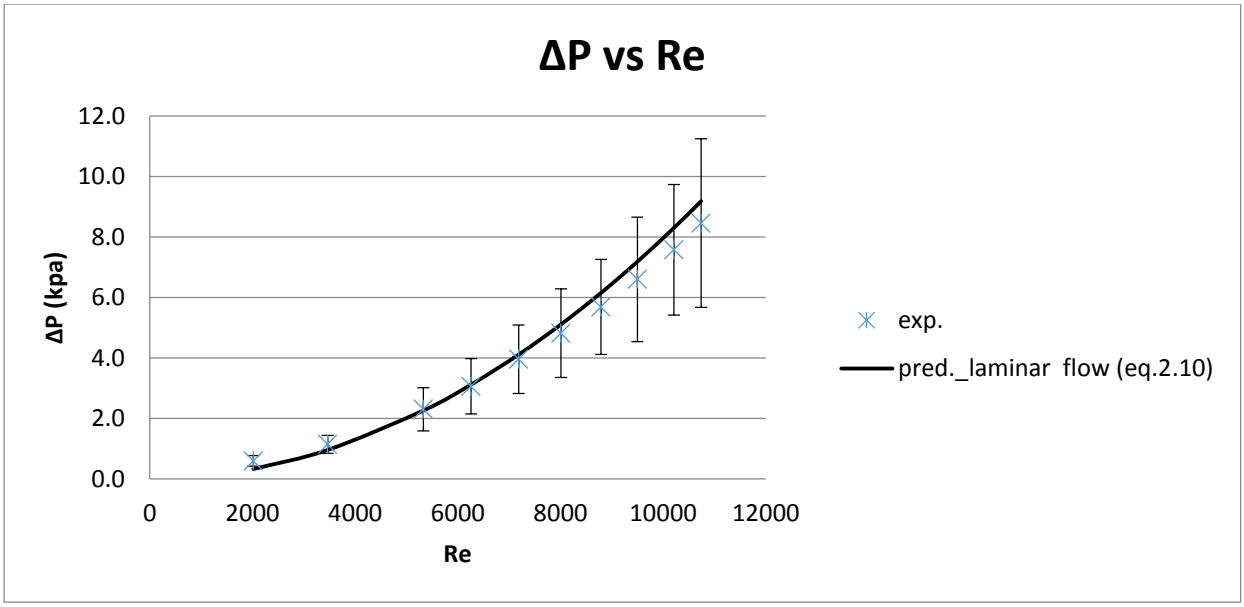

Figure 59: Pressure drop standard deviation for σ_c = 0.0784, $\dot{m}_L$ (g/s) = 5.63-30

The pressure drop prediction equation can have an accurate prediction and a good agreement with experimental data when area ratio (σ) and pressure differences are smaller. However, the pressure drop prediction in fully turbulent flow (flat flow) can give only rough

agreements with our experimental data. The experimental data might much more close to laminar flow than the fully turbulent flow.

4.2.2 Two phase performance

4.2.2.1 Pressure drop in contraction channels

For estimating the two phase flow pressure drop, many assumptions are made. The fluid is incompressible to ensure the density of the fluid keeps same everywhere in the test section. Homogeneous flow in the two fluids assumption is for keeping either liquid velocity and gas velocity are same all the time which makes slip ratio equals to one. The phase flow in contraction usually relates with vena contracta, therefore the consideration about whether or not vena contracta in the fluids flow for testing the experimental data become the critical and essential condition. Figure 60 gives the general prediction concepts as below.

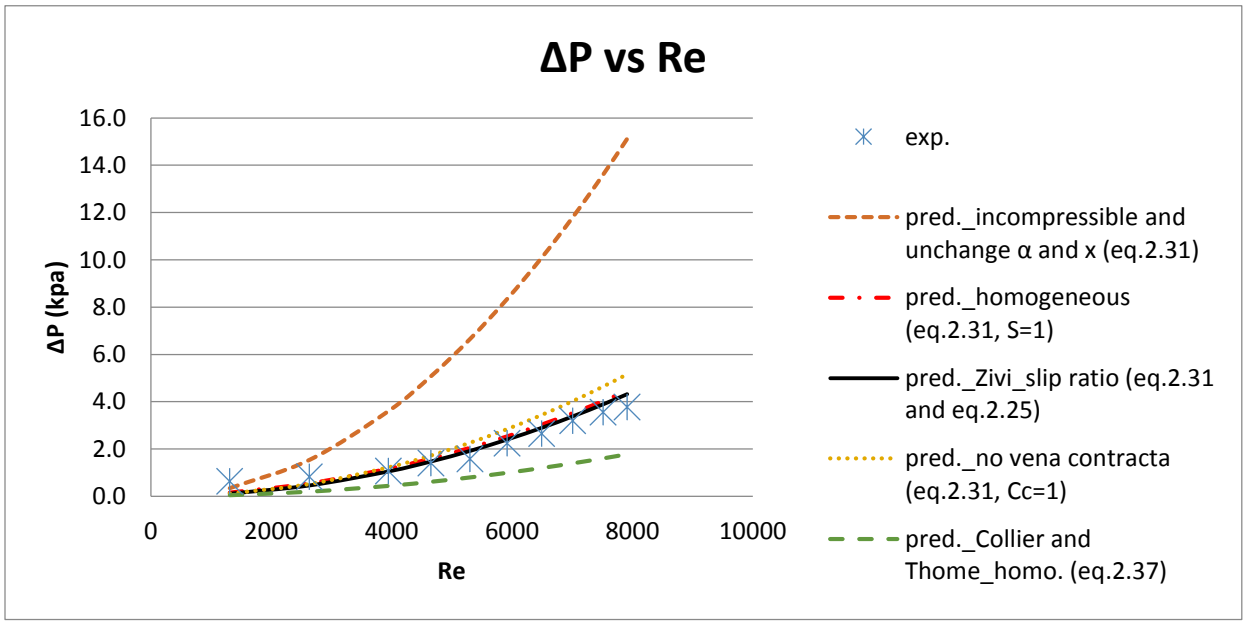

Figure 60: Pressure drop performance and predictions for σ_c = 0.1444, $\dot{m}_L$ (g/s) = 4.97-30, $\dot{m}_G$ (g/s) = 0.0019

In the Zivi's slip ratio model (Eq. 2.25), the pressure drop prediction in contraction can be received better estimation since Reynolds number larger than 4000. The pressure drop can be obtained from the experiment as the known value. The void fraction (α) can be calculated back and found it. However the new prediction formula of the pressure drop, which Reynolds number less than 4000, should be generated in the future.

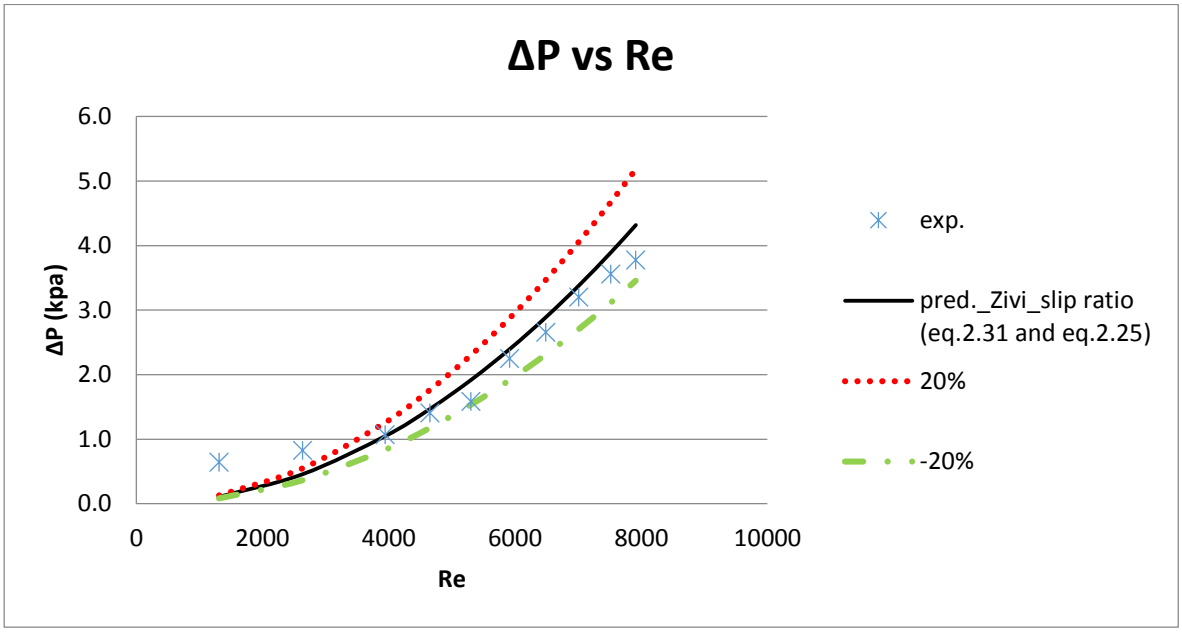

Figure 61: Pressure drop performance with ± 20% for σ_c = 0.1444, $\dot{m}_L$ (g/s) = 4.97-30, $\dot{m}_G$ (g/s) = 0.0019

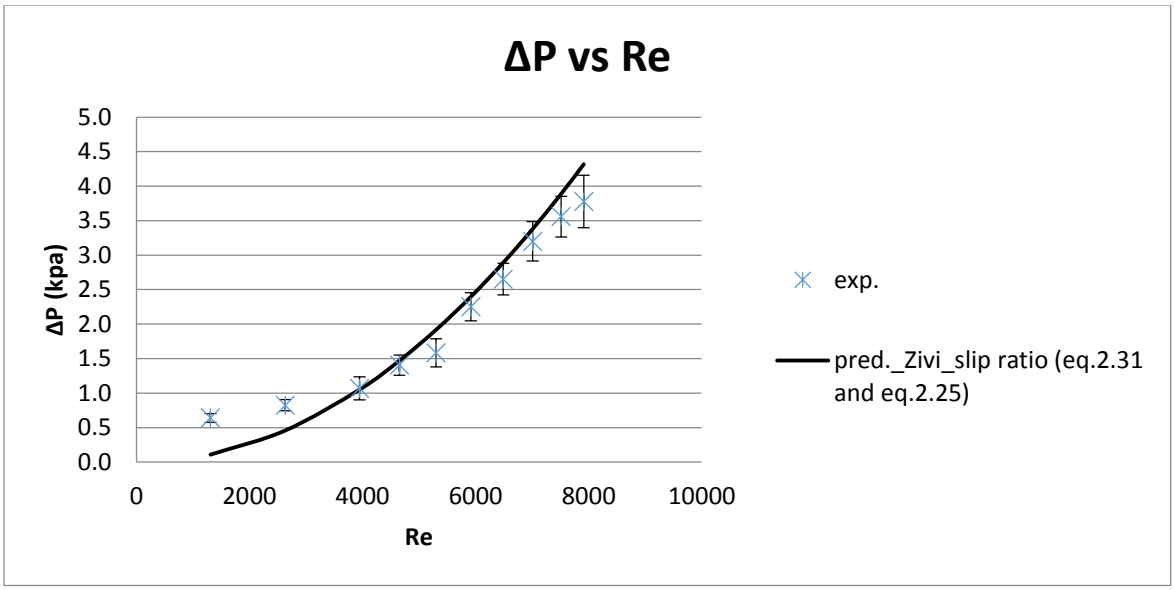

Figure 62: Pressure drop standard deviation for σ_c = 0.1444, $\dot{m}_L$ (g/s) = 4.97-30, $\dot{m}_G$ (g/s) = 0.0019

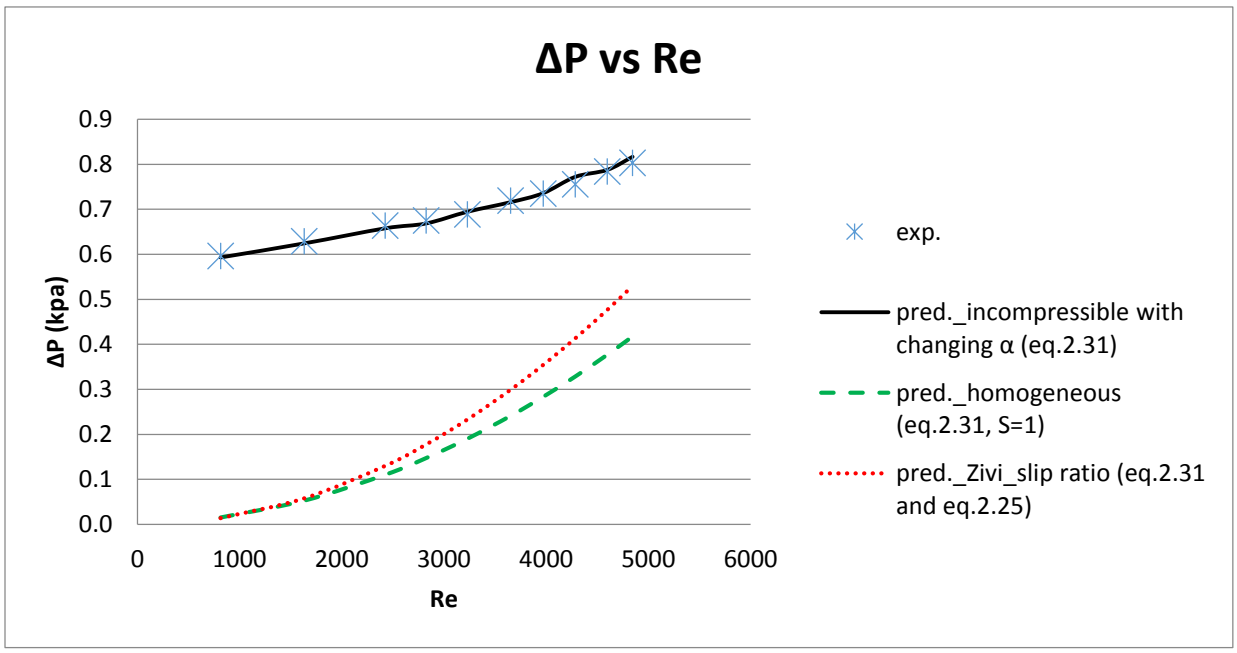

Figure 63: Pressure drop performance and predictions for σ_c = 0.3844, $\dot{m}_L$ (g/s) = 5.03-29.97, $\dot{m}_G$ (g/s) = 0.0019

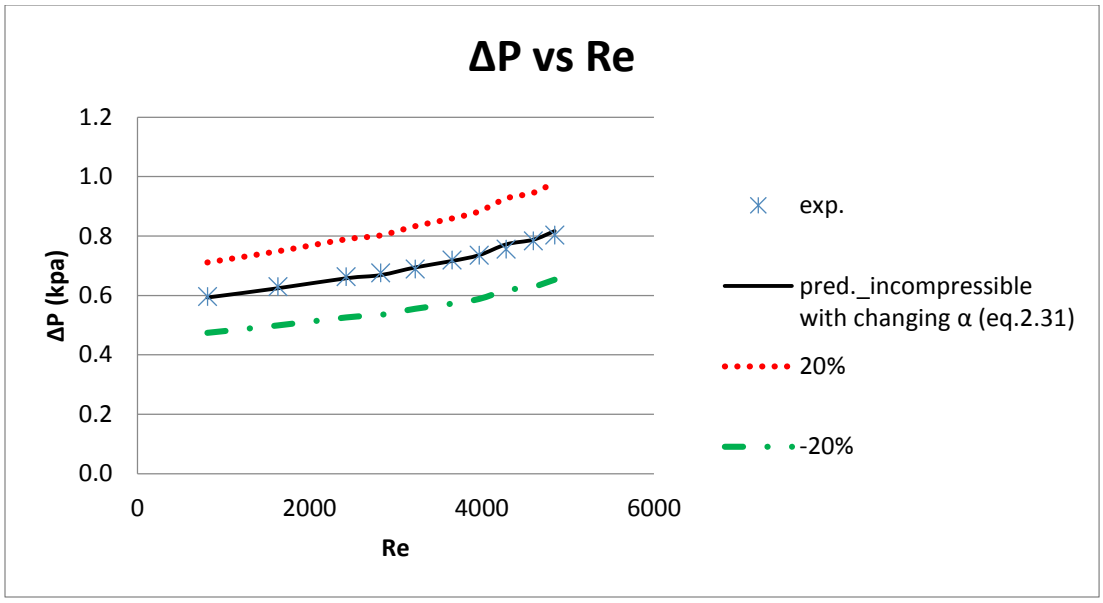

Figure 64: Pressure drop performance with ± 20% for σ_c = 0.3844, $\dot{m}_L$ (g/s) = 5.03-29.97, $\dot{m}_G$ (g/s) = 0.0019

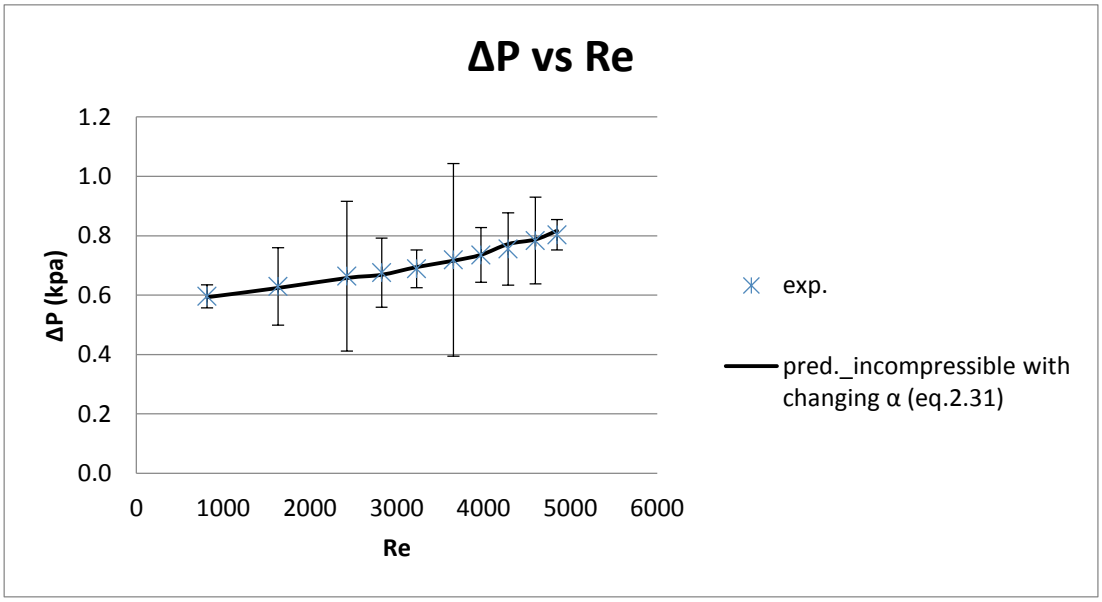

Figure 65: Pressure drop standard deviation for σ_c = 0.3844, $\dot{m}_L$ (g/s) = 5.03-29.97, $\dot{m}_G$ (g/s) = 0.0019

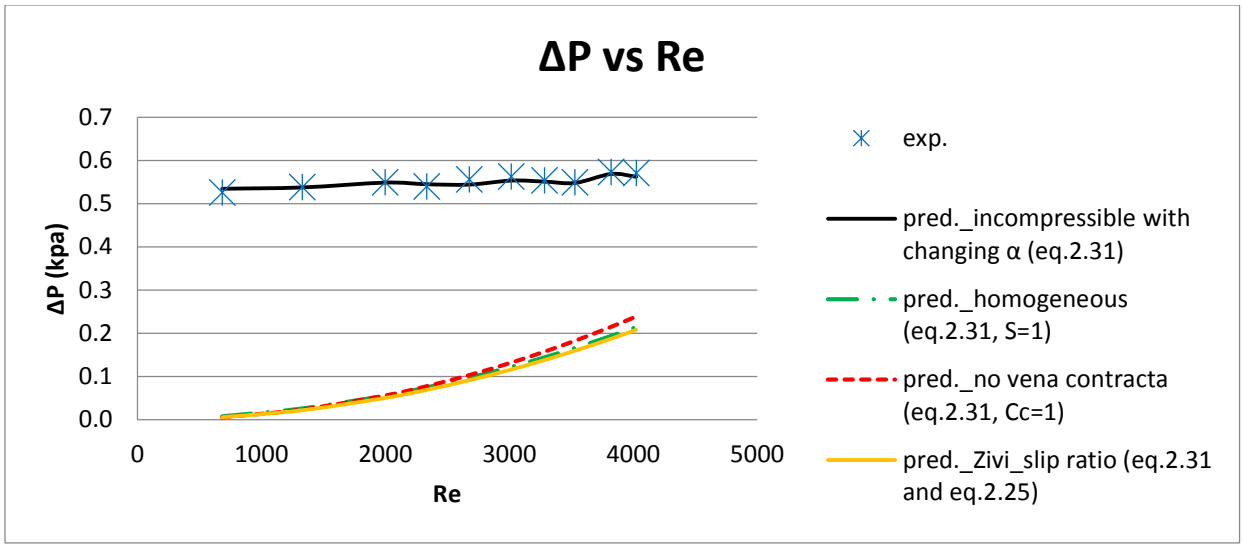

Figure 66: Pressure drop performance and predictions for σ_c = 0.5625, $\dot{m}_L$ (g/s) = 5.12-30.1, $\dot{m}_G$ (g/s) = 0.0019

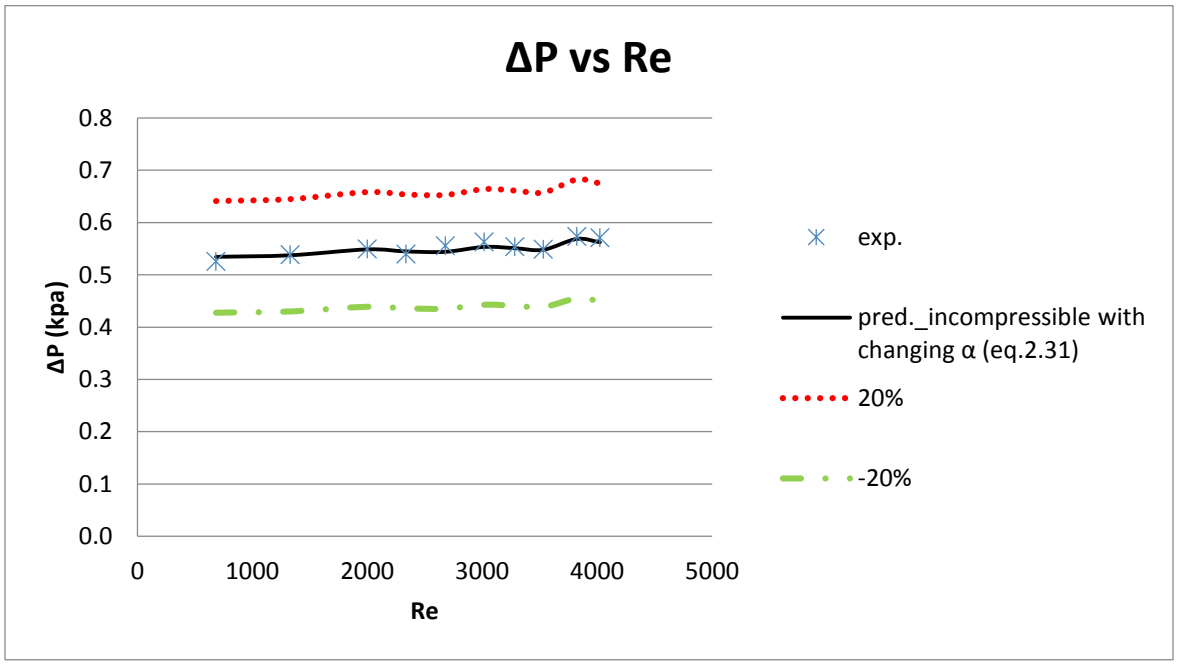

Figure 67: Pressure drop performance with ± 20% for σ_c = 0.5625, $\dot{m}_L$ (g/s) = 5.12-30.1, $\dot{m}_G$ (g/s) = 0.0019

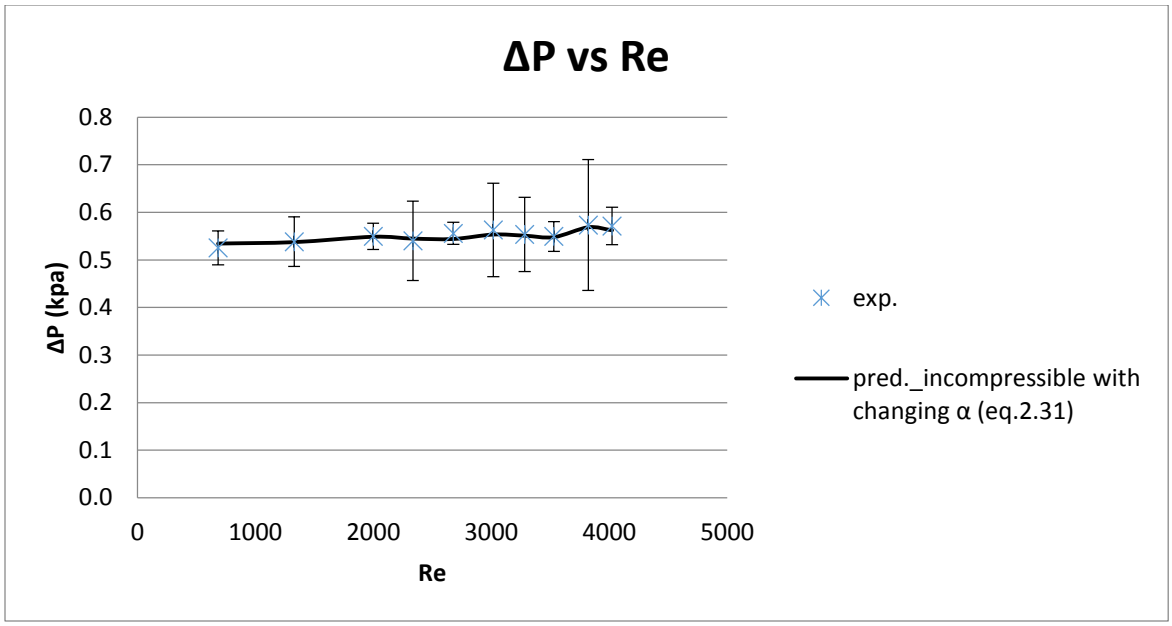

Figure 68: Pressure drop standard deviation for σ_c = 0.5625, $\dot{m}_L$ (g/s) = 5.12-30.1, $\dot{m}_G$ (g/s) = 0.0019

From the pressure drop result which shows above indicates that the pressure drop vs Reynolds number in the smaller area ratio, the pressure drop will increase gradually with Reynolds number increase. Yet, the pressure drop will not be significantly affected by increasing Reynolds number when the area ratio become larger. The Zivi's slip ratio model prediction equation seems to have good agreement results at the smaller area ratio and higher Reynolds number in the contraction channels. The incompressible model equation can be roughly predicted the larger area ratio when Reynolds number is smaller.

4.2.2.2 Pressure drop in expansion channels

The two phase flow pressure drop behavior in expansion channels show as below. The values of the static pressure are increasing according with the flow rate raising. Yet, the pressure drop performance with Reynolds number don't flow the regular pattern which the behavior is same

as single phase flow. Nevertheless, the most of the pressure drop will no long be affected apparently by Reynolds number changing.

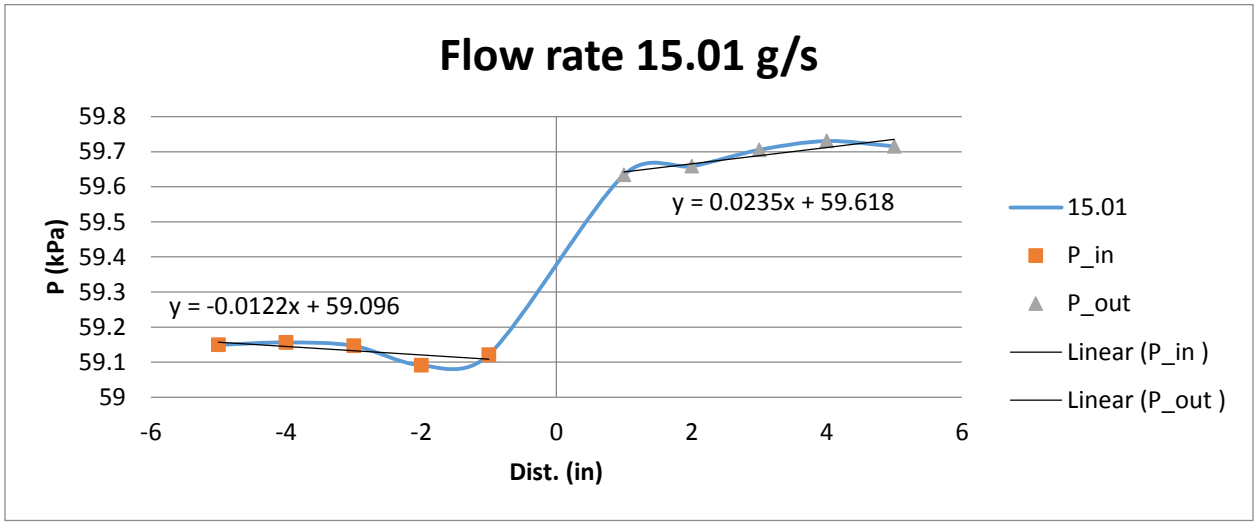

Figure 69: Pressure drop performance for σ_e = 0.5625, $\dot{m}_L$ (g/s) = 15.01 $\dot{m}_G$ (g/s) = 0.00954

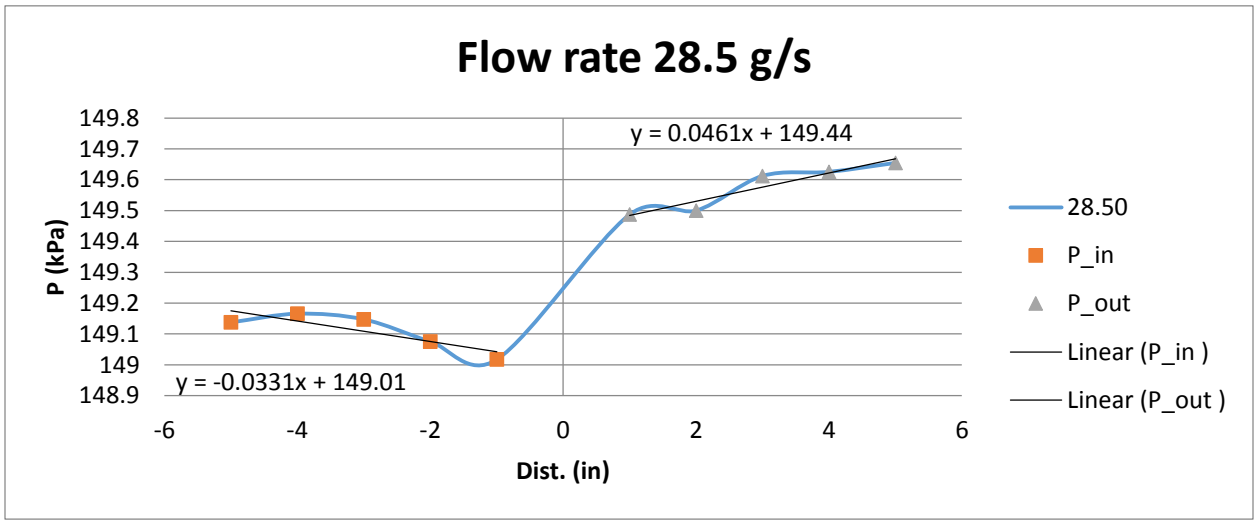

Figure 70: Pressure drop performance for σ_e = 0.5625, $\dot{m}_L$ (g/s) = 28.5 $\dot{m}_G$ (g/s) = 0.00954

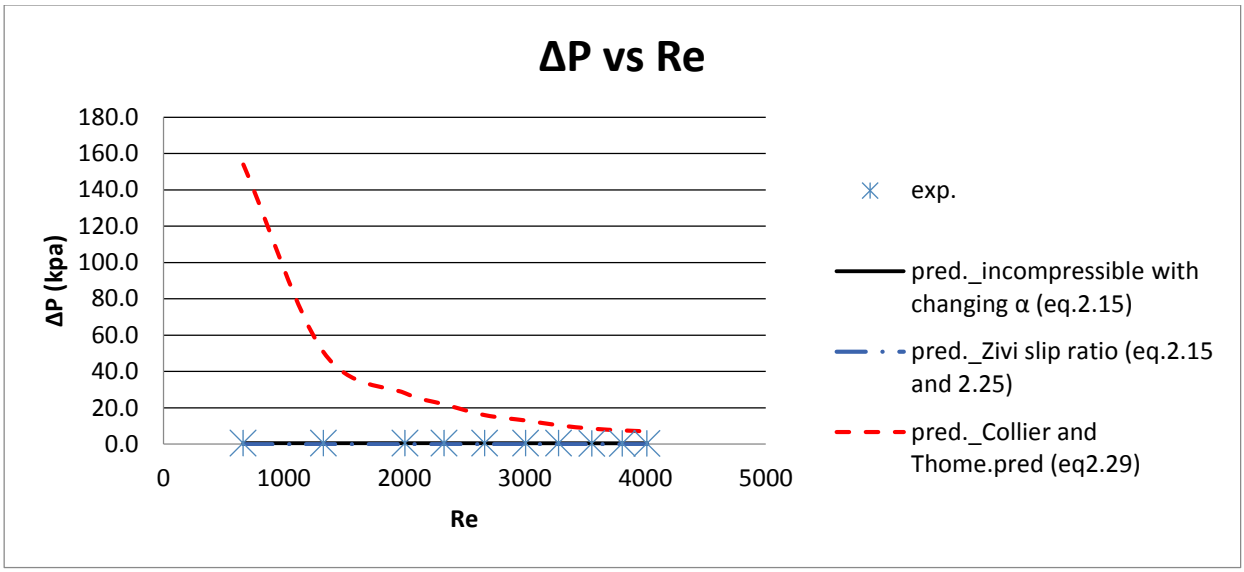

Figure 71: Pressure drop performance and predictions for σ_e = 0.5625, $\dot{m}_L$ (g/s) = 4.96-30.04 $\dot{m}_G$ (g/s) = 0.00954

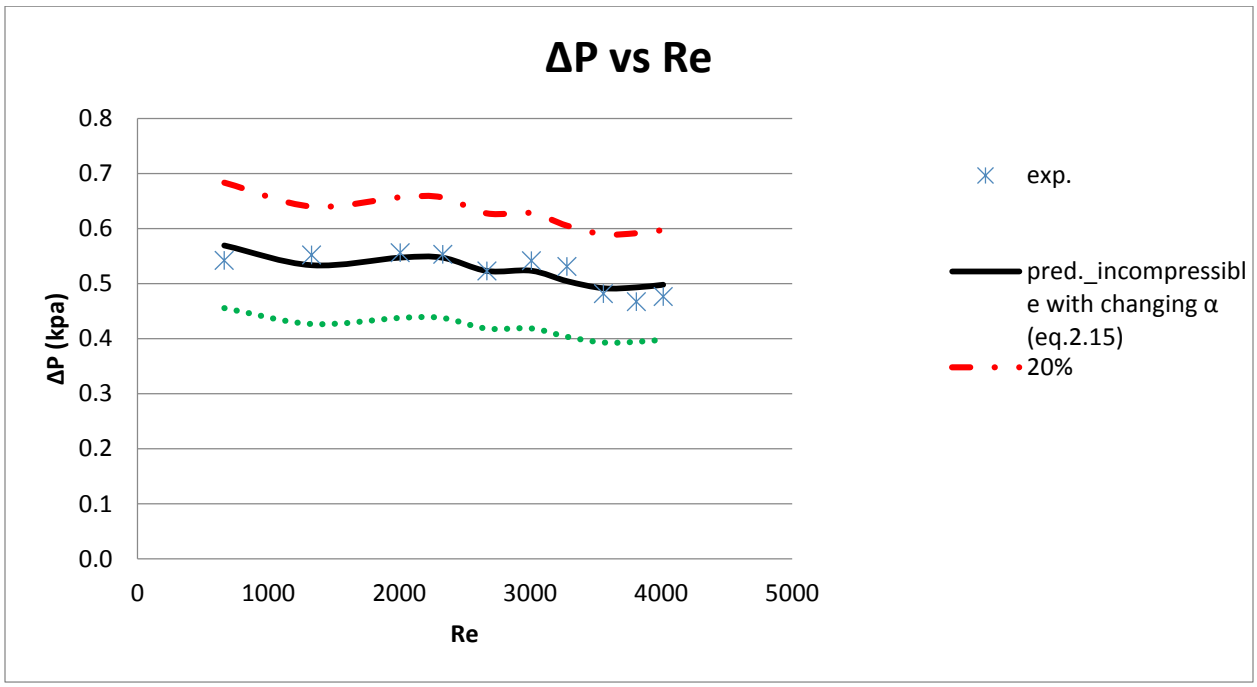

Figure 72: Pressure drop performance with ± 20% for σ_e = 0.5625, $\dot{m}_L$ (g/s) = 4.96-30.04 $\dot{m}_G$ (g/s) = 0.00954

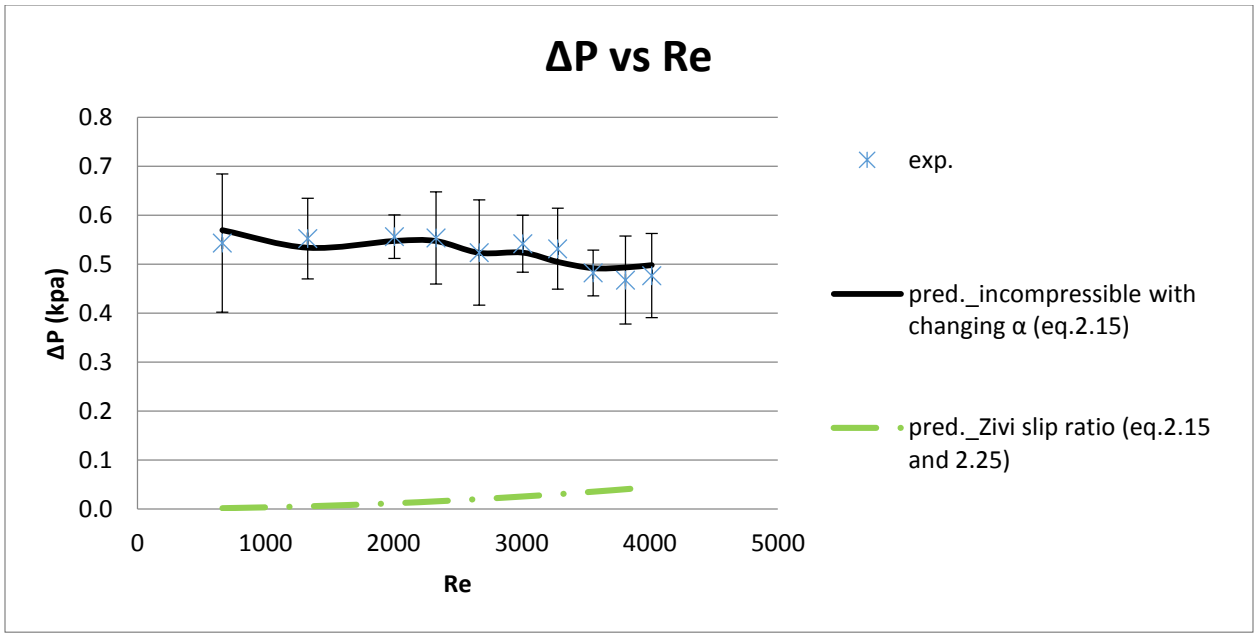

Figure 73: Pressure drop standard deviation for σ_e = 0.5625, $\dot{m}_L$ (g/s) = 4.96-30.04 $\dot{m}_G$ (g/s) = 0.00954

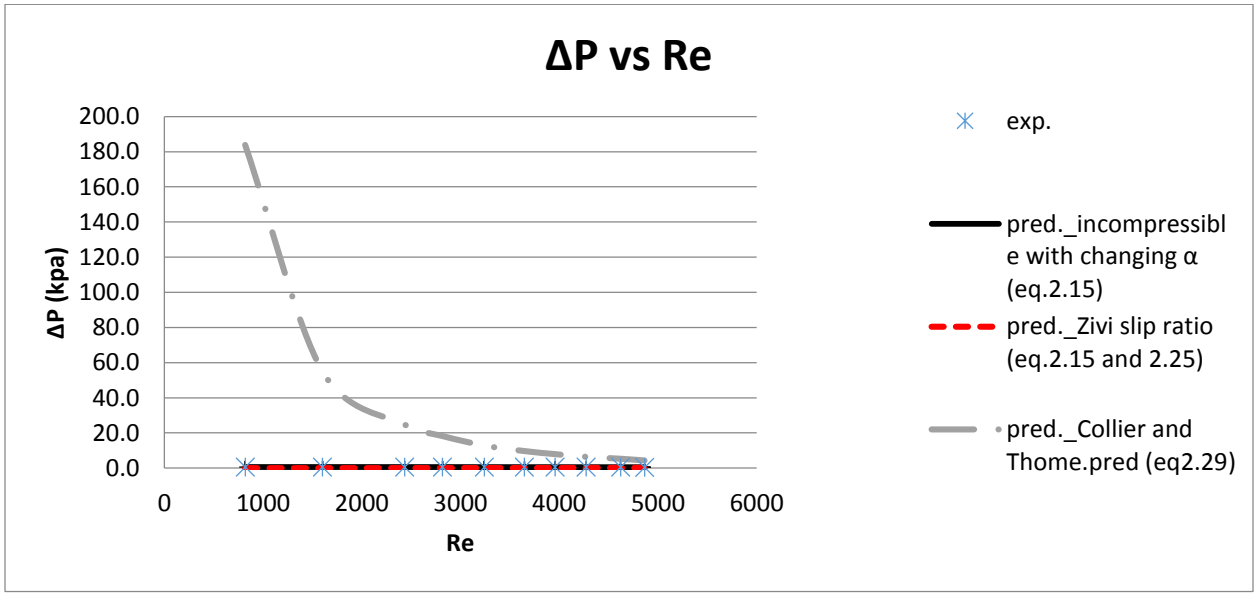

Figure 74: Pressure drop performance and predictions for σ_e = 0.3844, $\dot{m}_L$ (g/s) = 5.06-30.09 $\dot{m}_G$ (g/s) = 0.0019

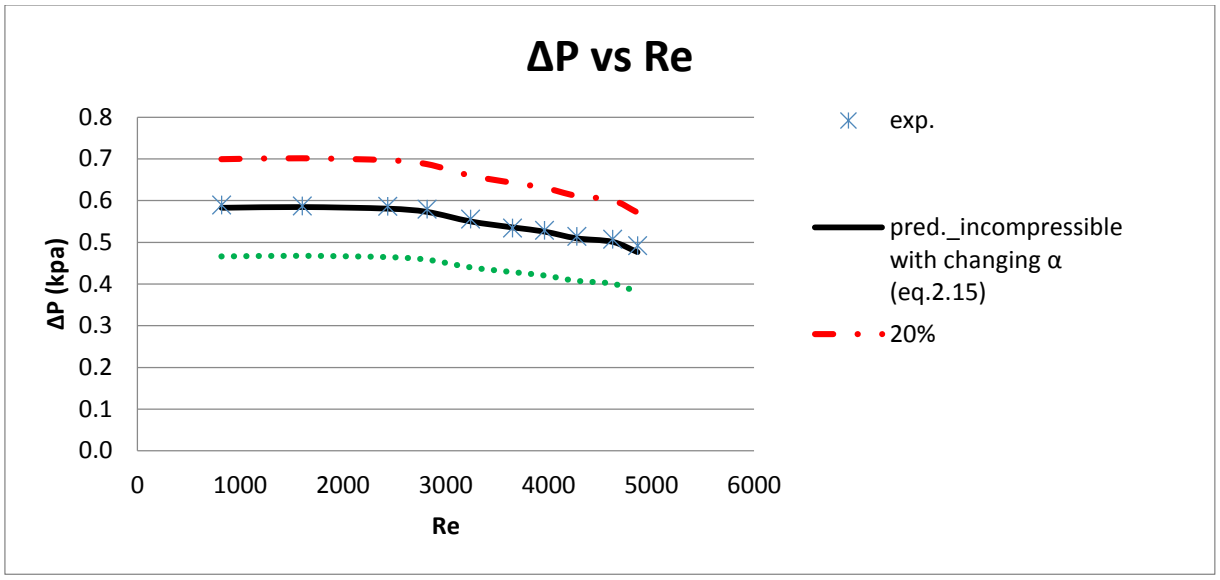

Figure 75: Pressure drop performance with ± 20% for σ_e = 0.3844, $\dot{m}_L$ (g/s) = 5.06-30.09 $\dot{m}_G$ (g/s) = 0.0019

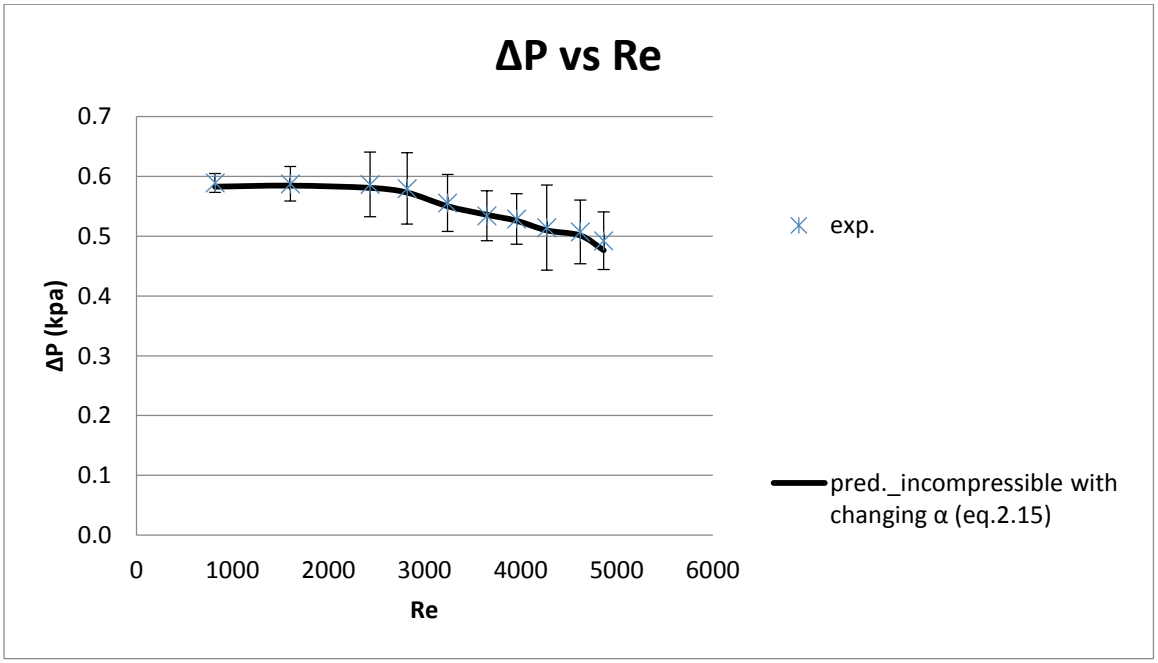

Figure 76: Pressure drop standard deviation for σ_e = 0.3844, $\dot{m}_L$ (g/s) = 5.06-30.09 $\dot{m}_G$ (g/s) = 0.0019

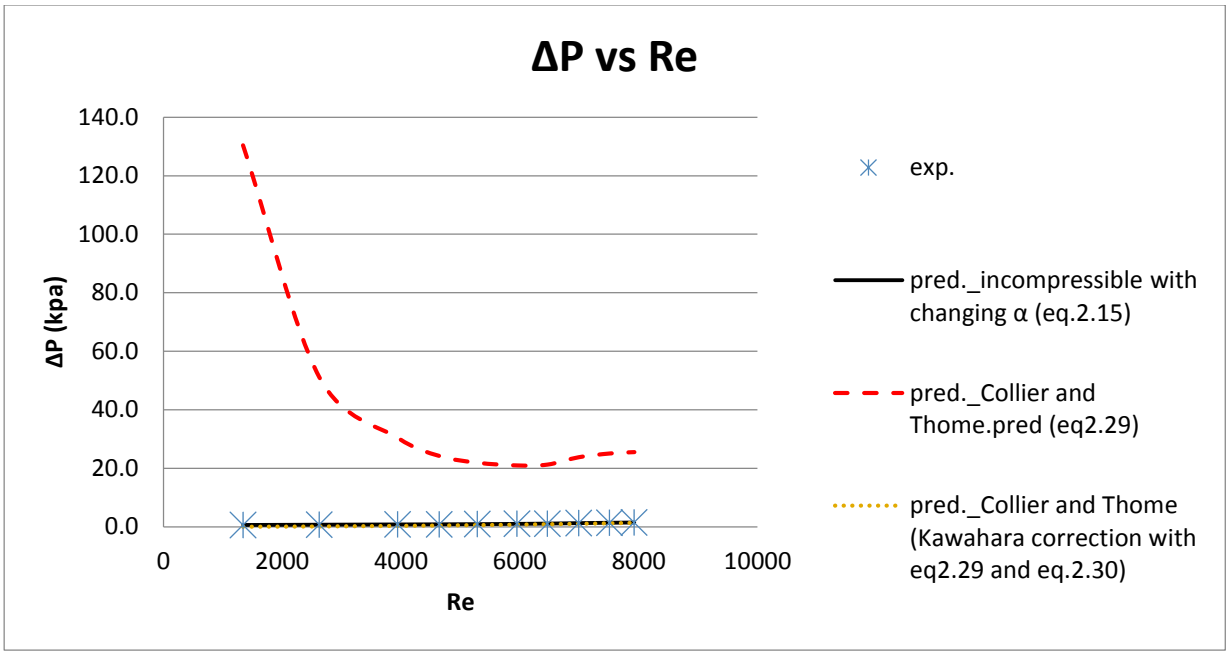

Figure 77: Pressure drop performance and predictions for σ_e = 0.1444, $\dot{m}_L$ (g/s) = 5.09-30.04 $\dot{m}_G$ (g/s) = 0.0019

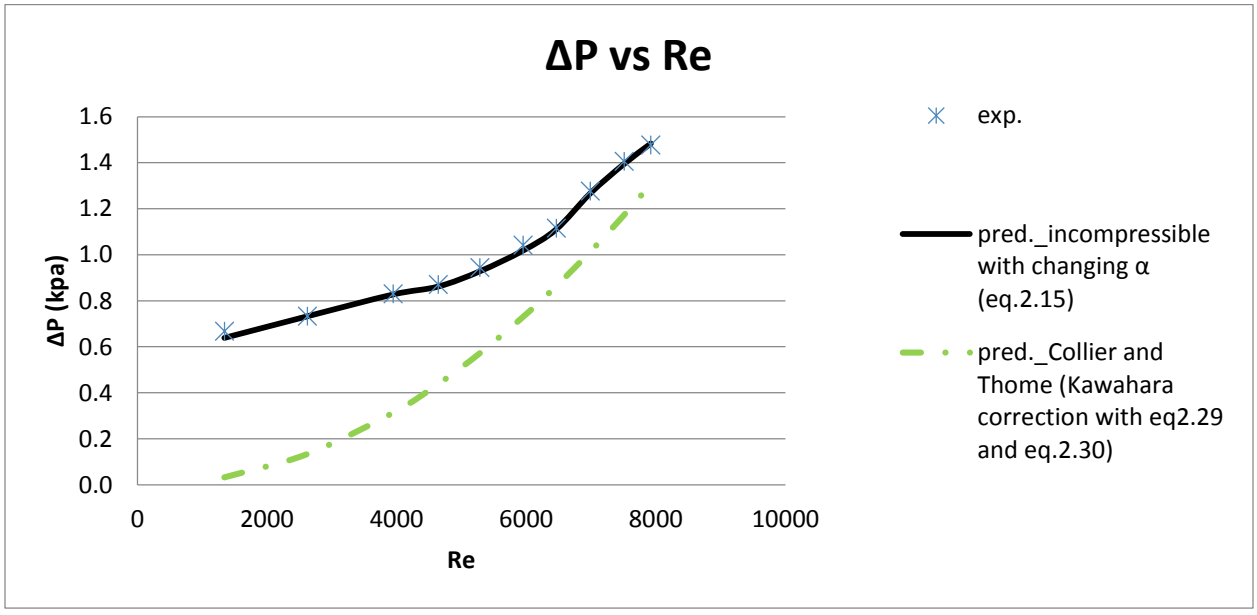

Figure 78 Pressure drop performance and predictions for σ_e = 0.1444, $\dot{m}_L$ (g/s) = 5.09-30.04 $\dot{m}_G$ (g/s) = 0.0019

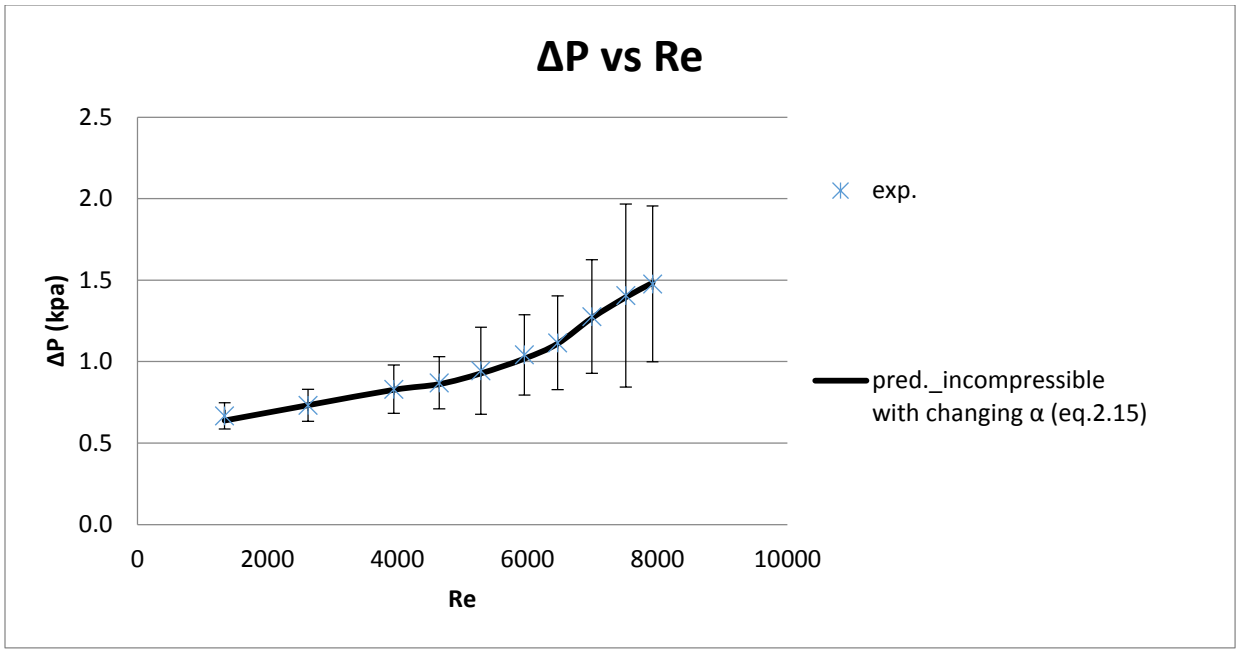

Figure 79: Pressure drop standard deviation for σ_e = 0.1444, $\dot{m}_L$ (g/s) = 5.09-30.04 $\dot{m}_G$ (g/s) = 0.0019

CHAPTER V

CONCLUSION AND RECOMMENDATIONS

5.1 Conclusion

The application of the single and two phase flow across abrupt contraction and expansion channels have been increasing dramatically in recent years. The most two phase studies are investigating for larger channels and the correlation equations normally can be proper used in their own experimental data. However, this studying are going to figure out the pressure drop behaviors and better prediction formulas for them. Loss coefficients are also the significant factor for observing the effect with test section geometrical changing and mass flow differences.

In order to gain the accurate and precise data result. The devices reliabilities and accuracies understanding are significantly important before the experimental data collecting. Also, the uncertainties estimation after the experimental data have been collected are necessary for precise and accurate true values. The experiment data results were received directly from the data acquisition system. The accuracy of the devices and instruments were significant affected the data result. For collecting static pressure transducers was with the ±0.02% accuracy. The flow meter sensor is ±0.05% accurate for mass flow rate and volume and ± 10°C for the temperature measurements. The gas mass flow controller was 0.8% of reading + 0.2% of full scale accuracy. Therefore the experimental data accuracy analysis was by describing in standard error, standard deviation and percent error. However, the pressure difference was the major factor for observation in the studying. The uncertainty of the pressure drop result, from appendix A, demonstrates that

most of the uncertainties are under 5 % and the uncertainties for gas mass flow, even better, are approximate below 2%.

From the experimental result approximate same water mass flow operating in various contraction channels for single phase flow, Reynolds number is going to be fully turbulent flow but not yet when area ratio as small as possible. Reynolds number is inversely proportional to the area ratio in our experimental result. The pressure drop becomes larger when area ratio is smaller with faster mass flow rate. The pressure drop is proportional to Reynolds number in this case. To estimate the better pressure drop prediction formula in this experiment, the turbulent, but not complete, flow model and flat velocity flow are applied at this time. The data points result demonstrates that the points are generally higher than these prediction loss coefficients. The performance of the loss coefficient is also suggested, approximate 0.85, in the result. The loss coefficient can be figure out by using Eq. 2.45. While the area ratio is getting larger, then Reynolds number is becoming smaller which the flow regimes local between the laminar and transition which are indicated in the experimental result. Also the pressure drop is reduced by increasing area ratio and the pressure drops don't significantly affect by increasing Reynolds number when the larger area ratio is applied. The prediction formulas for the pressure drops do not worked well for the turbulent not complete profiles model, the flat velocity profiles model or vena contracta model assumptions. The loss coefficients are generally recommended higher than the incomplete turbulent model and flat velocity model in the contraction channels.

The small area ratio in the expansion channels has same influences with the pressure drop performance, Reynolds number value and loss coefficient. The pressure drop stays higher when Reynolds number is also higher. The pressure drop is proportional to Reynolds number as the small area ratio in contraction channels as well. The pressure drop prediction can be a rough

agreement with experimental data. And then the loss coefficient is to suggest to use Eq. 2.43. The pressure drop is no long affecting by increasing Reynolds number in larger expansion area ratio. The prediction formulas don't agree with the experimental data, a new equation should be generated in the future for accurate prediction in this situation.

Two phase flow in the smaller area ratio contraction channels and lower gas mass flow rate, the pressure drop can be estimated highly accurate with experimental data by using Zivi's slip ratio model prediction. Reynolds number in this case is up to 7913 which means it's behaviors might close to fully turbulent flow regime. In the larger contraction test section and higher gas mass flow rate, the pressure drop can be predicted by using incompressible with Geiger's vena contracta model and unchanged void fraction. The estimation shows the fine agreement with the collecting data.

For the smaller area ratio and lower gas mass flow rate in two phase flow expansion channels, the result indicates that the incompressible model is the best prediction for this case but the void fraction obtaining needs a new investigation and result. In this situation, the void fraction is obtained by inverse method. The pressure drops, qualities, slip ratio and densities have been collected and calculated. The void fraction can be the only unknown value for calculating Eq. 2.19 by trial and error the new void fraction can be found. However even the new void fraction values have been found the new formula for void fraction should be investigated and generated in the future. Kawahara correction, Figure 78, shows great agreement when Reynolds number greater than 6000 in the small area ratio. The pressure drop experimental data are quite low compare to single phase pressure drop in this smaller area ratio condition. Nevertheless, Reynolds number is raising with constant gas flow rate and increasing water flow rate, but the Reynolds number in this situation is lower than single phase flow. The same situation occurred for two phase flow in the

larger expansion with lower gas mass flow rate. However when gas mass flow is increasing in larger expansion channels, the pressure drop becomes unstable and unpredictable.

5.2 Recommendations

Many prediction and correlation equations and formulas can be found from the previous works and studies for single and two phase flow with abrupt contraction and expansion. The correct assumption making and right equations selecting are major works need to deal with it. Normally, the prediction equations are only proper for their own experiments, thus for obtaining the experimental data prediction formulas need to treat with caution. In our experiment data, some prediction equation will be greatly agreed with the experimental data, some don't. Most equations with limit conditions and narrow ranges downward to particular cases. In our studying, the equations are quite fitted with previous work in approximate same area ratio but different flow rates, the equations cannot be used directly. The equations need to revise and give or take out new conditions or assumptions. Some new equations are suggested after this experiment. A new pressure drop equations or conditions for estimating the larger area ratio and faster gas mass flow should be generated and derived. The void fraction equations need to obtain for two phase flow in expansion and contraction. The proportion of water mass flow rate with gas mass flow rate are quite important. The slow water mass flow cannot flow itself fluently due to the stronger gas flow rate injects into the flow system. It might cause the water fluid counterclockwise drives the incorrect mass flow obtaining.

BIBLIOGRAPHY

[1] M. Yoda, F. Abdelall, G. Hahn, S. Ghiaasiaan, S. Abdel-Khalik, S. Jeter and D. Sadowski, "Pressure drop caused by abrupt flow area changes in small channels," *Experimental thermal and fluid science,* vol. 29, pp. 425-434, 2005.

[2] G. Hewitt and N.S. Hall-Taylor, Annular Two-Phase Flow, Oxford: Pergamon Press, 1970.

[3] E. Jansen and J.A. Kervinen, "Two-phase pressure drop across contractions and expansion, steam–water mixtures at 600–1400 psia," GEAP, 1964.

[4] I. Y. Chen, S. Wongwises, B.-C. Yang and C.-c. Wang, "Two-phase flow across small sudden expansions and contractions," vol. 31, no. 4, pp. 298-309, 2010.

[5] J. Schmidt and L. and Friedel, "Two-Phase Flow Pressure Change," *Chemical Engineering Communications,* no. 141, 1995.

[6] A. Attou and Bolle, "A New Correlation for the Two-phase Pressure Recovery Downstream From a Sudden Enlargement,," *Chemical Engineering Technology,,* vol. 20, 1997.

[7] "CODECOGS," Zyba Ltd , 2015. [Online]. Available: http://www.codecogs.com/library/engineering/fluid_mechanics/orifice/index.php. [Accessed 2015].

[8] G. E. Geiger, "Sudden contraction losses in single and two phase flow," University of Pittsburgh, Pittsburgh, 1964.

[9] D. Chisholm, in *Two-phase flow in pipelines and heat exchangers*, London, George Godwin, 1983, pp. 175-192.

[10] S. Zivi, "Estimation of steady state steam void fraction by means of principle of minmum entropy production," *ASME,* vol. C, no. 86, p. 237252, 1964.

[11] M. Wadle, "Anew formula for the pressure recovery in an abrupt diffuser," *Internaitonal Journal of Multiphase flow,* vol. 15, pp. 241-256, 1989.

[12] T. J. Collier J.G., in *Converctive boiling and condensation* , New York, Oxford, 1994, pp. 109-111.

[13] K. A.A., C. P.M.Y. and K. M., "International journal of heat and mass transfer," *Investigation of two phase flow pattern, void fraction and pressure drop in a microchannel,* vol. 28, pp. 1411-1435, 2002.

[14] Hewitt, G. Hewitt, G. Shires and T. Bott, Process Heat Transfer, Ann Arbor: CRC Press, 1993.

[15] W. Kays, "Loss coefficient for abrup changes in flow corss section with low Reynolds nuber flow in single and multiple tube systems," *ASME,* pp. 1067-1074, 1950.

[16] S. G. Toufik Y. Chalfi, "Pressure drop caused by flow area changes in capillaries under low flow conditions," *International journal of mutiphase flow,* pp. 1-11, 2007.

[17] P.-Y. Chung and M. Kawaji, "The effect of channel diameter on adiabatic two-phase flow characteristics in microchannels," *International Journal of Multiphase Flow,* no. 30, pp. 735-761, 2004.

[18] D. Chisholm and A. Laird, "Two-phase flow in rough tubes," *ASME,* no. 80, pp. 276-286, 1985.

[19] K. Triplett, S. Ghiaasiaan, S. Abdel-Khalik, A. LeMouel and B. McCord, "Ga-liquid two-phase flow in microchannels Part II: void fraction and pressure drop," *International Journal of Multiphase Flow,* no. 25, pp. 395-410, 1999.

[20] A. Armand and G. and Treschev, "The resistance during the movement of a two-phase system in horizontal pipes," pp. 16-23, 1946.

[21] R. P. Ching-Yi J. Hwang, "Flow of two-phase oil/water mixtures through sudden expansions and contractions," *Chemical Engineering Journal* , no. 68, pp. 157-163, 1997.

[22] R. Pal, *Ind. Eng. Chem. Res.,* vol. 33, pp. 1413-1435, 1994.

[23] P. Sookprasong, J. Brill and Z. Schmidt, *J. Energy Res.Technol.,* vol. 108, pp. 179-201, 1986.

[24] K. Triplett, S. Ghiaasiaan, S. Abdel-Khalik, Sadowski and D.L., "Gas-liquid two-phase flow in microchannels Part I: two-phase flow patterns," *International Journal of Multiphase Flow,* no. 25, pp. 377-394, 1999.

[25] T. Oya, "Upward liquid flow in small tube into which air streams," Bull, JSME, 1971, pp. 1320-1329.

[26] M. Fouran and Bories, "Experimental study of air-water two-phase flow through a fracture (narrow channel)," *Int. J. Multiphase Flow,* vol. 21, pp. 621-637, 1995.

[27] D. Beattie and P. Whalley, "A simple two-phase frictional pressure drop calculation method.," *Int. J. Multiphase Flow,* 1982.

[28] J. Chen and P. Spedding, "An analysis of holdup in horizontal two-phase gas-liquid FLow," *Int. J. Multiphase Flow,* 1983.

[29] J. Xu, P. Cheng and T. Zhao, "Gas±liquid two-phase ¯ow regimes in rectangular channels with mini/micro gaps," *International Journal of Multiphase Flow,* no. 25, pp. 411-432, 1999.

[30] Y. Taitel, D. Bornea and A. Dukler, "Modeling flow pattern transitions for steady upward gas-liquid flow in vertical tubes," *AIChE J,* vol. 26, pp. 345-354, 1980.

[31] K. Mishima and M. Ishii, "Flow regime transition criteria for upward two-phase ¯ow in vertical tubes," *Int. J. Heat Mass Transfer,* vol. 27, pp. 723-737, 1984.

[32] R. Knight, A. U. Auburn Univ., D. Hall, J. Goodling and R. Jaeger, "Heat Sink Optimization with Application to Microchannels," *IEEE,* vol. 15, no. 5, pp. 839-842, 1992.

[33] R. K. S. S. Kakac and W. Aung, in *Single-phase Convective Heat Transfer*, New York, Wiley, 1987.

[34] D. B. Tuckerman and R. F. W. Pease, "High-performance heat sinking for VLSI," *IEEE Electronic Device Lett,* vol. 2, pp. 126-129, 1981.

[35] N. Goldberg, "Narrow channel forced air heat sink," *IEEE Trans. Comp. Hybrids Manuf. Technol,* vol. 7, pp. 154-159, 1984.

[36] R. J. Phillips, "Micro-channel heat sinks," *Advances in Thermal Modeling of Electronic Components and Systems,* vol. 2, pp. 39-41, 1990.

[37] X. PENG and G. P. PETERSON, "Convective heat transfer and flow friction for water flow in microchannel structures," *Int. J. Heat Mass Transfer,* vol. 39, no. 12, pp. 2600-2607, 1996.

[38] J. Pfahler, J. Harley, H. H. Bau and J. Zemel, "Gas and liquid flow in small channels," *ASME,* vol. 32, pp. 49-60, 1991.

[39] G. M. Mala and D. Li, "Flow characteristics of water in microtubes," *International Journal of Heat and Fluid Flow,* vol. 20, pp. 142-148, 1999.

[40] J. Pfahler, J. Harley, H. Bau and J. Zemel, "Liquid and gas transport in small channels," *ASME,* pp. 149-157, 1990.

[41] Q. Weilin, G. M. Mala and L. Dongqing, "Pressure-driven water ¯ows in trapezoidal silicon microchannels," *International Journal of Heat and Mass Transfer,* vol. 43, pp. 353-364, 2000.

[42] R. Benedict, Fundamentals of Pipe Flow, New York: John Wiley & Son, 1980.

[43] A. L. R.K. Shah, Laminar flow forced convection in ducts, New York: Academic Press, 1978.

[44] W. M. Kays and M. E. Crawford, in *Convective Heat and Mass Transfer,* McGraw-Hill, 1980.

[45] W. M. Kays and A. L. London, in *Compact Heat Exchangers,* McGraw-Hill, 1964.

[46] M. N. Ozisik, in *Basic Heat Transfer,* McGraw-Hill , 1977.

[47] S. Sasaki and T. Kishimoto, "Optimal structure for micro-grooved cooling fin for high-power LSI devices," *Electron. Lett.,* vol. 22, no. 25, pp. 1332-1334, 1986.

[48] V. K. Samalam, "Convective heat transfer in microchannels," *J. Electron. Mater.,* vol. 18, no. 5, pp. 611-618, 1989.

[49] J.-M. K. L. J. M. A. Lian Zhang, "Measurements and Modeling of Two-Phase Flow in Microchannels With Nearly Constant Heat Flux Boundary Conditions," *JOURNAL OF MICROELECTROMECHANICAL SYSTEMS,* vol. 11, no. 1, pp. 12-19, 2002.

[50] R. S. Stanley, R. F. Barron and T. A. Ameel, "Two-phase flow in microchannels," *ASME,* no. 62, pp. 143-152, 1997.

[51] M. B. Bowers and I. Mudawar, "High flux boiling in low flow rate, low pressure drop mini-channel and micro-channel heat sinks," *Int. J. Heat Mass Transfer,* vol. 37, no. 2, pp. 321-332, 1994.